KU Leuven
Biomedical Sciences Group
Faculty of Medicine
Department of Imaging and Pathology
Nuclear Medicine & Molecular Imaging
Department of Cardiovascular Sciences

KU LEUVEN

DOCTORAL SCHOOL
BIOMEDICAL SCIENCES

MULTIMODAL IMAGING OF ISCHEMIC HEART DISEASE AND HEART FAILURE

Ganna Degtiarova

Dissertation presented in partial fulfilment of the requirements for the degree of

Doctor in Biomedical Sciences

Supervisor:	Prof. Dr. Piet Claus
Co-supervisor:	Prof. Dr. Jens-Uwe Voigt
	Prof. Dr. Johan Nuyts
Chair examining committee:	Prof. Dr. John Creemers
Chair public defence:	Prof. Dr. Werner Budts
Jury members:	Prof. Dr. Antti Saraste, Turku University Hospital, Finland
	Prof. Dr. Erwan Donal, University of Rennes, France
	Prof. Dr. Jan Bogaert, KU Leuven, Belgium
	Prof. Dr. Stefan Janssens, KU Leuven, Belgium

Leuven, May 29th, 2020

TABLE OF CONTENTS

ABBREVIATIONS

1(2)CM	=	One(two)-tissue compartment kinetic model
AR	=	Apical rocking
AC	=	Attenuation correction
AF	=	Atrial fibrillation
CAD	=	Coronary artery disease
CMR	=	Cardiac magnetic resonance
CRT	=	Cardiac resynchronization therapy
CT	=	Computed tomography
CZT	=	Cadmium-zinc-telluride
EDV	=	End-diastolic volume
EF	=	Ejection fraction
ESV	=	End-systolic volume
^{18}F-FDG	=	^{18}F-fluorodeoxyglucose
HF	=	Heart failure
IVCD	=	Intraventricular conduction delay
LBBB	=	Left bundle branch block
LAD	=	Left anterior descending artery
LCX	=	Left circumflex artery
LGE	=	Late-gadolinium enhancement
LV	=	Left ventricle
MBF	=	Myocardial blood flow
MFR	=	Myocardial flow reserve
MPI	=	Myocardial perfusion imaging
PET	=	Positron emission tomography
RAC	=	Right coronary artery
ROI	=	Region of interest
RV	=	Right ventricle
SF	=	Septal flash
SLR	=	Septal to lateral wall ratio
SPECT	=	Single photon emission tomography
SUV	=	Standardized uptake value
TAC	=	Time activity curve

SUMMARY

During the last decades important technological advances in both hardware and software for medical nuclear imaging, represented by single-photon emission computed tomography (SPECT) and positron emission tomography (PET), strengthened its position in the field of non-invasive cardiac imaging and expanded its opportunities for the evaluation of patients with cardiovascular diseases. This PhD project was intended to give an insight in some of the novel opportunities of nuclear cardiology to assess perfusion and metabolism that can assist in the diagnosis of CAD and therapy guidance in the context of heart failure (HF).

In particular, in the first part of this PhD project we explored how the assessment of perfusion and glucose metabolism, with ^{13}N-NH_3 and ^{18}F-fluorodeoxyglucose (^{18}F-FDG) PET, respectively, can help to unravel the pathophysiology of left ventricular (LV) remodelling in cardiac-resynchronization therapy (CRT) candidates and whether PET can help to reliably guide the necessity of CRT implantation in HF patients. For this, a large prospective multicenter clinical trial (WORK-CRT) was initiated, that included consecutive patients referred for CRT implantation in different European centers. In Chapter I-II we evaluated the regional alterations in myocardial perfusion and metabolism in non-ischemic HF patients with left bundle branch block (LBBB) and with mechanical dyssynchrony. The latter currently represents a promising marker of successful CRT response. We have demonstrated that these conditions are associated with the redistribution of myocardial perfusion and metabolism, with the lowest values in the septum and highest in the lateral wall (Chapter I-II) and that these changes are proportional to regional myocardial work (Chapter II). Furthermore, in the cohort of non-ischemic patients represented in Chapter II we showed that pre-CRT septal-to-lateral wall (SLR) glucose metabolism ratio linearly correlates with the extent of volumetric reverse remodelling after CRT, suggesting ^{18}F-FDG SLR as a possible marker of CRT response. In chapter III we focused more on the reverse remodelling process and expanded our patient cohort to those with HF of both ischemic and non-ischemic origin. We have shown that in non-ischemic HF patients low ^{18}F-FDG SLR alone predicts CRT response with high sensitivity and specificity, but in ischemic HF patients, however, the specificity of low ^{18}F-FDG SLR significantly drops, suggesting that in this patient cohort low SLR can also be caused by the presence of septal scar, characterized by the absence of metabolic activity and limited potential of regional functional recovery. We have demonstrated that combining low ^{18}F-FDG SLR, assessed with PET, with septal scar extent, assessed with cardiac magnetic resonance, could separate CRT responders from non-

responders with high sensitivity and specificity, independently of HF etiology of the patients, so for the first time suggesting ^{18}F-FDG SLR as a predictor of CRT response.

In the second part of this PhD project (Chapter IV) we focused on the recently introduced novel cardiac dedicated cadmium-zinc-telluride (CZT) SPECT cameras, that for the first time offered an opportunity to quantify myocardial perfusion with SPECT, providing a great potential for the improvement of management of patients with CAD. Acknowledging the disadvantages of clinically available SPECT perfusion tracers, we renewed our interest in ^{99m}Tc-Teboroxime - a perfusion tracer with more favourable characteristics, that for a long time was withdrawn from the market due to incompatibility of its fast kinetics with the slow conventional SPECT cameras. In Chapter IV we investigated if the fast kinetics of ^{99m}Tc-Teboroxime could be an advantage for the novel SPECT CZT camera and evaluated its performance to quantify myocardial perfusion. We have demonstrated the possibility to synthesize this tracer in our hospital and showed its high cardiac affinity and fast myocardial kinetics in rodents. Furthermore, we demonstrated the feasibility to image and quantify myocardial flow reserve with the novel SPECT CZT camera and ^{99m}Tc-Teboroxime in large animals, however the optimization of a suitable kinetic model for ^{99m}Tc-Teboroxime is necessary.

In the discussion chapter of this PhD thesis we reviewed the most crucial findings and important results of our work, while we shared the next research steps in the Future Perspectives chapter.

SAMENVATTING

Gedurende de laatste decennia hebben belangrijke technologische ontwikkelingen in zowel hardware als software voor medische nucleaire beeldvorming haar positie op het gebied van niet-invasieve cardiale beeldvorming versterkt en uitgebreid. Zowel “single-photon” emissie computertomografie (SPECT) als positron emissie tomografie (PET), worden ingezet voor de evaluatie van patiënten met hart- en vaatziekten. Dit doctoraatsonderzoek was bedoeld om inzicht te geven in enkele van de nieuwe mogelijkheden van nucleaire cardiologie om perfusie en metabolisme te beoordelen die kunnen helpen bij de diagnose van coronairlijden (CAD) en therapiebegeleiding in de context van hartfalen (HF).

In het eerste deel van dit onderzoek hebben we in het bijzonder bestudeerd hoe de beoordeling van perfusie en glucosemetabolisme, met respectievelijk ^{13}N-NH3 en ^{18}F-fluorodeoxyglucose (^{18}F-FDG) PET, kan helpen om de pathofysiologie van het linker-ventrikel (LV) remodelering te ontrafelen bij HF patiënten met linker bundeltakblok (LBBB) die in aanmerking komen voor cardiale resynchronisatietherapie (CRT) en of PET kan helpen de therapie response van CRT-implantatie bij HF-patiënten betrouwbaar kan voorspellen. Hiervoor werd een groot prospectief multicenter klinisch onderzoek (WORK-CRT) gestart, dat opeenvolgende patiënten includeerde die werden doorverwezen voor CRT-implantatie in verschillende Europese centra. In hoofdstuk I-II hebben we de regionale veranderingen in myocardperfusie en metabolisme geëvalueerd bij niet-ischemische HF-patiënten met LBBB, met of zonder mechanische dissynchronie, geëvalueerd met echocardiografie. Aanwezigheid van mechanische dissynchronie vertegenwoordigt momenteel een veelbelovende marker voor een succesvolle CRT respons. We hebben aangetoond dat deze gerelateerd is aan de herverdeling van myocardperfusie en metabolisme, met lage waarden in het septum en de hoge in de laterale wand (hoofdstuk I-II) en dat deze veranderingen evenredig zijn met regionale mechanische arbeid geleverd door de hartspier (hoofdstuk II) . Verder hebben we in deze cohort van niet-ischemische patiënten aangetoond dat de pre-CRT verhouding van septale-tot-laterale wand glucosemetabolisme (SLR) lineair correleert met de mate van inverse volumetrische remodelering na CRT. Dit suggereert dat ^{18}F-FDG SLR als een mogelijke predictor voor CRT-response kan worden gebruikt. In hoofdstuk III hebben we ons meer gericht op het proces van inverse remodelering en hebben we onze patiënten cohorte uitgebreid met mensen met HF van zowel ischemische als niet-ischemische oorsprong. We hebben aangetoond dat bij niet-ischemische HF-patiënten de lage ^{18}F-FDG SLR alleen CRT-respons voorspelt met een hoge

sensitiviteit en specificiteit, maar bij ischemische HF-patiënten daalt de specificiteit van lage ^{18}F-FDG SLR echter aanzienlijk, wat suggereert dat in deze patiënten lage SLR ook kan worden veroorzaakt door de aanwezigheid van littekenweefsel in het septum (na myocardinfarct) en dus ook gekenmerkt door de afwezigheid van metabole activiteit en beperkt potentieel van regionaal functioneel herstel. We hebben aangetoond dat het combineren van lage ^{18}F-FDG SLR, beoordeeld met PET, en omvang van littekenweefsel in het septum, beoordeeld met cardiale magnetische resonantie, CRT respons kan scheiden van non-respons met hoge gevoeligheid en specificiteit, onafhankelijk van de HF-etiologie van de patiënten.

In het tweede deel van dit doctoraatsonderzoek (hoofdstuk IV) hebben we ons gericht op de onlangs geïntroduceerde nieuwe speciale cardiale SPECT-camera's uitgerust met cadmiumzinktelluride (CZT) detectoren, die voor het eerst de mogelijkheid bood om myocardperfusie met SPECT te kwantificeren en daardoor potentieel het management van patiënten met CAD kunnen verbeteren. Gegeven de nadelen van klinisch beschikbare SPECT-perfusietracers, zoals onderschatting van perfusie bij hoge debieten, hernieuwden we onze interesse in ^{99m}Tc-Teboroxime - een perfusietracer met gunstiger kenmerken, die lange tijd uit de markt werd gehaald vanwege de onverenigbaarheid van zijn snelle kinetiek met de trage conventionele SPECT-camera's . In hoofdstuk IV hebben we onderzocht of de snelle kinetiek van ^{99m}Tc-Teboroxime een voordeel kan betekening in combinatie met de nieuwe SPECT CZT-camera en hebben we de prestaties ervan geëvalueerd om myocardperfusie te kwantificeren. We hebben de mogelijkheid aangetoond om deze tracer in ons ziekenhuis te synthetiseren en toonden zijn hoge hartaffiniteit en snelle myocardiale kinetiek bij knaagdieren. Verder hebben we aangetoond dat het mogelijk is om myocardiale flowreserve te kwantificeren met de nieuwe SPECT CZT-camera en ^{99m}Tc-Teboroxime bij grote dieren, maar de optimalisatie van een geschikt kinetisch model voor ^{99m}Tc-Teboroxime is noodzakelijk.

Deze dissertatie eindigt met een bespreking van de cruciale bevindingen en de belangrijkste resultaten, waarna we verder ingaan op mogelijke toekomstige onderzoekspistes die volgen uit onze resultaten.

PART I

INTRODUCTION

INTRODUCTION

During the last decades important technological advances in non-invasive cardiac imaging led to a tremendous progress in the management of patients with cardiovascular diseases. In particular, introduction of novel cameras and advanced hybrid techniques in the field of nuclear cardiology, represented by single-photon emission computed tomography (SPECT) and positron emission tomography (PET), expanded and sophisticated its ability to visualize molecular processes in cardiac tissue, increasingly attracting attention of scientists worldwide. The latest advances did not leave aside evaluation of myocardial perfusion and metabolism, that can be of interest for the diagnosis of coronary artery disease (CAD) and therapy guidance in the context of heart failure (HF). These diseases still represent a huge burden for society in terms of morbidity, mortality, quality of life and healthcare costs[1].

1. Management of patients with HF: role of PET

1.1 LV dyssynchrony

The electrical activation of the healthy heart is propagated throughout a specialized conduction pathway that originates in the sinus node of the right atrium, spreads over both atria to the atrioventricular node, goes further through the His bundle and the right and left Tawara branches, located correspondingly in the endocardium of right (RV) and left ventricles (LV) and ends in the Purkinje fibers (Figure 1).

The normal heart is characterized by simultaneous excitation of both ventricles, resulting in their synchronous contraction. In case of damage of this conduction system, the electrical signal cannot spread flawlessly throughout the regular conduction pathway anymore, causing a conduction delays. In case of a left bundle branch block (LBBB), the prominent feature of LV delay is represented by the first activation of the septum and delayed activation of the free wall, causing LV electrical dyssynchrony and corresponding changes of QRS morphology and duration (QRS $\geq$ 120 ms) [1,2].

Depending on the severity of the electrical activation delay between the different LV walls, asynchronous electrical LV activation can be coupled with a respective mechanical asynchrony, with initial contraction of the septum and late contraction of the lateral wall. This discoordinated

ventricular deformation results in a decreased and inefficient LV function, which is the basis of the harmful effect of LV dyssynchrony. Eventually, the changes in ventricular electromechanics associated with dyssynchrony are followed by regional molecular and structural alterations, leading to LV remodeling characterized by changes in LV configuration, mass, workload distribution, energetics and function. Serving first as physiological and adaptive mechanisms, these changes can provoke the development of HF, leading to vicious cycle with further progression of ventricular conduction abnormalities, chamber dilatation and functional deterioration[3].

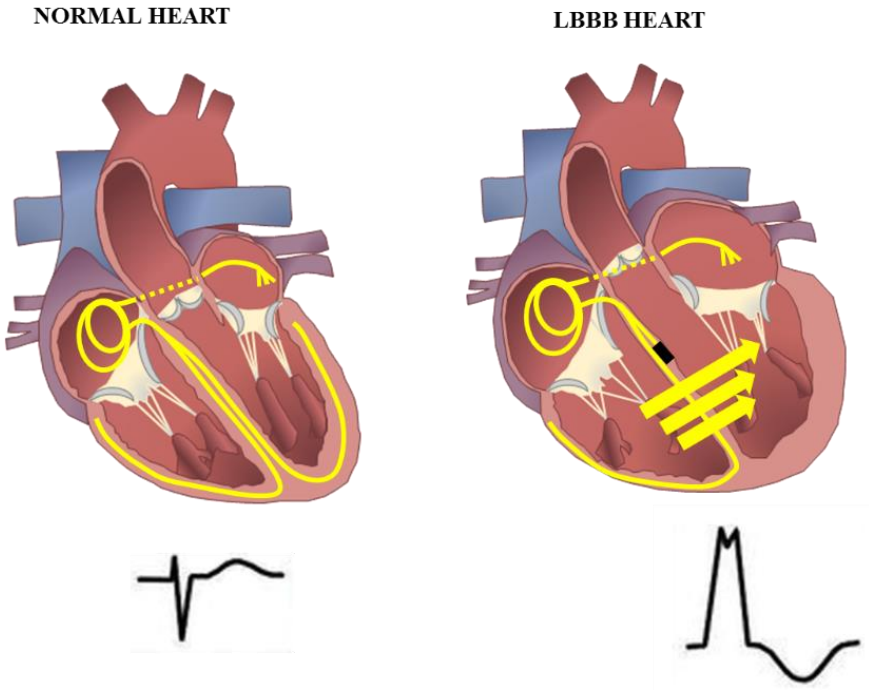

Figure 1. Schematic presentation of the electrical conduction pathway in the normal heart (left) and in the heart with a damaged LV conduction system due to LBBB (right). *Note the block in the LV conduction system in LBBB, that results in changes in electrical excitation pathway and leads to the corresponding changes in duration and morphology of QRS complex on ECG below. Adapted from* [4]

Ventricular dyssynchrony is present in patients with left LBBB, nonspecific intraventricular conduction delay (IVCD) or RV pacing. While the first one represents a complete block of the left His bundle branch, with slow propagation of electrical activation from normally activated non-affected RV to the endocardium of LV septum and afterwards to the LV free wall (Figure 1), IVCD implies only partial damage of the LV conduction pathway, with a combination of

normal and abnormal propagation of the electrical wave [5]. It has been demonstrated that patients with RV pacing with the lead positioned at the RV apex, share an electrical activation pattern similar to that in LBBB, which can likewise cause a deleterious effects on LV function and structure[6]. The evidence suggests that a prolonged QRS duration on ECG, irrespective of the type of conduction delay, is strongly associated with increased rate of all-cause mortality, cardiac mortality and sudden cardiac death [7].

1.2 LV dyssynchrony can be treated with cardiac resynchronization therapy

Despite continuous improvements in medical therapies for HF, the prognosis of many patients remains poor. The introduction of cardiac resynchronization therapy (CRT) has dramatically changed the management of patients with symptomatic HF and conduction delay. By means of biventricular pacing, with the pacing leads placed in the RV apex and lateral or posterolateral veins of the LV, CRT restores the synchronous contraction of the heart, leading to the improvement in clinical symptoms, quality of life and LV function, and causing reverse myocardial remodelling with associated decrease in hospitalization and mortality [8] (Figure 2). The activation pattern of the dyssynchronous hearts, however, is not always homogeneous, that is why some investigators emphasize the necessity to decide on the lead position individually in every patient, based on the region of the latest activation/contraction. Promising results of this approach have been demonstrated in the TARGET and STARTER studies, but the methods haven't been yet incorporated to the routine clinical practice [9,10].

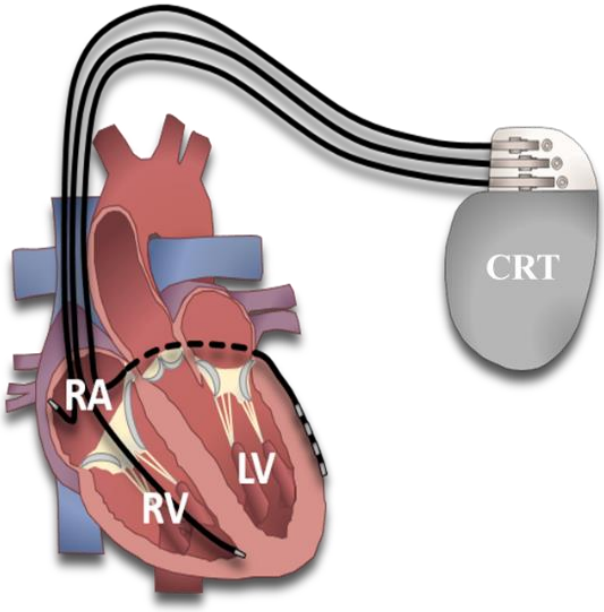

Figure 2. A schematic illustration of a cardiac resynchronization therapy device. *The device consists of three leads that are respectively placed in the right atrium (RA), apex of the right ventricle (RV) and in one of the veins of the lateral wall (LV). Courtesy of J.Duchenne, Department of Cardiovascular Sciences, KU Leuven, Leuven, Belgium.*

According to the latest ESC Heart Failure Association guidelines, CRT is recommended in patients with symptomatic drug-refractory HF with decreased LV function and increased QRS duration with preferably LBBB QRS morphology (Table 1) [11]. This guidelines does not differ significantly from the previous European guidelines, released in 2013 by ESC European Heart Rhythm association, except for the management of patients with QRS duration 120-129 ms [8,11]. While the European Heart Rhythm association (2013) strongly recommended CRT treatment in these patients (class I), the recent Heart Failure association guidelines (2016) do not (class III), what is mainly driven by the results of the ECHO CRT study[12].

Table 1. Recommendations for CRT implantation in HF patients [11]

Recommendations	Class	Level
CRT is recommended for symptomatic patients with HF in sinus rhythm with a QRS duration ≥150 msec and LBBB QRS morphology and with LVEF ≤35% despite OMT in order to improve symptoms and reduce morbidity and mortality.	I	A
CRT should be considered for symptomatic patients with HF in sinus rhythm with a QRS duration ≥150 msec and non-LBBB QRS morphology and with	IIa	B

LVEF ≤35% despite OMT in order to improve symptoms and reduce morbidity and mortality.		
CRT is recommended for symptomatic patients with HF in sinus rhythm with a QRS duration of 130–149 msec and LBBB QRS morphology and with LVEF ≤35% despite OMT in order to improve symptoms and reduce morbidity and mortality.	I	B
CRT may be considered for symptomatic patients with HF in sinus rhythm with a QRS duration of 130–149 msec and non-LBBB QRS morphology and with LVEF ≤35% despite OMT in order to improve symptoms and reduce morbidity and mortality.	IIb	B
CRT rather than RV pacing is recommended for patients with HFrEF regardless of NYHA class who have an indication for ventricular pacing and high degree AV block in order to reduce morbidity. This includes patients with AF	I	A
CRT should be considered for patients with LVEF ≤35% in NYHA Class III–IVd despite OMT in order to improve symptoms and reduce morbidity and mortality, if they are in AF and have a QRS duration ≥130 msec provided a strategy to ensure bi-ventricular capture is in place or the patient is expected to return to sinus rhythm.	IIa	B
Patients with HFrEF who have received a conventional pacemaker or an ICD and subsequently develop worsening HF despite OMT and who have a high proportion of RV pacing may be considered for upgrade to CRT. This does not apply to patients with stable HF	IIb	B
CRT is contra-indicated in patients with a QRS duration < 130 msec.	III	A

AF – atrial fibrillation; HFrEF – heart failure with reduced ejection fraction; LBBB – left bundle branch block; OMT – optimal medical treatment; RV - right ventricle.

Despite huge clinical benefit for the majority of patients, it has been demonstrated that about 30 to 40% of candidates who meet CRT implantation criteria show little or no improvement after CRT, suggesting that QRS duration is not the ideal parameter to predict CRT response [13]. This is the reason why optimization of the current selection criteria for CRT remains an active area of investigation. A better understanding of the pathophysiology of ventricular conduction abnormalities as well as the heart's (reverse) remodeling process is essential for

future research. Several parameters such as presence of mechanical dyssynchrony and myocardial scar, LV lead position and venous anatomy have already shown encouraging results for the prediction of CRT response. The recent advances in non-invasive cardiovascular imaging, including nuclear imaging and cardiac magnetic resonance (CMR), are expected to further improve selection of patients who will most likely benefit from CRT implantation.

1.3 Left bundle branch block as one of the causes of LV dyssynchrony

The prevalence of LBBB in the general population is less than 1% but increases with age, reaching 6% by the age of 80. In the presence of HF, its frequency approaches 30% [14,15]. LBBB can develop primarily, due to degeneration of the conduction pathway, or secondary, due to heart remodeling in patients with e.g. CAD, cardiomyopathy or myocarditis. [16]. There is ample evidence form the literature that the presence of LBBB is an independent cause of HF and is associated with an increased rate of hospitalization, cardiovascular mortality and sudden cardiac death. However, the magnitude of these effects has a high individual variability [3,17]. The presence of LBBB in patients with LV dyssynchrony and HF has emerged as a criterion for favorable CRT response and is currently listed with highest recommendation level in the CRT guidelines (Table 1). However, the definition of LBBB remains not fully standardized. Defined initially as a QRS ≥ 120ms with specific QRS morphology on the surface ECG, the criteria for complete LBBB mistakenly encompassed patients with LV hypertrophy and patients with only left anterior fascicular block (incomplete LBBB), who are less likely to have a successful CRT response[1,2]. Indeed, it has been shown that the 1/3 of the patients with LBBB defined according to the abovementioned conventional criteria do not present significant regional activation delay. The latter explains why not all LBBB patients are CRT responders and necessitates the introduction of more strict criteria for defining a complete LBBB, e.g. such as Strauss criteria[18]. The Strauss criteria are more strict in defining complete LBBB and include a larger QRS duration for men (QRS ≥ 140 ms) than for women (QRS ≥ 130 ms) as well as QRS notching or slurring in two or more ECG leads V1, V2, V5, V6, I and aVL [18] (Figure 3). Some studies demonstrated that Strauss LBBB criteria are more often coupled to dyssynchronous LV contraction and potentially might improve patient selection for CRT, but its definitive value in CRT field has yet to be established [19]. Therefore the current LBBB definition mentioned by CRT implantation guidelines is still characterized by less strict criteria such as QRS ≥120 ms, QS or rS pattern in lead V1, broad R wave in I, aVL, V5, V6 and absence of Q waves in V5 or V6[8]. Insight in the pathophysiology of LBBB has been steadily

increasing and might become an important step towards a final change in the LBBB definition adopted for CRT implantation.

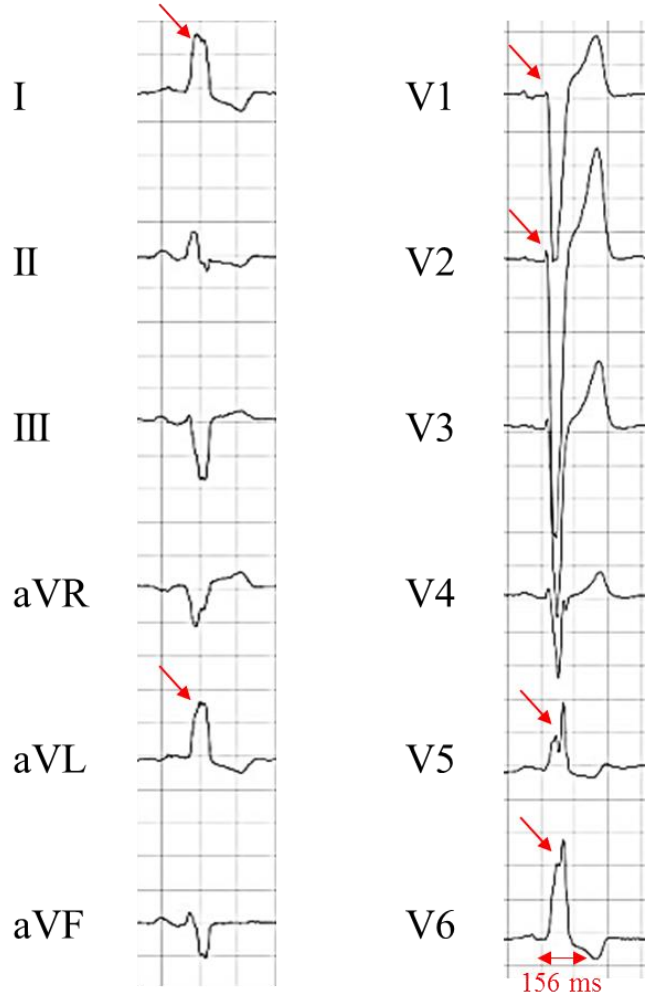

Figure 3. *Example of ECG of the female patient, meeting Strauss LBBB criteria [18]. Note QRS width 156 ms, presence of rS in V1, V2, mid-QRS notching/slurring in I, aVL,V5 and V6.*

1.4 Mechanical and electrical dyssynchrony are not the same

It is important to acknowledge that electrical dyssynchrony, induced by inhomogeneous electrical activation of the ventricles and represented by a wide QRS complex on the surface ECG, differs from mechanical dyssynchrony, characterized by a different timing of contraction of the LV walls. Since CRT is mainly a treatment to correct mechanical consequences of conduction disturbances, targeting mechanical dyssynchrony might improve the CRT selection process. Initially mechanical dyssynchrony was assumed to always couple to electrical dyssynchrony, and since the latter was so easy to measure with the widely available surface ECG, prolonged QRS width has become the main target of CRT. Later on, extensive research has demonstrated that mechanical dyssynchrony does not always follow electrical dyssynchrony and is present in about 30-40% of patients with normal QRS duration[20]. Lack of mechanical dyssynchrony has become a reasonable explanation for patients, who despite meeting the guidelines criteria, do not respond to CRT [21]. It has also become evident that a substantial number of patients with narrow QRS complex that do not receive CRT, but exhibit mechanical dyssynchrony, might still benefit from the device implantation[22,23]. These findings initiated an intensive search to reliably assess and quantify this parameter.

Echocardiography has emerged as the first modality suitable for mechanical dyssynchrony assessment. The association between quantitative echocardiography-derived M-mode and tissue Doppler parameters of dyssynchrony and favorable CRT response was shown in multiple small single-center studies [24–26]. However, the results of the multicenter PROSPECT (predictors of response to CRT) trial, testing the performance of all quantitative echocardiographic parameters of dyssynchrony, demonstrated that none of these could reliably predict clinical and echocardiographic response to CRT, mainly due to their low reproducibility[27]. Furthermore, the EchoCRT trial has even shown a deleterious effect of CRT in patients with mechanical dyssynchrony on echocardiography and narrow QRS complex[28]. The results mentioned above challenged the routine implementation of quantitative echocardiography indices for dyssynchrony assessment and prompted to search for other approaches to evaluate mechanical dyssynchrony.

In contrast to quantitative M-mode and tissue Doppler parameters, septal flash (SF) and apical rocking (AR) are qualitative dyssynchrony indices that represent specific deformation patterns of the LV, amendable by CRT. SF and AR are relatively novel, simple markers of mechanical dyssynchrony that can be visually assessed by echocardiography[29]. SF is an active inward motion of the septum predominantly during the isovolumetric contraction phase,

immediately followed by a fast outward motion (Figure 4). The shortening of the septum, contracting first and against the low LV pressure and relaxed LV wall, pulls the apex to the septal side. Afterwards, the contraction of the late activated lateral wall pulls the apex towards the lateral wall. This right-left apical motion pattern is known as AR. Both parameters, SF and AR, represent the direct mechanical consequences of a dyssynchronous activation of the LV myocardium with an early contraction of the septum and a delayed contraction of the lateral wall.

SF and AR have emerged as promising surrogate markers for mechanical dyssynchrony and have been shown to reliably predict CRT response as well as long-term survival [30]. The simplicity of their assessment and interpretation, that do not require any special software, in combination with good reproducibility have made them as one of the most attractive markers of mechanical dyssynchrony.

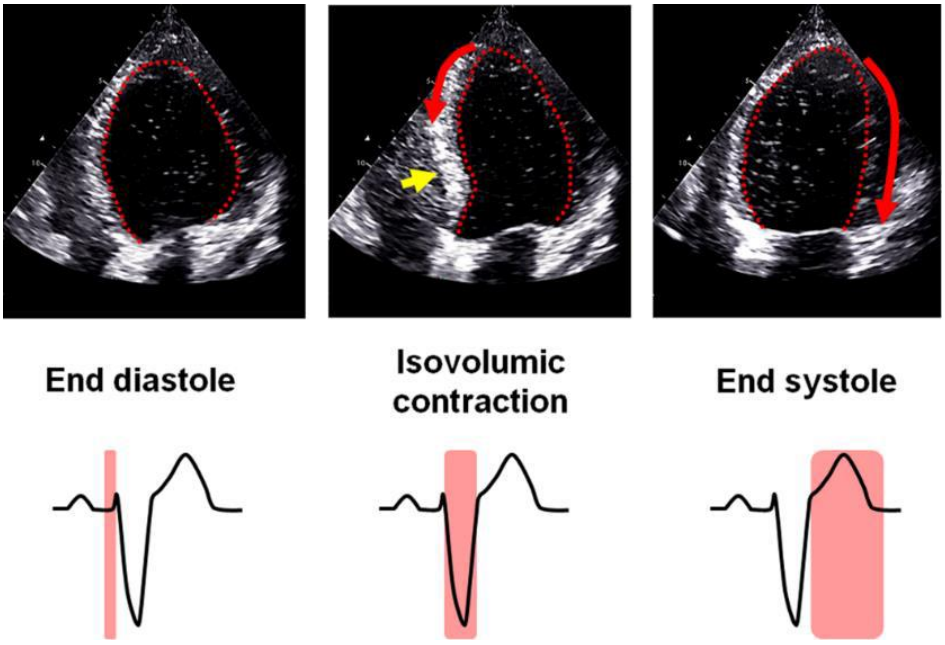

Figure 4. Typical pattern of mechanical dyssynchrony assessed visually with echocardiography*. Upper panel: An early fast septal contraction marked with the yellow arrow corresponds to septal flash. Red arrows identify apical rocking, represented by the initial movement of the apex towards the early contracting septum followed by an opposite movement towards the later activated lateral wall. Lower panel: representative ECG with orange rectangles indicating the onset and duration of septal flash and apical rocking, described in the upper panel. Reproduced with permission from* [31].

Nuclear cardiology has become another alternative that evoked a lot of interest for the assessment of mechanical dyssynchrony. Several parameters derived from SPECT and to a

lesser extent from PET phase analysis, that is based on the assessment of the onset of regional LV contraction, have shown some potential to improve patients selection for CRT implantation [32]. Among the main advantages of the approach is the possibility to retrospectively derive necessary indices from previously performed nuclear scans, omitting extra radiation burden for the patient. Another advantage is an automated calculation of mechanical dyssynchrony extent with high reproducibility and repeatability [33]. The challenge of this modality though is the lack of randomized trials and standardized cut-off values for phase analysis indices, what makes the wide implementation of the approach rather difficult. The recently proposed alternative is based on the identification of either an U or non-U shaped LV contraction pattern on polar maps derived from phase analysis, however more investigations should be performed to assess their prognostic value before clinical implementation[34].

Assessment of mechanical dyssynchrony with different cardiac magnetic resonance (CMR) techniques, among which myocardial tagging with assessment of cardiac motion and deformation has emerged as the most popular, has shown an important predictive value for clinical improvement and reverse remodeling after CRT in several small studies [35,36]. However, the low temporal resolution of cine images (usually 30 phases per cardiac cycle), lack of clinical experience in dyssynchrony assessment with CMR, low availability of CMR scanners and their incompatibility with pacemakers that are often present in CRT candidates, have so far precluded its widespread clinical application.

Despite the promising results, mechanical dyssynchrony has not yet been included in the clinical CRT guidelines, leaving the current decision for device implantation mainly based on the presence of electrical dyssynchrony. The reason is the lack of a clear definition of mechanical dyssynchrony, a continuing debate on the best way it should be measured, the distrust in visual and thus subjective techniques (even with clear underlying mechanisms) as well as lack of understanding of this phenomenon. Deeper insights into pathophysiological processes induced by or related to mechanical dyssynchrony, including changes in perfusion and metabolism, might help to better understand the influence of mechanical dyssynchrony on adverse and reverse cardiac remodeling of CRT patients and eventually facilitate the wide recognition of mechanical dyssynchrony and change guidelines.

1.5 Investigation of the pathophysiology of LV dyssynchrony with PET

PET has emerged as a reliable modality for the visualization of cellular and molecular processes in the heart. With the use of radioactive tracers, PET allows accurate assessment of myocardial

perfusion, metabolism, innervation, inflammation and other biological processes, involved in disease development and progression. This technique currently represents an important tool for investigating the underlying pathophysiology of a variety of cardiovascular diseases. Deeper insight in alterations of perfusion and metabolism in the failing dyssynchronous heart may help to enhance the understanding of the fundamental molecular processes involved in LV remodelling and may improve patient selection for CRT.

1.5.1 PET for the assessment of cardiac metabolism

PET has gained a lot of recognition for the evaluation of cardiac glucose metabolism. Using the radiolabelled glucose analogue ^{18}F-fluorodeoxyglucose (^{18}F-FDG), that undergoes cellular transport similar to glucose, but is trapped in the cells in the form of ^{18}F-FDG-6-phosphate, PET imaging can reliably assess regional glucose uptake and thus provide information on regional energy consumption in the heart (Figure 5).

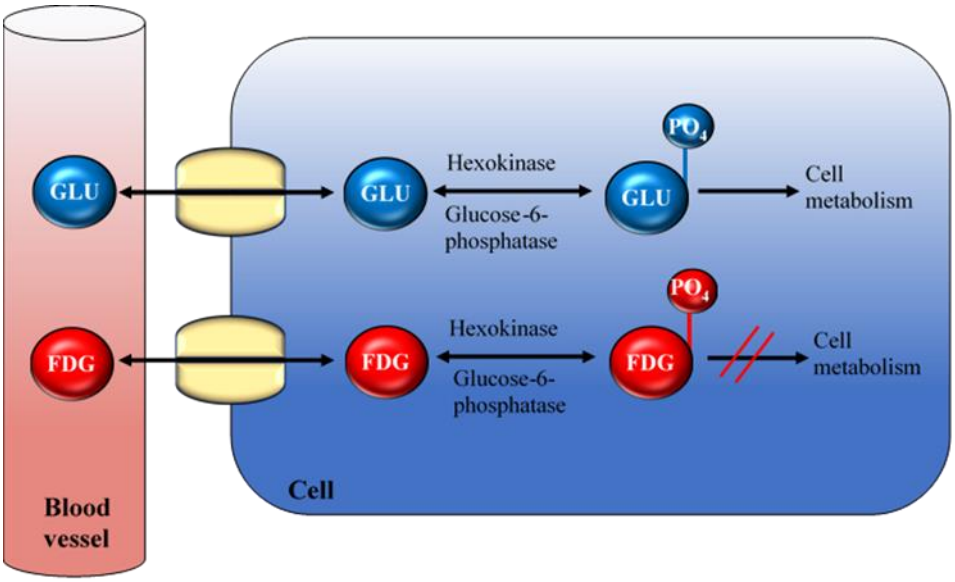

Figure 5. Schematic comparison of glucose and ^{18}F-FDG cellular uptake and metabolism. *Both glucose and ^{18}F-FDG are transported into the cell by membrane glucose transporters. After phosphorylation by hexokinase, phosphorylated glucose participates in the subsequent cell metabolism (glycolytic pathway), while phosphorylated ^{18}F-FDG is not further metabolized and is trapped in the cell.*

Previous preclinical and clinical cardiac PET studies in subjects with ventricular conduction abnormalities have consistently demonstrated a reduced septal and increased lateral wall

glucose metabolism[37–39]. These findings correspond to the regional systolic deformation pattern, with a poorly contracting septum and strongly contracting lateral wall, as assessed with CMR, and to the regional redistribution of myocardial work, with a reduced loading of the early activated septal wall versus an increased loading of the late activated lateral wall, as assessed with echocardiographic strain techniques[37,40]. One of the major limitations of cardiac ^{18}F-FDG PET imaging is the variable physiologic myocardial glucose consumption, requiring optimal patient preparation in order not to compromise image quality and diagnostic performance of the modality. Indeed, fatty acid oxidation represents the main source of energy in the normal heart under basal conditions, while physiological glucose uptake is usually limited, but very variable[41]. The avid consumption of glucose can be provoked by some pathological conditions, such as ischemia/hibernating myocardium or inflammation [41–43]. Therefore, indication-specific and standardized patient preparations protocols are absolutely needed to evaluate glucose uptake in a reliable way. For example, in order to assess the presence of hibernating myocardium, patients should be prepared with an oral glucose load or euglycemic hyperinsulinemic clamping method to facilitate glucose consumption. In contrast, to assess inflammatory/infectious lesions such as endocarditis or sarcoidosis, patient should be prepared with a high-fat, low carbohydrate diet in combination with prolonged fasting to completely suppress physiological ^{18}F-FDG uptake [44].

1.5.2 PET for the assessment of cardiac perfusion

In addition to metabolism, PET has also emerged as a validated and highly reproducible tool for the assessment of myocardial perfusion. Due to its unique possibility to quantify myocardial blood flow (MBF) in absolute units (ml/g/min), PET represents a "gold standard" for perfusion assessment. Moreover, in general PET is more sensitive and has higher spatial resolution (PET 4-7mm, SPECT 12-15 mm) compared to conventional gamma cameras, resulting in a higher diagnostic performance for evaluating CAD[45,46]. The currently available and routinely used perfusion PET tracers include ^{15}O-H_2O, ^{13}N-NH_3, and ^{82}Rb, while usage of ^{18}F-fluripidaz is currently limited to the clinical trials. These tracers are different in terms of half-life, extraction, kinetics and production which make one preferable above another depending on the clinical situation and research center expertise (Table 2). ^{82}Rb is a potassium analog that is actively transported into the cell through the Na/K ATP transporter, while ^{13}N-NH_3 enters the cells through the combination of both active transport and passive diffusion [47,48]. After extraction and upon entering the cellular compartment, both tracers are metabolically trapped enabling to obtain 'late' static images of tracer uptake in addition to absolute perfusion quantification

(Figure 6). These static images have a high myocardial-to-blood pool ratio enabling relative/semiquantitative assessment of perfusion distribution, expressed as standardized uptake value (SUV) or percentages relative to area with maximal tracer uptake. When combined with ECG gating, myocardial function, volumes and wall motion can also be assessed[49] (Figure 6). In contrast to ^{82}Rb and ^{13}N-NH_3, ^{15}O-H_2O is a freely diffusible agent with 100% extraction and represents the ideal tracer for myocardial perfusion quantification. However, ^{15}O-H_2O is metabolically inert and is not retained in the myocardium, resulting in the inability to obtain good quality static images.

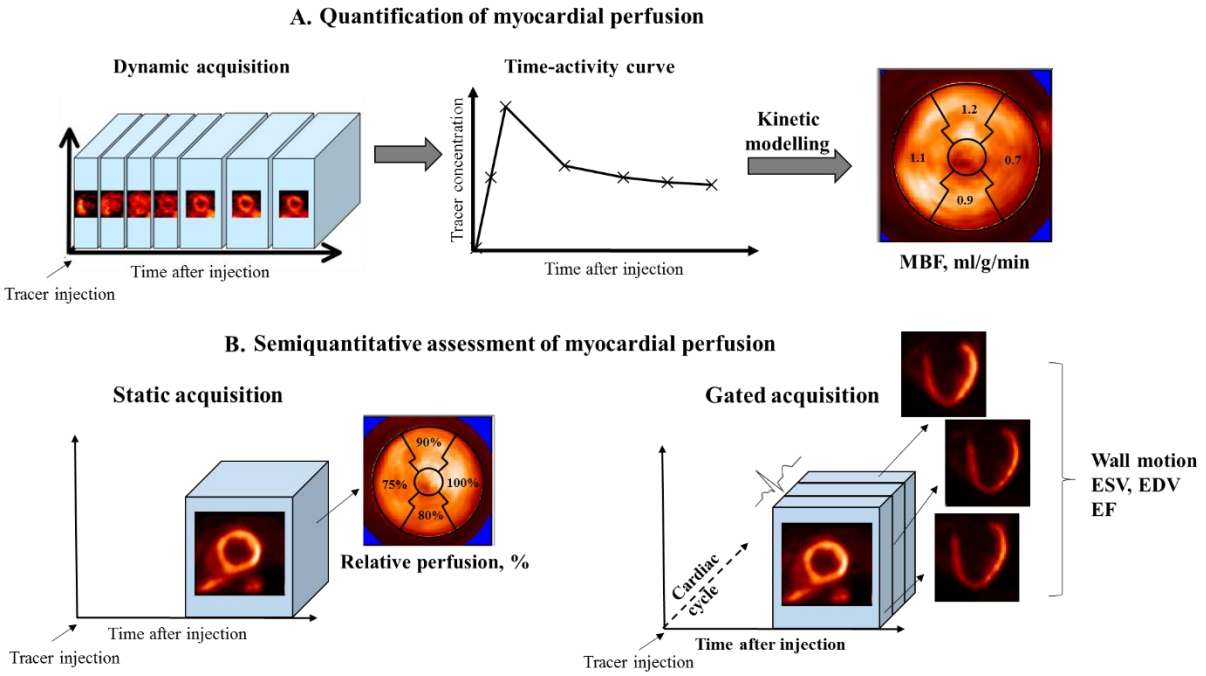

Figure 6. Schematic difference between quantitative (A) and semiquantitative (B) assessment of myocardial perfusion. *Quantification of myocardial perfusion requires the start of a dynamic PET acquisition simultaneously with tracer injection (A). Dynamic acquisition enables generation of time-activity curves, which can be converted to absolute myocardial blood flow (MBF) values using tracer-specific kinetic models. Semiquantitative assessment of perfusion requires a static PET reconstruction at predefined intervals after tracer administration (B). At this time near absence of tracer in the blood pool and high concentration in the myocardium provides a good quality PET image, that can be used to assess myocardial tracer distribution in standardized uptake values or as percentage (B, left panel). When static acquisition is combined with ECG-gating, assessment of myocardial ejection fraction (EF), end-diastolic volume (EDV), end-systolic volume (ESV) and regional wall motion abnormalities can be performed (B, right panel). Adapted from* [50].

Nevertheless currently ^{15}O-H_2O is considered the gold standard for absolute perfusion quantification. ^{18}F-Flurpiridaz is a novel PET perfusion tracer that has promising biological and imaging characteristics. Among them are the short positron range, that provides superior image quality, high fist pass myocardial extraction, favorable for reliable perfusion quantification and relatively long half-life, that does not require the proximity of cyclotron and makes the tracer effective for both exercise and pharmacological stress testing[51–53]. Already performed preclinical and clinical trials with 18F-Flurpiridaz have demonstrated promising results and the tracer is awaiting further validations and clinical approval[54,55]. ^{11}C-acetate has also demonstrated a potential for the quantification of myocardial perfusion, mainly due to its high initial myocardial extraction fraction[56]. However, the inability to use late static images as a surrogate for the relative regional perfusion and the necessity of kinetic modelling, hampered its wide implementation in routine clinical practice.

Table 2. Characteristics of cardiac PET perfusion tracers

	^{15}O-water	^{13}N-ammonia	^{82}Rb	^{18}F-flurpiridaz
Half-life (minutes)	2.06	9.96	1.25	109.8
Positron range in water (mean, mm)[53]	2.96	1.73	7.49	0.66
Production	Onsite cyclotron	Onsite cyclotron	Generator	Offsite/onsite cyclotron
Myocardial extraction fraction	100%	80%	65%	94%
Data acquisition	Dynamic	Dynamic, static	Dynamic, static	Dynamic, static

In the past decade, a lot of experimental and clinical studies have focused on the influence of ventricular dyssynchrony on regional myocardial perfusion, however, in contrast to the well-established changes in glucose uptake, conflicting results on perfusion have been reported. While experimental data with microspheres have shown a hypoperfusion in the septal wall compared to the lateral wall, PET and SPECT clinical studies predominantly reported a rather homogeneous perfusion across the LV, with few studies showing septal hypoperfusion[38,39,57]. The reasons for the different perfusion results among the studies might be attributed amongst others to different imaging modalities, radiopharmaceuticals and study protocols, while differences in perfusion results obtained with the same tracer, remain to be elucidated.

1.5.3 PET for the assessment of cardiac perfusion-metabolism relation

Assessment of myocardial viability with PET by combining perfusion and metabolism has gained a lot of recognition in the management of patients with CAD with LV systolic dysfunction [58,59]. In particular, differentiating viable but dysfunctional myocardium from myocardial scar plays an important role in therapy decision making. It has been shown that the presence of significant amount of viable myocardium is associated with improved patient outcome after revascularization, while medical treatment of these patients results in worse prognosis[58,60]. Widely used combination of ^{13}N-NH_3/^{18}F-FDG PET, that represents respectively myocardial perfusion and metabolism, has been a well-validated and sensitive method for the assessment of myocardial viability. It allows to reliably delineate myocardial segments with perfusion-metabolism match and mismatch, corresponding to normal tissue/myocardial scar and hibernation respectively.

Identification of perfusion-metabolism patterns with PET has been challenging in patients with LV dyssynchrony. It has been demonstrated that "mismatch"/"reverse mismatch" patterns can be present in CRT eligible patients irrespective of the presence of ischemia or hibernation, which questions the reliability of the method in ischemic dyssynchronous hearts. Interestingly, some studies have demonstrated that the presence of reverse mismatch patterns in non-ischemic HF CRT candidates might have a value in the prediction of CRT response[61,62].

A more detailed investigation of regional glucose metabolism, perfusion and their relation in a failing dyssynchronous heart might provide a better insight in the pathophysiological mechanisms of LV remodelling.

1.6 Nuclear imaging might have a value in guiding HF therapy

It has been demonstrated that patients eligible for CRT present with a typical pattern of low septal and high lateral wall glucose metabolism, as assessed with ^{18}F-FDG-PET [37,40]. Interestingly, immediately after CRT implantation homogenization of glucose uptake in the heart was observed, suggesting that evaluating regional ^{18}F-FDG metabolism may be a promising option to select patients for CRT[37]. So far, data on the prediction of CRT response using nuclear imaging are scarce, with a couple of published studies, reporting an association between the extent of perfusion-metabolism reverse mismatch areas in the septum and

favourable reverse remodelling after CRT [61,62]. However, the septal-to-lateral ^{8}F-FDG uptake ratio, that might provide a measure of regional differences in energetic requirements within the heart, has not been explored yet as a possible CRT response predictor.

It has been shown that patients with non-ischemic etiology of HF are more prone to favourable CRT response, while the presence of scar tissue decreases the chances of reverse remodelling [27,63]. It does not come as a surprise that CRT requires not only the presence of correctable dyssynchrony, but also enough viable myocardium to restore LV function. CMR is the gold standard technique for the assessment of myocardial structure and function and due to its high spatial resolution, it allows a reliable differentiation between viable and non-viable myocardium, providing qualitative and/or quantitative information on scar extent and localization. Scar is characterized by the absence of metabolic activity and when present in the septum or lateral wall, can significantly influence ^{8}F-FDG SLR. Therefore, it would be interesting to explore, if combination of regional LV glucose metabolism and myocardial scar could be used for the prediction of CRT response.

2. Management of patients with CAD: role of SPECT

2.1 Non-invasive imaging in the diagnostics of CAD

The contemporary toolbox of diagnostic modalities used to identify CAD includes electrocardiography (ECG), echocardiography, CMR, computed tomography (CT), SPECT and PET (Table 3)[64]. These modalities allow to detect functional and structural evidence of coronary stenosis, but the diagnostic accuracy of each modality is highly dependent on the disease stage, which is linked to the pathophysiologic ischemic cascade [65]. For instance, signs of ischemia on exercise ECG mainly occur in the latest stages of CAD and the method therefore has low sensitivity (46-69%). The specificity of stress ECG is also low and varies between 54 and 69%[66]. Higher sensitivity and specificity have been reported for stress echocardiography (80-89% and 72-89%, respectively) and stress CMR (83-94% and 69-88%, respectively) for the detection of inducible wall motion abnormalities, that also occur at the more advanced stages of the disease [66]. In contrast, coronary CT allows revealing pathological anatomical lesions at the early phase of CAD, but fails to provide sufficient information about the hemodynamic significance of these lesions. The method has high sensitivity (93-99%), but moderate-to-low specificity (67-86% for anatomically and 37-68% for functionally significant stenosis) [66]. Meanwhile, radionuclide myocardial perfusion imaging with SPECT and PET has shown high sensitivity (78-96%) and specificity (63-91%) in detecting myocardial perfusion abnormalities which is one of the earliest hallmarks of CAD [66]. While continuous research efforts to improve hardware and software of echocardiography, CMR and CT for assessing myocardial perfusion have increased their performance, radionuclide myocardial perfusion imaging has been widely implemented in the work-up of patients with suspected or known CAD for several decades. It has been routinely used in clinical practice and has demonstrated its value in assessing myocardial ischemia, treatment choice and prognosis [67,68].

Table 3. The main advantages and disadvantages of different non-invasive imaging modalities to detect coronary artery disease

	Stress echocardiography	SPECT	PET	Stress CMR	Coronary CT
Time to perform test	++	+++	+++	++	+
Spatial resolution	++	+	++	+++	+++
Temporal resolution	+++	+	+	++	++
Cardiac function	++	+	+	+++	++
Cardiac anatomy	++	+/-	+/-	+++	+
Coronary vessel anatomy	-	-	-	++	+++
Functional information on stenosis severity	++	++	+++	++	-
Wall motion abnormalities	++	+	+	+++	+
Stress test	Exercise or pharmacological	Exercise or pharmacological	Pharmacological	Pharmacological	Pharmacological
Costs	+	++	+++	+++	++
Contrast	+	-	-	+	+
Radiation	-	+++	++	-	+
Operator dependance	+++	++	+	+	+
Availability	+++	+++	+	+	++
Contra-indications	No	Pregnancy	Pregnancy	Claustrophobia, renal insufficiency, metallic implants	Pregnancy, Renal insufficiency
Limitations	Poor image quality in obese, lung disease	Tissue attenuation and motion artifacts	Motion artifacts	Heart rate/rhythm control and breath-hold instructions	Heart rate control and breath-hold instructions; Heavy calcification limits reliable assessment of lumen stenosis

2.2 Role of PET and SPECT in the assessment of myocardial perfusion

2.2.1 Current status

Despite being an established technique that is widely implemented in clinical practice, SPECT is limited by only visual/relative assessment of myocardial perfusion by normalizing myocardial tracer uptake in a particular region to the myocardial region with maximal tracer uptake. This approach may underestimate the extent of atherosclerotic burden, especially in patients with multi-vessel or main stem disease. In those patients, either balanced ischemia can be present or only the vascular territory with the most severe hemodynamic impact can be identified, hence resulting in a lower sensitivity for those subgroups [69,70]. In contrast to SPECT, PET imaging allows to perform dynamic acquisition and absolute quantification of myocardial perfusion in ml/g/min, thus overcoming the shortcomings of SPECT [71,72] (Figure 7).

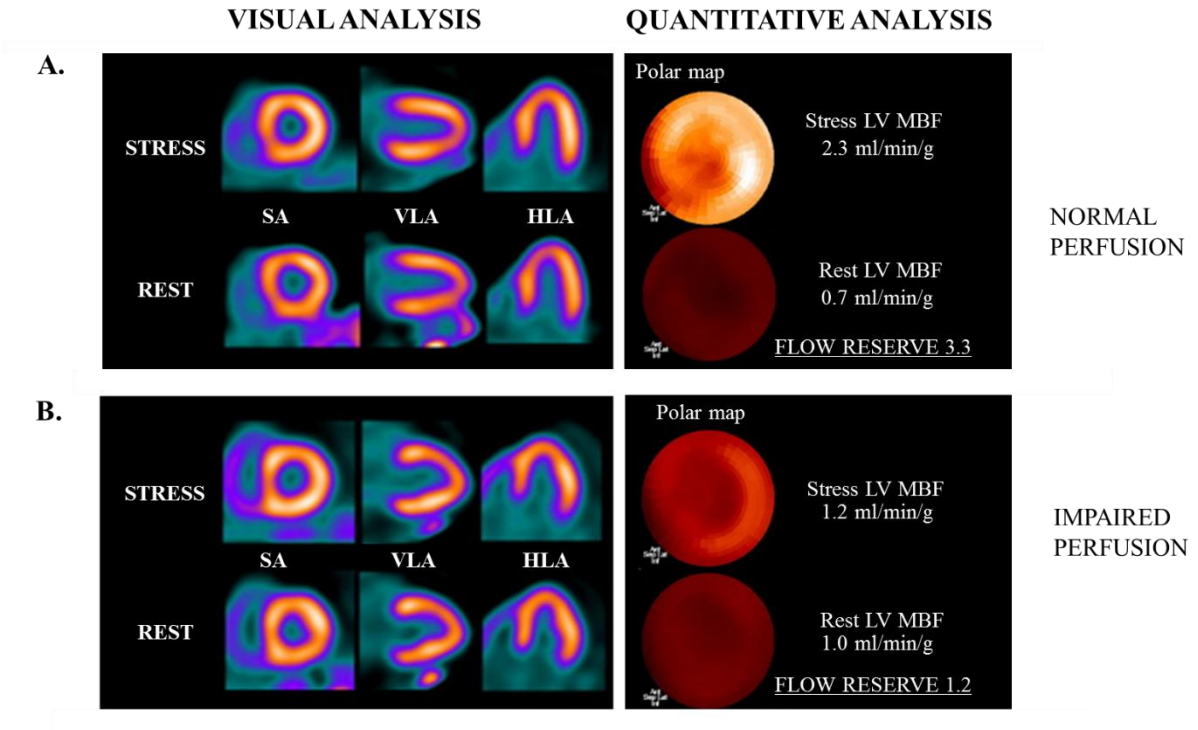

Figure 7. Importance of flow quantification. *Representative example of rest/dipyridamole stress ^{82}Rb PET scan in two subjects showing visually normal myocardial perfusion on static tomographic reconstructions, normalized to the maximum activity within each heart, in both patients (left panel A,B). However, quantification of myocardial perfusion, derived from dynamic images, shows normal absolute perfusion at stress and rest in patient A and significantly reduced stress MBF and MFR in patient B, who has angiographically proven triple-vessel disease (balanced ischemia) (right panel A, B). Adapted from* [50].

Quantification of myocardial perfusion requires the application of a mathematical modelling to time-activity curves, to produce quantitative information on myocardial perfusion, represented by myocardial blood flow (MBF, ml/g/min) (Figure 6) [46,73]. MBF can be assessed during rest and at pharmacological stress, to reveal ischemia by inducing flow heterogeneity [74]. The ratio between rest and stress MBF is called myocardial flow reserve (MFR). MBF and MFR provide an overall measure of coronary vasomotor (dys)function integrating the hemodynamic consequences of focal lesions, diffuse lesions, small vessel disease and microvascular dysfunction on tissue perfusion. Furthermore, these parameters have shown to improve risk stratification in CAD patients compared to the information provided by relative assessment of perfusion defects alone[46]. In addition, MFR has shown the ability to assess the severity of coronary lesions, similar to invasive fractional flow reserve hence eliminating the need for diagnostic catheterizations[75,76]. Despite obvious advantages of PET perfusion imaging, its wide implementation is currently hampered by a relatively high cost, limited availability and requirement of an on-site cyclotron due to the short half-life of tracers or on-site generator. As a result, the majority of cardiac scintigraphies for evaluating CAD (especially in Europe) is still performed on conventional Anger cameras which do not allow dynamic imaging, thus prohibiting to obtain quantitative perfusion information.

2.2.2 Latest technological advances

The recent introduction of novel cardiac-dedicated high sensitivity SPECT systems revolutionized the field of nuclear cardiology. Both, Discovery NM 530c (GE Healthcare, Haifa, Israel) and D-SPECT (Spectrum-Dynamics, Cesarea, Israel), are composed of ultra-fast, solid state cadmium zinc telluride (CZT) pixilated detectors, that in contrast to conventional NaI detectors allow a direct conversion of the collected photons into an electrical signal, leading to higher sensitivity [77] (Figure 8). The optimized collimator design (pinholes for Discovery and parallel-hole for D-SPECT) in combination with the unique gantry design consisting of a ‘C’ shape allows for the first time high-sensitive dynamic acquisition, similar to PET technology. In addition to dynamic imaging, acquisition time and administered activity can be significantly reduced. Several recent experimental and clinical studies have demonstrated the possibility to obtain quantitative information on perfusion and flow reserve[76,78]. However, it is worthwhile to mention that the tracers used in those studies (^{99m}Tc-Sestamibi, ^{99m}Tc-Tetrofosmin, and ^{201}Tl) are routinely used radiotracers in clinical practice, which all have limitations in terms of absolute perfusion quantification[78].

Figure 8. Gantry design of the novel cardiac dedicated SPECT cameras.

2.3 Radiotracers for perfusion assessment

The ideal perfusion agent is characterized by a perfect linear relationship between regional blood flow and myocardial tracer uptake at any flow rate, currently represented by ^{15}O-water (Figure 9). Every significant deviation from this linearity (Figure 9) may impact the diagnostic performance of myocardial perfusion imaging, hereby limiting its value for the reliable assessment of presence, extent and severity of perfusion defects, guidance and monitoring of the treatment as well as prognostic assessment in CAD patients. The commercially available SPECT perfusion tracers such as ^{99m}Tc-Sestamibi and ^{99m}Tc-Tetrofosmin preserve this linear relationship at low flow rates, but develop a plateau at higher regional flow known as the 'roll-off phenomenon' [79,80].

The latter can lead to an underestimation of the apparent flow increase during stress tests. On the other hand, ^{201}Tl has a higher and more favourable linear extraction fraction, but has worse image quality due to low photon energy and has higher radiation burden for the patient [79,80]. The introduction of novel CZT SPECT cameras with the possibility of perfusion quantification opens the door to look for a better SPECT perfusion agent with improved extraction properties. The previously developed neutral agent ^{99m}Tc-Teboroxime with high extraction fraction, linear myocardial uptake at relatively high flow rates and fast myocardial kinetics might be of particular interest [81–83]. Its rapid wash-out rate impeded its wide implementation with conventional SPECT cameras due to a slow rotating gantry and the tracer was out of the market. However, with the introduction of novel cardiac-dedicated cameras allowing dynamic acquisitions, ^{99m}Tc-Teboroxime might be of interest again.

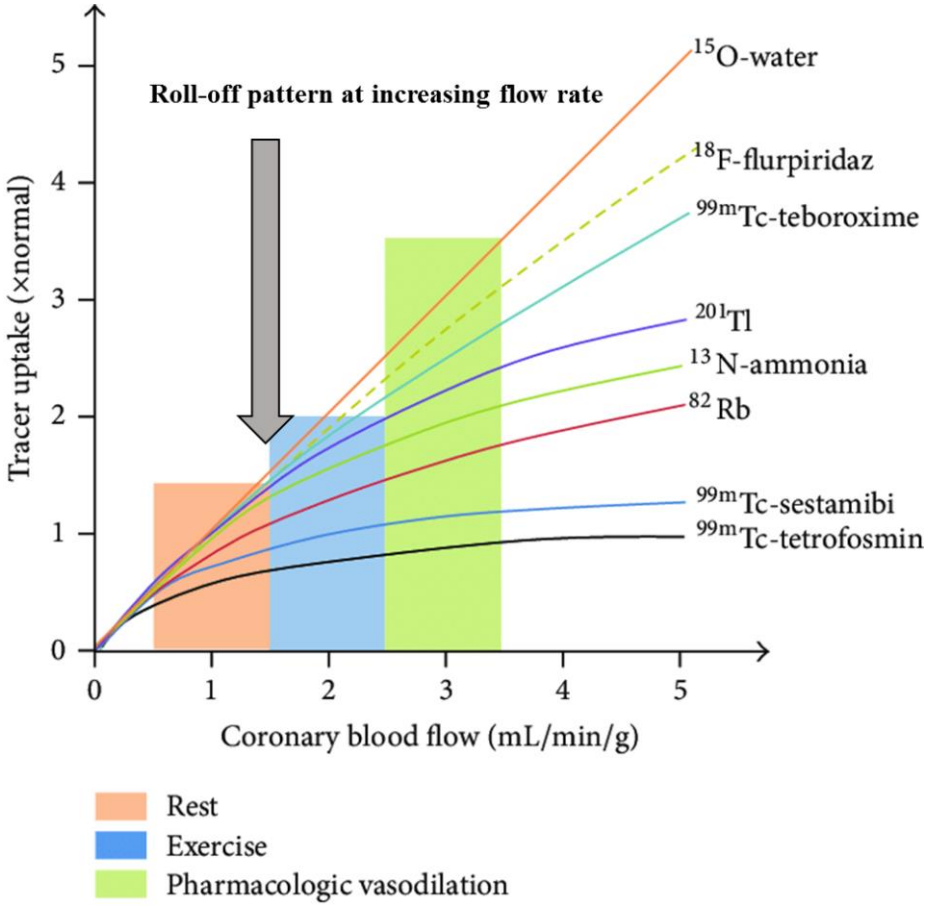

Figure 9. Relationship between myocardial blood flow and myocardial tracer uptake, represented for SPECT and PET perfusion tracers. *Note a roll-off phenomenon with the increase of flow rates observed for most of the tracers. Reproduced with permission from* [84].

PART II

PROJECT AIMS AND RESEARCH QUESTIONS

PROJECT AIMS AND RESEARCH QUESTIONS

Our **central research hypothesis** presumed that visualization of molecular processes in the myocardium using nuclear imaging techniques, will provide more insights into disease pathophysiology and further improve management of patients with CAD and HF.

The ***first general aim*** of this PhD project was to investigate how the assessment of myocardial perfusion and metabolism with ^{13}N-NH3 and ^{18}F-FDG PET, respectively, can provide insights into the pathophysiology of prominent markers of successful CRT response (LBBB, mechanical dyssynchrony) and influence the decision making for CRT implantation. Therefore, a prospective multicenter clinical study was initiated and registered as "WORK-CRT" at ClinicalTrials.gov (NCT02537782) with two out of 5 research centers (Oslo University Hospital and University Hospitals Leuven) mainly focusing on the imaging part of the study.

The following research questions were formulated:

1. **What is the influence of LBBB on regional myocardial perfusion and metabolism? (CHAPTER I)**

   We evaluated regional myocardial perfusion and metabolism with ^{13}N-NH_3 and ^{18}F-FDG PET, respectively, in a homogenous group of non-ischemic HF patients with LBBB, who were referred for CRT implantation. In this patient cohort, LBBB was defined according to the Strauss criteria, as they were shown to more likely represent a complete block of LV conduction pathway and be associated with favourable CRT response.

2. **Can the different approaches of perfusion assessment with ^{13}N-NH_3 PET influence the perfusion results in patients with LBBB? (CHAPTER I)**

   In order to understand if conflicting perfusion results in LBBB patients, reported in the literature, can be at least partially explained by different approaches of perfusion assessment, we evaluated ^{13}N-NH_3 perfusion in two ways – quantitatively, using different kinetic models (either one or two tissue compartments), and semi-quantitatively, based on tracer concentration in the myocardium on "late" static images.

3. **Is a reliable assessment of viability with PET possible in LBBB patients? (CHAPTER I)**

Using a standard PET technique to assess myocardial viability, we investigated the presence of different perfusion-metabolism patterns in non-ischemic HF patients with LBBB. This will help us to understand whether viability assessment can be reliably applied in ischemic HF patients with LBBB.

4. **What is the influence of mechanical dyssynchrony on cardiac perfusion and metabolism? (CHAPTER II)**

We evaluated absolute perfusion and metabolism in septal and lateral walls, assessed with ^{13}N-NH_3 and ^{18}F-FDG PET, respectively, in non-ischemic HF patients with and without mechanical dyssynchrony, who were undergoing CRT implantation. Mechanical dyssynchrony was defined visually based on the presence of SF or AR on echocardiography. Regional differences in myocardial perfusion and metabolism, represented as perfusion and metabolism SLR, were also correlated with regional distribution of myocardial work.

5. **Is there any association between regional perfusion and metabolism, assessed with PET before CRT implantation, and the extent of volumetric reverse remodelling after CRT implantation? (CHAPTER II)**

In the same cohort of non-ischemic HF patients, we correlated perfusion and metabolism SLR before CRT implantation with the extent of volumetric reverse remodelling 12 months after CRT implantation. PET parameter(s) that correlated best with volumetric reverse remodelling will be tested as independent predictor(s) of CRT response (ΔESV$\geq$15%) in a larger and more diverse cohort of patients in the next chapter.

6. **Can ^{18}F-FDG PET reliably guide therapy of HF patients? (CHAPTER III)**

In ischemic and non-ischemic HF CRT candidates we explored whether ^{18}F-FDG SLR alone or in combination with myocardial scar could be used to predict response to CRT.

The ***second general aim*** of this PhD project was to explore whether it is feasible to image and quantify myocardial perfusion/flow reserve with a novel cardiac-dedicated SPECT camera using ^{99m}Tc-Teboroxime in a porcine model.

The research questions to be answered were the following:

7. Are the characteristics of ^{99m}Tc-Teboroxime suitable for perfusion assessment? (CHAPTER IV)

In a number of rats we evaluated biodistribution, initial myocardial uptake, retention, and clearance of ^{99m}Tc-Teboroxime in order to understand if the properties and kinetics of the tracer are favourable for perfusion assessment.

8. Is it feasible to image and quantify myocardial perfusion with ^{99m}Tc-Teboroxime using a dedicated cardiac camera in a pig model? (CHAPTER IV)

We investigated the possibility to image and quantify MBF and MFR in a number of healthy and infarcted pigs that underwent a two day rest - adenosine stress SPECT scans with a dedicated cardiac CZT camera using ^{99m}Tc-Teboroxime. In healthy animals SPECT derived MBF values were correlated with coloured microspheres, which served as gold standard.

PART III

PERFORMED STUDIES

CHAPTER I

Impact of left bundle branch block on myocardial perfusion and metabolism: a positron emission tomography study

Published in: J Nucl Cardiol. 2019; [Epub ahead of print]

DOI: 10.1007/s12350-019-01900-y.

Ganna Degtiarova, MD[1,2], Piet Claus, PhD[3], Jürgen Duchenne, PhD[3,4], Georg Schramm, PhD[1], Johan Nuyts, PhD[1], Hein J. Verberne MD,PhD[5], Jens-Uwe Voigt, MD, PhD[3,4], Olivier Gheysens MD, PhD[1,2]

1. Department of Imaging and Pathology, KU Leuven, Leuven, Belgium
2. Nuclear Medicine and Molecular Imaging, University Hospitals Leuven, Belgium
3. Department of Cardiovascular Sciences, KU Leuven, Leuven, Belgium
4. Department of Cardiovascular Diseases, University Hospitals Leuven, Leuven, Belgium
5. Department of Radiology and Nuclear Medicine, Amsterdam UMC, location AMC, University of Amsterdam, The Netherlands

This chapter addresses the following research questions:

- What is the influence of LBBB on regional myocardial perfusion and metabolism
- Can the different approaches of perfusion assessment with ^{13}N-NH_3 PET influence the perfusion results in patients with LBBB?
- Is reliable assessment of viability with PET possible in LBBB patients?

ABSTRACT

Background: Better understanding of pathophysiological changes, induced by left bundle branch block (LBBB), may improve patient selection for cardiac resynchronization therapy (CRT). Therefore, we assessed the effect of LBBB on regional glucose metabolism, ^{13}N-NH_3-derived absolute and semiquantitative myocardial blood flow (MBF), and their relation in non-ischemic CRT-candidates.

Methods: Twenty-five consecutive non-ischemic patients with LBBB underwent ^{18}F-FDG and resting dynamic ^{13}N-NH_3 PET/CT prior to CRT implantation. Regional ^{18}F-FDG uptake, absolute MBF and late ^{13}N-NH_3 uptake were analyzed and corresponding septal-to-lateral wall ratios (SLR) were calculated. Segmental analysis was performed to evaluate "reverse mismatch", "mismatch" and "match" patterns, based on late ^{13}N-NH_3/^{18}F-FDG uptake ratios.

Results: A significantly lower ^{18}F-FDG uptake was observed in the septum compared to the lateral wall (SLR 0.53±0.17). A similar pattern was observed for MBF (SLR 0.68±0.18), whereas late ^{13}N-NH_3 uptake showed a homogeneous distribution (SLR 0.96±0.13). ^{13}N-NH_3/^{18}F-FDG "mismatch" and "reverse mismatch" segments were predominantly present in the lateral (52%) and septal wall (61%), respectively.

Conclusions: Non-ischemic CRT-candidates with LBBB demonstrate lower glucose uptake and absolute MBF in the septum compared to the lateral wall. However, late static ^{13}N-NH_3 uptake showed a homogenous distribution, reflecting a composite measure of altered regional MBF and metabolism, induced by LBBB.

INTRODUCTION

Left bundle branch block (LBBB) is characterized by inhomogeneous activation of the ventricular myocardium resulting in inefficient contraction of the left chamber. Being a risk factor for the development and progression of adverse remodelling and heart failure, LBBB is associated with an increased risk of all-cause mortality[85]. Even though cardiac resynchronization therapy (CRT) is a promising therapy for heart failure patients with LBBB, a significant number of patients do not respond to this therapy, and establishing optimal selection criteria for CRT candidates is still an area of active investigation. Deeper insights into the pathophysiological changes induced by or related to LBBB is needed in order to assess the complex mechanism of disease progression, including causes of adverse remodelling, changes in perfusion, metabolism and their relation with regard to CRT response or failure.

^{18}F-fluorodeoxyglucose (^{18}F-FDG) positron emission tomography (PET) studies, both quantitative and semiquantitative, in patients with LBBB have shown regional changes in glucose metabolism with a relatively low glucose uptake in the septum and high in the lateral wall[39,40]. These findings correlated with regional differences in myocardial mechanics and structure, as evaluated by cardiac magnetic resonance imaging (CMR) and correspond to the regional redistribution of myocardial work, as assessed with echocardiographic strain techniques[37,40].

In contrast to the well-established changes in glucose uptake, data on myocardial perfusion in LBBB patients remain controversial. Experimental data have consistently shown a relative hypoperfusion in the septal wall compared to the lateral wall, while clinical nuclear studies predominantly reported a rather homogeneous tracer uptake across the left ventricle (LV) with few studies showing septal hypoperfusion[39,57].

Identification of different perfusion-metabolism patterns with PET, widely implemented in clinical practice for the assessment of myocardial viability, has been challenging in LBBB patients. It has been demonstrated that “mismatch”/”reverse mismatch” patterns can be present in LBBB/CRT eligible patients irrespective of the presence of myocardial hibernation and might have a value in the prediction of CRT response[61].

Therefore, we investigated the effect of LBBB on regional absolute ^{13}N-NH_3 myocardial perfusion, semiquantitative late ^{13}N-NH_3 uptake and ^{18}F-FDG uptake as well as their relation in a homogenous group of patients with non-ischemic dilated cardiomyopathy eligible for CRT.

MATERIAL AND METHODS

Study Population

Patients with non-ischemic heart failure and LBBB (according to the Strauss criteria), referred for CRT implantation, were recruited at the University Hospital Leuven from the Leuven cohort of patients of the WORK-CRT study (Clinical trials NCT02537782). Inclusion for CRT was based on the ESC criteria[8]. Coronary artery disease was excluded by CMR and/or coronary angiography obtained no more than 3 months before CRT implantation. Exclusion criteria were presence of right bundle branch block, permanent atrial fibrillation, flutter or tachycardia (>100 bpm), difficulties to obtain LV volumes by echocardiography, history and findings suggestive of ischemic myocardial disease, valve surgery within 90 days prior to enrolment, history of heart transplantation or presence of the patient on the heart transplantation list, implanted LV assist device, severe aortic stenosis, complex and uncorrected congenital heart disease, pregnant and breastfeeding women, enrolment in one or more concurrent studies that would confound the results of this study. The study was approved by the institutional ethics committee and all patients gave written and informed consent prior to inclusion.

PET acquisition protocol

All patients underwent resting ^{13}N-NH_3 and ^{18}F-FDG PET studies (Biograph HiRez 16 PET/CT, Siemens, Erlangen, Germany) 1 week before CRT implantation (except for one patient that underwent a ^{99m}Tc-tetrofosmin perfusion scintigraphy). A scout acquisition followed by a low-dose CT (80 kVp, 11 mAs) was performed before each PET emission for optimal patient positioning and subsequent CT-based attenuation correction.

For ^{13}N-NH_3 PET, a slow bolus intravenous administration of 10 MBq/kg ^{13}N-NH_3 was performed and a 30 minute dynamic list-mode acquisition was started together with radiotracer injection. In case of a one-day protocol, ^{13}N-NH_3 always preceded ^{18}F-FDG imaging with a minimal 60 min interval between tracer administrations.

^{18}F-FDG PET was performed using the euglycemic hyperinsulinemic clamp technique in accordance with the method of Lewis et al[86]. After plasma glucose levels achieved a plateau, 4.25 MBq/kg ^{18}F-FDG was administered intravenously and a 40 minute ECG-gated acquisition was performed approximately 45 minutes after tracer administration.

Image processing

Before image reconstruction, alignment between PET and CT images was evaluated and manual realignment was performed if deemed necessary by the investigator. All PET images were reconstructed using ordered-subsets expectation maximization algorithms (4 iterations and 8 subsets), matrix size 256x256, 5.0 mm Gaussian filter and corrected for attenuation using the low-dose CT.

^{18}F-FDG PET static images, both gated and non-gated, were generated from the whole 40 min acquisition. For ECG gated reconstructions, that included 8 gates, the end-systolic gate was used based on previous results from our group[87]. ^{13}N-NH_3 list-mode file was rebinned into 22 frames (12 frames x 10 sec, 4 frames x 30 sec, 3 frames x 120 sec, 1 frame x 180 sec, 1 frame 420 sec, and 1 frame x 600 sec). The last 20 min frame was used to analyze ^{13}N-NH_3 late uptake.

PET image analysis

All reconstructed ^{13}N-NH_3 and ^{18}F-FDG PET images were analyzed using in-house developed software[88]. Briefly, each myocardial image was resampled into 16 radial slices and a polar map was generated according to previously validated methods[88]. The subsequent analysis was performed both on a segmental and regional level. For segmental analysis, the LV was divided into 17-segment American Heart Association model, but segment 17 was not included for further analysis (Supplemental Figure 1) [89]. For regional/wall analysis, LV polar map was divided into 4 regions corresponding to the septal, lateral, anterior and inferior wall (Supplemental Figure 1).

Regional quantification of myocardial blood flow with ^{13}N-NH_3

Absolute quantification of myocardial blood flow (MBF) was performed per region by modelling the 10-minute and 2-minute time activity curves of ^{13}N-NH_3 uptake using a two-tissue (2CM) and one tissue compartment model (1CM), respectively[90,91]. Estimated rate constants were calculated using a weighted least-square method and were corrected for partial volume effect and spillover, as previously reported[90]. Because the amount of ^{13}N-NH_3 metabolites is known to be negligible during the first 2 minutes after tracer administration, metabolite correction (based on time-metabolites curves from a previous study[92]) was only performed for the 2CM kinetic modelling.

Regional late ^{13}N-NH$_3$ and ^{18}F-FDG uptake

Regional ^{13}N-NH$_3$ and ^{18}F-FDG uptake were expressed as mean standardized uptake values (SUV). Septal to lateral wall ratios (SLR) were calculated by dividing mean uptake in the septum by mean uptake in the lateral wall.

Segmental perfusion – metabolism relation

The segmental perfusion metabolism relation was evaluated using a method that is routinely used to assess myocardial viability. In brief, segmental ^{18}F-FDG uptake was expressed as percentage of the segment with the highest mean late ^{13}N-NH$_3$ uptake, assuming that the segment with the highest "perfusion" should have normal metabolism. Segmental "reverse mismatch", "mismatch" and "match" patterns between ^{13}N-NH$_3$ uptake and ^{18}F-FDG metabolism were defined as ^{13}N-NH$_3$/^{18}F-FDG uptake ratio $\geq$1.2, $\leq$0.8 and 0.8-1.2, respectively[93].

Statistical Analysis

Statistical analysis was performed using SPSS Statistics 20 (IBM, Chicago, IL, USA). Shapiro-Wilk test was used to check the normality of data distribution. Continuous variables are presented as mean ± standard deviation, categorical variables are presented as percentages. Comparison between septal, lateral, anterior and inferior walls was performed using one-way ANOVA test with Bonferroni post-hoc correction. T-test was used for comparison of continuous variables, contingency tables - for categorical variables. The correlation between parameters was assessed with Pearson correlation coefficients for normally distributed data, otherwise Spearman coefficient was used. Comparison of 1CM and 2CM-derived MBF was performed with Bland-Altman analysis. All statistical tests were 2-tailed. A p-value of less than 0.05 was considered as statistically significant.

RESULTS

Patient characteristics

Twenty-five patients (mean age 67±10 years, 13 (52%) males) were included in the study. Three patients had suboptimal quality of their ^{18}F-FDG scans and 1 patient underwent SPECT ^{99m}Tc-sestamibi scan instead of ^{13}N-NH_3 PET scan. After excluding these studies from the analysis, 22 patients remained with an ^{18}F-FDG PET and 24 with an ^{13}N-NH_3 PET, with 21 patients having had both PET imaging protocols successfully completed.

All patients had stable sinus rhythm. Clinical characteristics of patients are represented in Table 1.

Table 1. Clinical characteristics of patients

Parameter	All patients (n=25)
Male (% of total)	13 (52%)
Age (y)	67±10
Diabetes mellitus (% of total)	3 (12%)
Blood pressure:	
Systolic blood pressure (mmHg)	135±21
Diastolic blood pressure (mmHg)	70±16
Left ventricular function:	
EDV (ml)	162±86
ESV (ml)	113±68
EF (%)	33±8
NYHA class:	
NYHA 1	0(0%)
NYHA 2	15(60%)
NYHA 3	10(40%)
NYHA 4	0(0%)
QRS width (ms)	161±13
Medication:	
β-blockers	21(84%)
ACEi/ARB	22(88%)
Aldosterone antagonists	13(52%)

ACEi - angiotensin converting enzyme inhibitors; ARB - angiotensin-receptor blockers; EDV – end-diastolic volume; ESV – end-systolic volume, EF - ejection fraction.

Regional ^{18}F-FDG uptake

Regional ^{18}F-FDG uptake on gated and non-gated images revealed a similar pattern of tracer distribution, with higher SUVmean values on gated acquisitions, predominantly in the lateral wall (Figure 1). Because no statistically significant difference was observed between the gated and non-gated derived regional ^{18}F-FDG uptake, non-gated ^{18}F-FDG images were used for subsequent analysis.

Regional ^{18}F-FDG uptake was significantly higher in the lateral wall compared to all other walls ($p \leq 0.01$). A significantly lower ^{18}F-FDG uptake in the septum was noticed compared to all other regions ($p < 0.05$), except for the inferior wall ($p = 0.6$). There was no statistically significant difference in ^{18}F-FDG uptake between anterior and inferior walls (Figure 1).

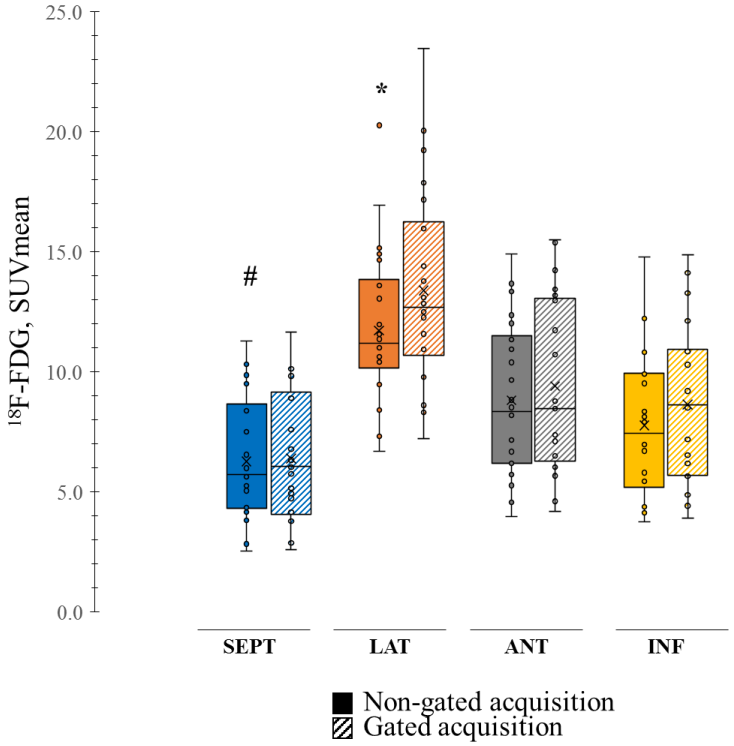

Figure 1. Regional ^{18}F-FDG uptake. *Regional ^{18}F-FDG uptake derived from cardiac gated and non-gated images. SEPT–septum, LAT–lateral wall, ANT–anterior wall, INF–inferior wall, *p≤0.01 compared to all other walls, #p<0.05 compared to the lateral and anterior wall.*

Regional MBF and late ^{13}N-NH$_3$ uptake

Absolute regional MBF derived from 1CM and 2CM ^{13}N-NH$_3$ kinetic models was strongly correlated ($r = 0.9$, $p < 0.05$) and showed a good agreement on Bland-Altman plot (bias 0.05 ml/g/min, 95% limits of agreements from -0.14 to 0.23 ml/g/min) (Supplemental Figure 2).

Mean absolute MBF in the lateral wall was significantly higher, whereas mean absolute septal MBF was significantly lower than in all other walls, when quantified with 2CM (Figure 2A). Similar results for absolute MBF were obtained with a 1CM (Supplemental Figure 3). In contrast to absolute MBF, regional late ^{13}N-NH$_3$ SUVmean was homogeneously distributed across the LV myocardium (p=0.16) (Figure 2B). Only a weak overall correlation (r=0.4, p<0.001) was found between regional absolute MBF and late ^{13}N-NH$_3$ SUVmean.

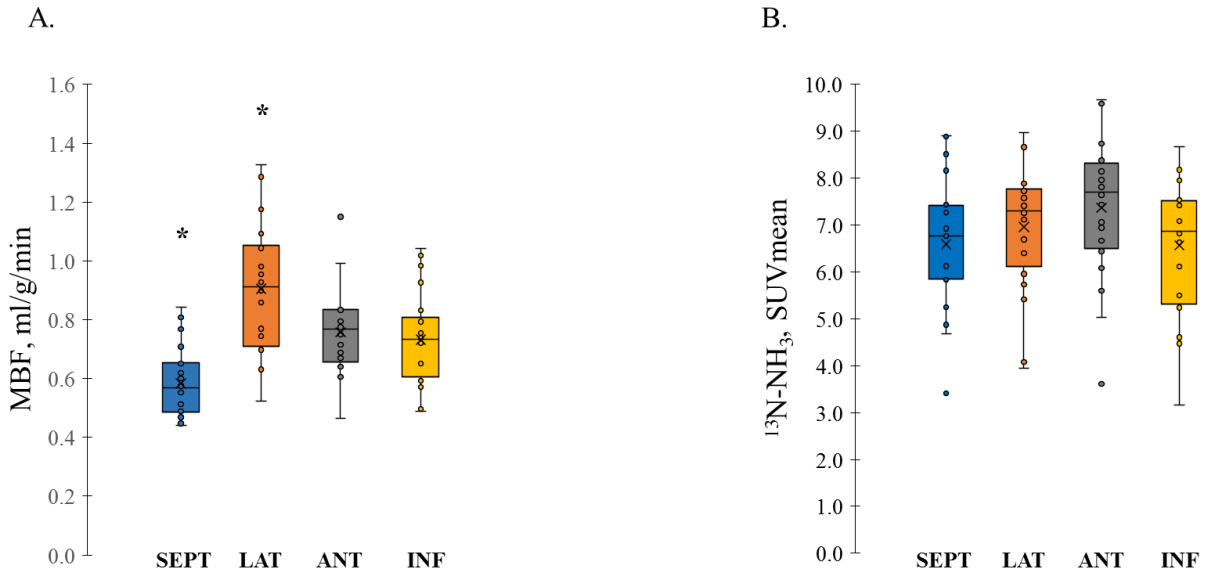

Figure 2. Regional absolute MBF and late ^{13}N-NH$_3$ uptake. *Regional myocardial blood flow (MBF), derived from 2CM kinetic model (A) and late ^{13}N-NH$_3$ uptake (B) in patients with LBBB. Note, the heterogeneous distribution of absolute perfusion across LV regions (A) vs homogeneous regional late ^{13}N-NH$_3$ uptake (B). SEPT–septum, LAT–lateral wall, ANT–anterior wall, INF–inferior wall, *p ≤ 0.01 compared to all other walls.*

Visual comparison of regional ^{13}N-NH$_3$ time activity curves (TACs) demonstrated a different pattern, with a plateau in the lateral wall compared to a steadily increased tracer accumulation in the other walls (Figure 3 A).

Detailed analysis of regional ^{13}N-NH$_3$ SUVmean changes between 3 and 30 min post tracer administration demonstrated a significant increase in tracer accumulation in the septum (5.42±1.17 vs 6.55±1.35, p<0.01), anterior (6.61±1.38 vs 7.23±1.43, p<0.01) and inferior (5.80±1.31 vs 6.47±1.43, p<0.01) walls, while no significant changes were observed in the lateral wall (6.82±1.36 vs 6.84±1.27, p=0.9). The temporal changes in SUV were most pronounced in the septal wall, with a 21% increase in tracer accumulation during the 30 min acquisition period, while smaller changes were observed in the lateral, anterior and inferior wall

with respectively +0.2%, +9% and +11%. The differences between the temporal changes in ^{13}N-NH$_3$ uptake reached the significance level only between septal and lateral wall (p=0.01) (Figure 3 B).

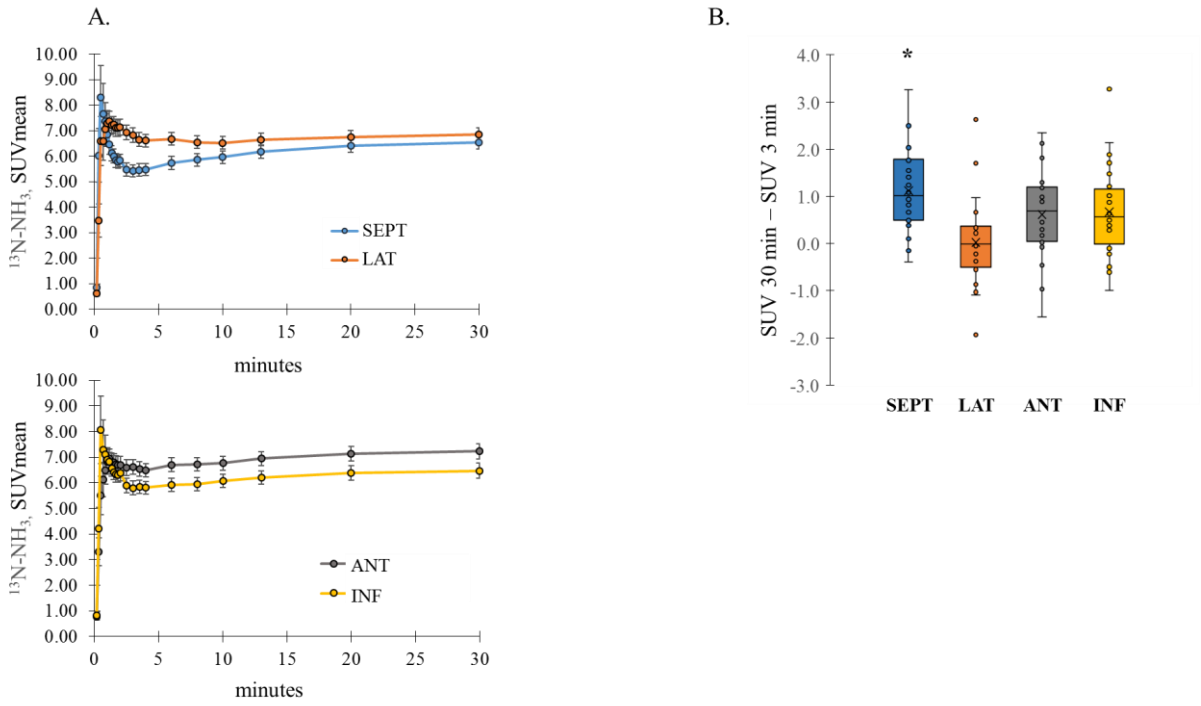

***Figure 3. Regional temporal ^{13}N-NH$_3$ kinetics**. Regional time-activity curves, representing changes in mean ^{13}N-NH$_3$ SUV as a function of time (A) and regional changes in ^{13}N-NH$_3$ SUV between 3 and 30 min postinjection (B) in all patients with LBBB. Vertical bars in figure A represent the standard error. SEPT–septum, LAT–lateral wall, ANT–anterior wall, INF–inferior wall, *p<0.01 compared to the lateral wall.*

Septal-to-lateral absolute MBF, late ^{13}N-NH$_3$ and ^{18}F-FDG uptake ratio

Mean absolute 2CM-MBF SLR, late ^{13}N-NH$_3$ SLR and ^{18}F-FDG SLR are represented in Figure 4. ^{18}F-FDG SLR was significantly lower compared to absolute MBF SLR and late ^{13}N-NH$_3$ SLR (0.53±0.17 vs 0.68±0.18 vs 0.96±0.13, respectively, p≤0.01). The significantly lower resting absolute MBF in the septum compared to the lateral wall with MBF SLR of 0.68±0.18 was no longer observed on late ^{13}N-NH$_3$ uptake (SLR 0.96±0.13), indicating a more homogenous distribution of ^{13}N-NH$_3$ in the LV. There was a significant but moderate correlation between ^{18}F-FDG and late ^{13}N-NH$_3$ SLR (r=0.55, p=0.01).

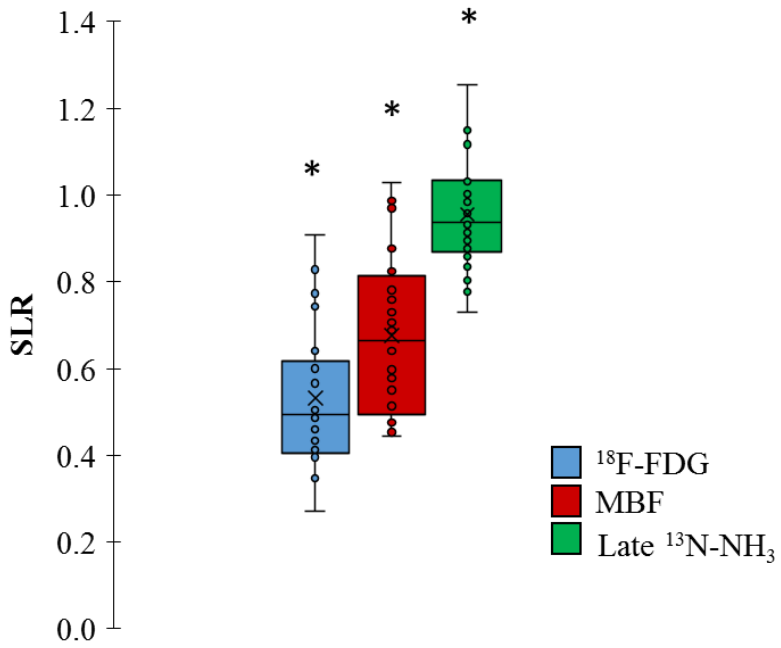

Figure 4. Septal-to-lateral ratios. *Mean septal-to-lateral ^{18}F-FDG, absolute 2CM-MBF and ^{13}N-NH$_3$ late uptake ratios (SLR). *p ≤ 0.01 compared to other SLRs.*

Segmental perfusion – metabolism relation

Overall segmental analysis of perfusion-metabolism relation revealed "mismatch", "reverse mismatch" and "match" patterns in 70 (21%), 111 (33%) and 155 (46%) segments, respectively.

"Mismatch" pattern was observed in 3 (3%), 55 (52%), 6 (10%) and 6 (10%) segments in the septum, lateral, anterior and inferior wall, respectively. "Reverse mismatch" patterns in these regions corresponded to 64 (61%), 0 (0%), 25 (40%) and 22 (35%) segments, respectively (Figure 5).

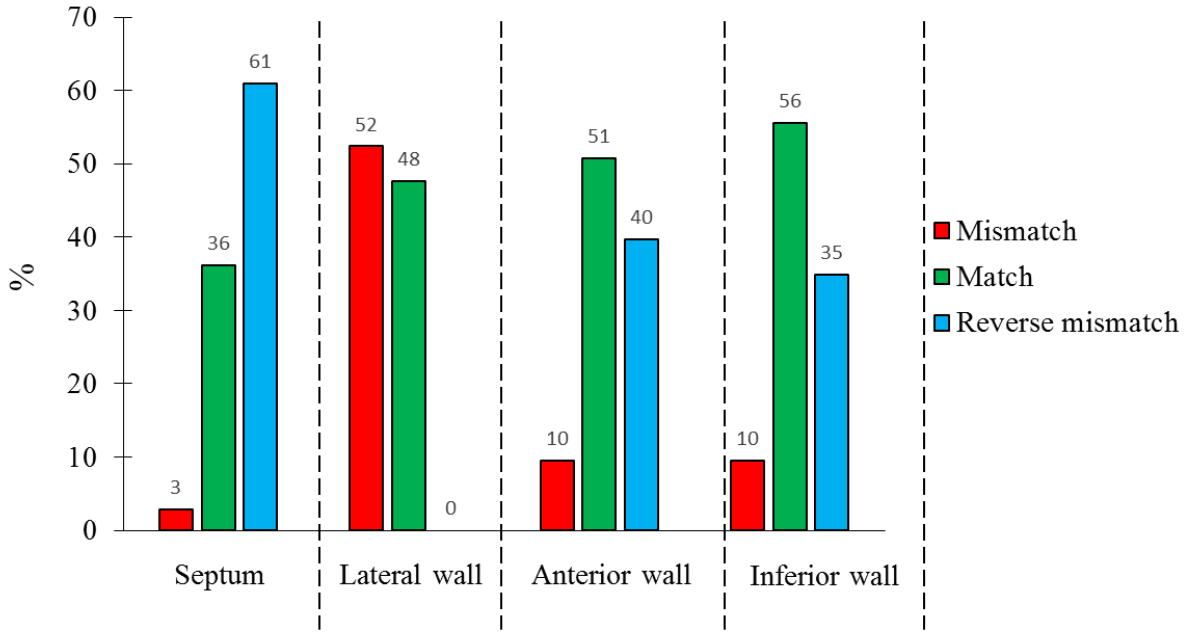

Figure 5. Perfusion-metabolism patterns. *Distribution of late ^{13}N-NH_3/^{18}F-FDG "reverse mismatch", "mismatch" and "match" patterns between septal, lateral, anterior and inferior wall.*

DISCUSSION

The main finding of our study is the presence of regional heterogeneity in glucose metabolism and perfusion with lower glucose uptake and absolute MBF in the septum compared to the lateral wall in non-ischemic CRT-candidates with LBBB. In contrast, late ^{13}N-NH_3 uptake did not show significant regional differences, hence being a poor parameter for MBF but rather reflecting a composite measure of altered regional MBF and metabolism, induced by LBBB.

Several studies have demonstrated regional changes in glucose metabolism in the presence of LBBB. Among those, an experimental study of Ono et al. showed a significantly lower ^{18}F-FDG uptake in the septum compared to the lateral wall (67.4±12.1% versus 88.0±5.2%, $p<0.05$) in right ventricular pacing-induced LBBB[38]. Similar findings were reported in a clinical study of Nowak et al. in patients with LBBB with lowest ^{18}F-FDG uptake in the septum (56±12%), highest in the lateral wall (89±6%) and intermediate values in the anterior and inferior wall (66±12% and 69±8%, respectively)[39]. The low ^{18}F-FDG SLR in dyssynchronous hearts were also postulated by Neri et al. (0.59±0.17) and Nowak et al. (0.62±0.12)[39,94]. Our results are in line with above-mentioned papers, demonstrating a heterogeneous regional glucose metabolism in non-ischemic LBBB heart failure patients with lowest ^{18}F-FDG uptake in the septum, highest in the lateral wall and intermediate ^{18}F-FDG values in anterior and inferior wall. Furthermore, ^{18}F-FDG SLR obtained in our study (0.53±0.17) perfectly matches the range shown by other groups.

These results presented in our and previous studies in patients with LBBB, can be explained by the fact that the early activated septum does not contribute much to LV contraction or is even wasting work due to systolic stretching, whereas the lateral wall bears most of the load and compensates for the septal dysfunction[37]. Earlier work by our group in a preclinical sheep model has shown that ^{18}F-FDG uptake is linearly correlated with the amount of work performed by the myocardium, which indicates, that the observed regional differences in ^{18}F-FDG uptake are an adaptive mechanism to compensate for the difference in regional workload in an asynchronously contracting ventricle[37].

In contrast to glucose metabolism, findings on regional myocardial perfusion in LBBB patients are controversial. Conflicting results may be attributed amongst others to different imaging modalities, radiopharmaceuticals, study protocols, and approaches for flow assessment. Earlier studies using SPECT perfusion have shown a decreased perfusion of the septum, that can be the result of partial-volume effect in the reported thinned septum, which is less pronounced when recent PET technology is used[95]. Discrepant results for absolute MBF

in non-ischemic LBBB patients have also been described with PET depending on the radiotracer used. The study by Baller et al. showed a low absolute MBF for the septum and high MBF for the lateral wall with ^{11}C-acetate, while the study of Koepfli et al. showed a more homogeneous resting perfusion using ^{15}O-water[96,97]. However, in the latter study, stress imaging induced regional perfusion inhomogeneities, which may be explained by the fact that 'stress' increases mechanical dyssynchrony resulting in regional perfusion changes[98]. Additionally, exercise leads to an increased oxygen demand mainly in the extensively working lateral wall leading to a more distinct redistribution of myocardial flow. In our study, regional differences in absolute MBF were similar to metabolic changes, with a low perfusion in the septum, high values in the lateral wall and intermediate values in anterior and inferior wall. It is unlikely that this difference can be explained by differential partial volume effects since we did not observe a significant difference in septal and lateral wall thickness (6.99±1.64 mm vs 6.62±1.55 mm, respectively, p=0.36) as assessed with CMR in 21 out of 25 patients.

In contrast to our study, Masci et al. reported a rather homogeneous ^{13}N-NH_3-derived MBF between septal and lateral walls[40]. One of the possible explanations for their findings could be the exclusion of patients with advanced disease, allowing to assume that LV dyssynchrony was not pronounced enough to induce perfusion heterogeneities. Another explanation could be the different modeling approach to obtain absolute perfusion values. The authors used a simplified perfusion model proposed by Bellina et al. , in which absolute MBF is not quantified by fitting a kinetic model to the TAC, but is derived from a fixed myocardial ^{13}N-NH_3 concentration measured at a particular time point[99]. Consequently, this derived MBF is always proportional to the tracer uptake at that time point. In our study we have demonstrated that late ^{13}N-NH_3 uptake is homogeneously distributed between all LV regions and therefore, when absolute MBF is computed with this simplified model, MBF will also be homogeneous across the regions. In our study, perfusion quantification was performed using a richer kinetic model (full 1CM and 2CM models) which does not impose the perfusion to be proportional to the late myocardial tracer concentration. This can explain the different regional patterns for absolute MBF distribution between both studies.

We hypothesize that perfusion heterogeneity in LBBB patients observed in our study is an example of coronary autoregulation where redistribution of local myocardial workload is associated with similar changes in oxygen demand, hence alterations in blood supply. Differences in regional workload and imbalance in oxygen consumption in asynchronously contracting ventricles has been demonstrated with highest values in the lateral wall and lowest

in the septum, which may support the theory of a functional rather than structural adaptive mechanism[38,100].

In contrast to the regional differences in absolute MBF, late ^{13}N-NH_3 uptake was homogeneously distributed across the LV in our study. These findings correspond with other ^{13}N-NH_3 PET studies in patients with LBBB reporting an average late ^{13}N-NH_3 SLR in the order of one[101]. Earlier reports have demonstrated that ^{13}N-NH_3 fixation in the heart occurs mainly through its ATP-dependent conversion into glutamine via the glutamate-glutamine pathway[48]. The latter suggests a particular role of myocardial metabolism for ^{13}N-NH_3 incorporation which is further supported by the significant, even though moderate, correlation between late ^{13}N-NH_3 and ^{18}F-FDG SLR, observed in our study. Furthermore, our and other studies did not show a perfect linear correlation between MBF and late ^{13}N-NH_3 uptake, illustrating that late ^{13}N-NH_3 myocardial uptake is rather a combined assessment of MBF and metabolism[102]. The latter is supported by the study of Choi et al. reporting ^{13}N-NH_3 SUV to be a poor indicator of MBF by comparing six different methods for the assessment of myocardial perfusion in dogs and healthy volunteers[103].

The different regional temporal kinetics of ^{13}N-NH_3 shown in our study with a plateau in the lateral wall and steadily increased tracer accumulation in the rest of the heart is not fully understood, but explains the homogenous late ^{13}N-NH_3 uptake despite significant differences in absolute MBF. One of the possible hypotheses for the different regional ^{13}N-NH_3 kinetics between myocardial walls can be linked to regional metabolic alterations secondary to functional adaptive mechanisms, with different levels of glutamate, glutamate synthtetase, free available ATP, intracellular level of NH_3, intracellular pH, that all may play a role in myocardial tracer fixation. However, further studies are needed to fully understand and explain the observed regional differences.

Finally, a differential relation between perfusion and metabolism in septal and lateral walls characterized as “mismatch” and “reverse mismatch” patterns using a common method for viability assessment has been shown in LBBB patients in our study. Similarly to the study of Masci et al., “mismatch” segments were predominantly present in the lateral wall (52%) while “reverse mismatch” segments were mainly observed in the septum (61%)[40]. The presence of these perfusion/metabolism “mismatch” and “reverse mismatch” patterns in LBBB patients are most likely attributed to the physiological changes induced by the presence of LBBB and should be taken into account when patients with LBBB are referred for viability assessment prior to revascularization procedures. In addition, further investigations are needed to evaluate whether specific perfusion/metabolism patterns in LBBB patients may predict

response to CRT, however one study has shown that the presence of reverse mismatch patterns in the septum was associated with good prognosis after [61].

Our study had several limitations. Although ischemia was excluded in our patient cohort based on CMR and/or coronary angiography 3 months prior to CRT implantation, one cannot completely rule out ischemia at the time of CRT implantation, however these chances are negligible. In the current study, clinically used reconstruction algorithms and software programs were applied without correcting for partial volume effect, which may lead to a slight underestimation of the true tracer concentration in the thinned walls. Furthermore, we did not perform absolute quantification of cardiac glucose metabolism, but only mean glucose uptake defined by SUV was used in the current study. Quantification of glucose consumption as well as using other metabolic PET tracers such as ^{11}C-acetate could help to better understand the pathophysiological mechanisms and metabolic adaptations during abnormal LV activation patterns. The presence of a comparable control group with non-ischemic cardiomyopathy without LV dyssynchrony would have been informative to define whether the alterations observed in myocardial perfusion and metabolism in non-ischemic LBBB patients are absolute or rather relative. This control group would also provide more insights into the temporal kinetics of ^{13}N-NH_3 uptake in different walls to further support the assumption that the different regional temporal kinetics are attributed to abnormal LV activation.

CONCLUSIONS

Non-ischemic heart failure patients with LBBB demonstrate lower myocardial glucose uptake and absolute MBF in the septum compared to the lateral wall. However, late static ^{13}N-NH_3 uptake did not show significant regional differences, demonstrating that there is no perfect correlation between absolute MBF and late ^{13}N-NH_3, with the latter being a composite measure of absolute MBF and myocardial metabolism. Regional differences in temporal ^{13}N-NH_3 kinetics in LBBB patients are present but further investigations are warranted to elucidate the underlying pathophysiological mechanism.

SUPPLEMENTAL MATERIAL

Impact of left bundle branch block on myocardial perfusion and metabolism: a positron emission tomography study

SUPPLEMENTAL MATERIAL AND METHODS

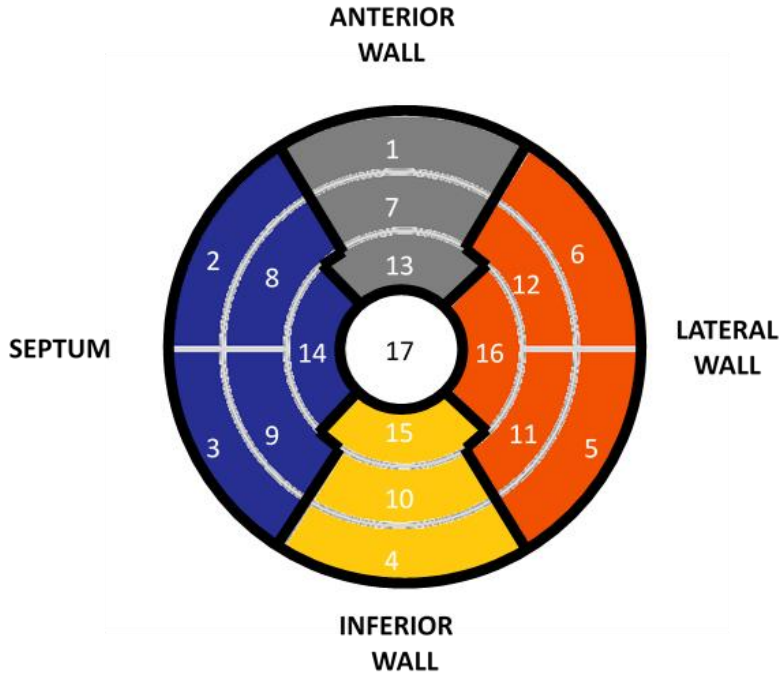

Supplemental Figure 1. LV segmentation. *Bull`s-eye polar map divided into 17 segments and 4 left ventricular regions*

SUPPLEMENTAL RESULTS

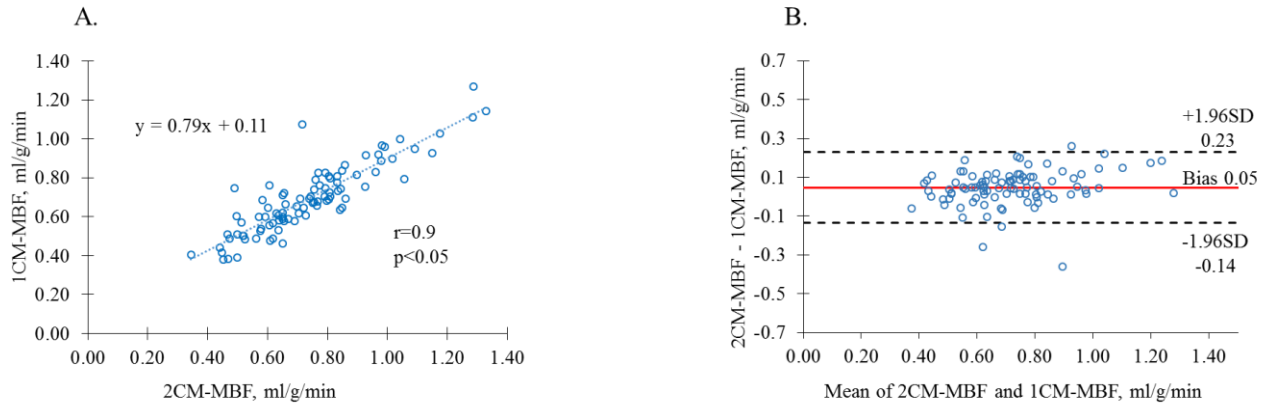

Supplemental Figure 2. Comparison of 1CM and 2CM kinetic model. *Correlation plot (A) and Bland-Altman plot (B) between regional myocardial blood flow (MBF) derived from one-(1CM) and two tissue compartment(2CM) ^{13}N-NH_3 kinetic model. The broken line in figure A, red line and broken lines in figure B represent the correlation line, mean bias and the 95% confidence intervals, respectively.*

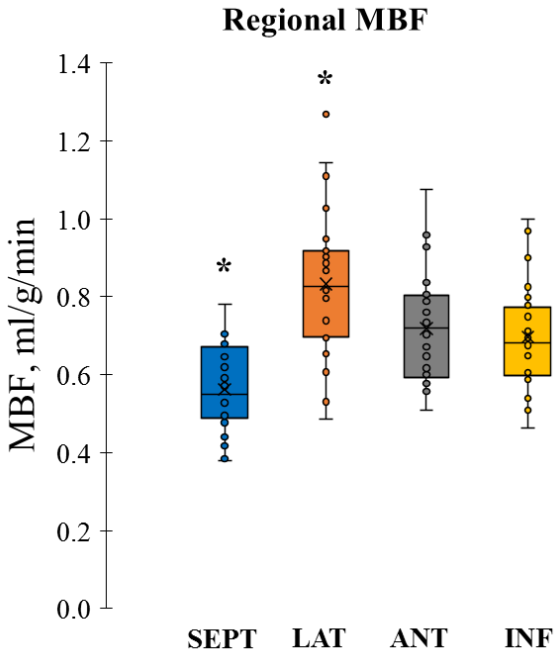

Supplemental Figure 3. Regional myocardial blood flow (MBF), derived from 1CM kinetic model. *Note, the similar regional perfusion pattern between 1CM and 2CM-derived MBF with the highest MBF in the septum and the lowest in the lateral wall. SEPT–septum, LAT–lateral wall, ANT–anterior wall, INF–inferior wall, *p ≤ 0.01 compared to all other walls.*

CHAPTER II

Low septal to lateral wall ^{18}F-FDG ratio is highly associated with mechanical dyssynchrony in non-ischemic CRT candidates

Published in: EJNMMI Res. 2019 Dec 9;9(1):105.

doi: 10.1186/s13550-019-0575-9.

Ganna Degtiarova, MD[a,b], Piet Claus, PhD[c], Jürgen Duchenne, PhD[c,d], Marta Cvijic, MD, PhD[d], Georg Schramm, PhD[a], Johan Nuyts, PhD[a], Jens-Uwe Voigt, MD, PhD[c,d], Olivier Gheysens, MD, PhD[a,b]

a) Department of Imaging and Pathology, KU Leuven, Leuven, Belgium

b) Nuclear Medicine and Molecular Imaging, University Hospitals Leuven, Belgium

c) Department of Cardiovascular Sciences, KU Leuven, Leuven, Belgium

d) Department of Cardiovascular Diseases, University Hospitals Leuven, Leuven, Belgium

This chapter addresses the following research questions:

- What is the influence of mechanical dyssynchrony on cardiac perfusion and metabolism?
- Is there any association between regional perfusion and metabolism, assessed with PET before CRT implantation, and the extent of volumetric reverse remodelling after CRT implantation?

ABSTRACT

Background: In order to better understand the concept of mechanical dyssynchrony, a promising hallmark of cardiac resynchronization therapy (CRT) response, we investigated its effect on regional myocardial metabolism and myocardial blood flow (MBF) in non-ischemic CRT-candidates.

Results: 30 consecutive non-ischemic CRT eligible patients underwent static ^{18}F-FDG and resting dynamic ^{13}N-NH_3 PET/CT. ^{18}F-FDG uptake and MBF for septal and lateral wall were analyzed and septal-to-lateral wall ratios (SLR) were calculated. Based on the presence of mechanical dyssynchrony (septal flash and/or apical rocking) on echocardiography, patients were divided into 2 groups, with (n=23) and without (n=7) mechanical dyssynchrony.

Patients with mechanical dyssynchrony had significantly lower ^{18}F-FDG SUVmean in the septum compared to the lateral wall (5.58±2.65 vs 11.19±4.10, p<0.0001), while patients without mechanical dyssynchrony had a more homogeneous ^{18}F-FDG distribution (7.33±2.88 vs 8.31±2.50, respectively, p=0.30). Similarly, MBF was significantly different between the septal and lateral wall in the dyssynchrony group (0.57±0.11 ml/g/min vs 0.92±0.23 ml/g/min, respectively, p<0.0001), whereas no difference was observed in the non-dyssynchrony group (0.61±0.23 ml/g/min vs 0.77±0.21 ml/g/min, respectively, p=0.16). ^{18}F-FDG SLR, but not MBF SLR, was associated with the presence of mechanical dyssynchrony and showed a significant correlation with volumetric reverse remodelling after CRT (r=0.62,p=0.001).

Conclusions: Non-ischemic heart failure patients with mechanical dyssynchrony demonstrate heterogeneous regional metabolism and MBF compared to patients without dyssynchrony. However, only ^{18}F-FDG-SLR appeared to be highly associated with the presence of mechanical dyssynchrony.

INTRODUCTION

During the last decade, ventricular conduction disturbances have been shown to be associated with adverse cardiac remodelling and to contribute to the development of heart failure (HF) and an increased risk of all-cause mortality[85]. Even though cardiac resynchronization therapy (CRT) is a promising therapy for patients with ventricular conduction abnormalities, 30-40% of patients do not respond to this treatment and therefore optimization of selection criteria for CRT candidates is still an active area of investigation[104]. Along with electrical dyssynchrony induced by inhomogeneous electrical activation of the left ventricle (LV), about 60-70% of patients also develop mechanical dyssynchrony, characterized by discoordinate myocardial deformation and inefficient contraction[31]. Septal flash (SF) and apical rocking (AR), surrogate markers of mechanical dyssynchrony, have been shown to be associated with favorable CRT response[31]**.** Deeper insights into pathophysiological processes related to mechanical dyssynchrony are needed, including changes in perfusion and metabolism, in order to better understand the adverse cardiac remodelling and to further improve patient selection for CRT.

Different non-invasive imaging techniques are currently available to evaluate regional changes in perfusion and metabolism and their interplay. ^{18}F-fluorodeoxyglucose (^{18}F-FDG) positron emission tomography (PET) studies in patients with ventricular conduction abnormalities have shown regional changes in glucose metabolism with a relatively reduced glucose uptake in the septum compared to an increased uptake in the lateral wall[39,101].

In contrast to the well-established changes in glucose uptake, data on myocardial perfusion in patients with ventricular dyssynchrony remain controversial. Experimental data have consistently shown a relative hypoperfusion in the septal wall compared to the lateral wall, while clinical studies predominantly reported a rather homogeneous perfusion across the LV, with only few studies showing septal hypoperfusion[38,39,95].

Despite several studies investigating myocardial metabolism and perfusion in patients with ventricular conduction abnormalities, data on the influence of mechanical dyssynchrony on these physiologic parameters are lacking.

The aim of our study was to investigate the effect of mechanical dyssynchrony on regional ^{18}F-FDG uptake and absolute myocardial blood flow (MBF) (derived from ^{13}N-NH_3 kinetic models) in patients with non-ischemic cardiomyopathy, eligible for CRT.

METHODS

Study Population

Patients with non-ischemic HF referred for CRT implantation were recruited at the University Hospital Leuven and were part of the Leuven cohort of the WORK-CRT study (Clinical trials NCT02537782). Inclusion for CRT was based on the ESC guidelines[8]. Coronary artery disease was excluded by late gadolinium enhancement cardiac magnetic resonance (CMR) and/or coronary angiography obtained no more than 3 months before CRT implantation and/or thorough evaluation of patient history and complaints by an experienced treating cardiologist. Exclusion criteria comprised the presence of a right bundle branch block, permanent atrial fibrillation/flutter or tachycardia (>100bpm), difficulties to obtain LV volumes by echocardiography, history and findings suggestive of ischemic myocardial disease, valve surgery within 90 days prior to enrolment, history of or listing for heart transplantation, implanted LV assist device, severe aortic stenosis, complex and uncorrected congenital heart disease, pregnant and breastfeeding women, enrollment in one or more concurrent studies that would confound the results of this study. The study was approved by the institutional ethics committee and all patients gave written informed consent prior to inclusion and any study procedure.

Echocardiography

All patients underwent a standard two-dimensional echocardiography within 1 week before CRT implantation and approximately 12 months after CRT implantation using commercially available systems (Vivid E9 and E95, GE Vingmed Ultrasound, Horten, Norway). Acquired data were stored digitally and analysed off-line using an EchoPAC workstation (version 202, GE Vingmed Ultrasound). LV end-diastolic volume (EDV), end-systolic volume (ESV) and LV ejection fraction (LVEF) were measured using the modified biplane Simpson's method. Volumetric remodelling after CRT (Δ LV ESV, %) was defined as the relative reduction in LV ESV between baseline and 12 months post-CRT (Δ LV ESV,% = (ESV 12M – ESV baseline) / ESV baseline). Mechanical dyssynchrony was visually assessed by two independent readers (JD and MC) on pre-CRT echocardiography images. A third reader (JUV) blinded to previous readings was asked in case of disagreement. Patients were divided into 2 groups – one group with mechanical dyssynchrony defined by the presence of either AR or SF, or both, and another group without mechanical dyssynchrony (neither AR nor SF).

Additionally, pre-CRT echocardiography was used to calculate segmental myocardial work, using an 18 segment model and a method, previously described by our group[105]. In short, a dedicated, MATLAB-based (version 2017b, The MathWorks, Inc., Natick, MA,USA) research software (TVA version 22.00, JU Voigt, Leuven) was used to determine LV pressure estimates according to the method described by Russell[106]. LV segmental mid-wall curvature was dynamically estimated from full trace export of the speckle tracking software and used together with the segmental wall thickness measurements to estimate segmental wall stress according to the formula of Laplace. Segmental stress-strain loops were generated, the area of which was considered to represent myocardial work per volume-unit[105]. Regional myocardial work in the septum and lateral wall was calculated as average of the stress-strain loop areas of the basal, mid, and apical segments of the respective wall.

PET acquisition protocol

All patients underwent resting dynamic ^{13}N-NH_3 and static ^{18}F-FDG PET studies (Biograph HiRez 16 PET/CT, Siemens, Erlangen, Germany) 1 week before CRT implantation (except for one patient who underwent a ^{99m}Tc-tetrofosmin perfusion scintigraphy). A scout acquisition followed by a low-dose CT (80 kVp, 11 mAs) was performed for optimal patient positioning and subsequent CT-based attenuation correction of the PET emission data.

For ^{13}N-NH_3 PET, a 30 minute dynamic list-mode acquisition was started together with a slow bolus intravenous administration of 10 MBq/kg ^{13}N-NH_3. In case of a one-day protocol, the ^{13}N-NH_3 scan always preceded the ^{18}F-FDG scan with a minimum interval of 60 minutes between tracer administrations.

^{18}F-FDG PET scan was performed using the hyperinsulinemic euglycemic clamp technique in accordance with the method of Lewis et al.[86]. After reaching a steady state plasma glucose level, 4.25 MBq/kg ^{18}F-FDG was administered intravenously and a 40 minute acquisition was performed approximately 45 minutes after tracer administration.

Image processing

Before image reconstruction, alignment between PET and CT images was evaluated and manual realignment between both images was performed if deemed necessary by the investigator. All PET images were reconstructed using the ordered-subsets expectation maximization algorithms (4 iterations and 8 subsets), matrix size 256x256, 5.0 mm Gaussian filter. Attenuation correction was performed using a low-dose CT scan.

^{18}F-FDG PET static images were generated from the whole 40 min acquisition. ^{13}N-NH_3 list-mode file was rebinned into 22 frames (12 frames x 10sec, 4 frames x 30 sec, 3 frames x 120sec, 1 frame x 180sec, 1 frame 420 sec, and 1 frame x 600sec).

PET image analysis

All reconstructed ^{13}N-NH_3 and ^{18}F-FDG PET images were analyzed using in-house developed software [88]. Briefly, each myocardial image was resampled into 16 radial slices and a 17 segment polar map was generated according to previously validated methods [88,89]. LV polar map was divided into 4 regions corresponding to the septal, lateral, anterior, and inferior wall with exclusion of the apex (segment 17). Analysis of perfusion and metabolism was performed focusing on the septal and lateral wall.

Absolute quantification of MBF with ^{13}N-NH_3

Absolute quantification of MBF per region was performed by modelling the first 10-minute emission data of ^{13}N-NH_3 using a two-tissue compartment model [90]. Estimated rate constants were calculated using a weighted least-square method and were corrected for spillover and partial volume effect, as previously reported [90]. Because the amount of ^{13}N-NH_3 metabolites is known to increase after the first 2 minutes after tracer administration, metabolite correction was performed [92]. In addition to regional absolute MBF, septal-to-lateral wall MBF ratio (SLR) was calculated by dividing mean MBF in the septum by mean MBF in the lateral wall.

Analysis of ^{18}F-FDG uptake

Regional ^{18}F-FDG uptake was expressed as mean standardized uptake value (SUVmean). Septal to lateral wall ratio (SLR) was calculated by dividing mean ^{18}F-FDG uptake in the septum by mean uptake in the lateral wall.

Cardiac resynchronization therapy

CRT implantation was performed according to the guidelines[107]. In short, LV pacing leads were positioned, guided by coronary venography, preferably in the lateral and postero-lateral venous branches. After implantation, the device was set to bi-ventricular pacing in all patients.

Statistical Analysis

Statistical analysis was performed using SPSS Statistics 20 (IBM, Chicago, IL, USA). Shapiro-Wilk test was used to check the normality of data distribution. Normally distributed continuous variables were expressed as mean ± standard deviation, otherwise median and interquartile range was used. Categorical variables were represented as percentages. Paired and unpaired t-test with Bonferroni correction was used for comparison of continuous variables, while contingency tables were used for categorical variables. The correlation between parameters was assessed with Pearson correlation coefficients for normally distributed data, otherwise Spearman coefficient was used. Inter- and intraobserver variability of echocardiographic measurements of mechanical dyssynchrony (SF, AR) was performed in the whole study population using Kappa statistics. All statistical tests were 2-tailed. A p-value of less than 0.05 was considered statistically significant.

RESULTS

Patient characteristics

Thirty patients (mean age 68±10 years, 16 (53%) males) were included in the study. Coronary artery disease was excluded by late gadolinium enhancement CMR in 23/30 patients, by coronary angiography in 2/30 patients and all patients underwent thorough evaluation of patient history and complaints by an experienced treating cardiologist.

All patients had echocardiography pre-CRT. Two patients died during the first 6 months of follow-up so post-CRT echocardiography was available in only 28 patients. On pre-CRT echocardiography, 23 (77%) patients had mechanical dyssynchrony, while 7 (23%) patients had no mechanical dyssynchrony. Among patients with mechanical dyssynchrony, 2 patients had only AR, 1 patient had only SF and 20 patients had both AR or SF. The QRS morphology on surface ECG in patients with mechanical dyssynchrony was represented mainly by LBBB (91%), while QRS pattern in patients without mechanical dyssynchrony was represented by LBBB (57%), nonspecific intraventricular conduction delay (29%) and right ventricular pacing (1%). Clinical characteristics of our study cohort are presented in Table 1.

Three patients had suboptimal quality of ^{18}F-FDG scan and 1 patient underwent ^{99m}Tc-tetrofosmin perfusion scintigraphy instead of ^{13}N-NH_3 PET scan. After excluding these studies from the analysis, 27/30 and 29/30 patients have successfully completed respectively a ^{18}F-FDG and ^{13}N-NH_3 PET scan. These scans were included in the further analysis independently of each other and were distributed between both patient groups as follows: 21 ^{18}F-FDG and 22 ^{13}N-NH_3 scans belonged to the group of mechanical dyssynchrony while 6 ^{18}F-FDG and 7 ^{13}N-NH_3 scans represented the group without mechanical dyssynchrony.

Regional ^{18}F-FDG uptake

A significantly lower ^{18}F-FDG SUVmean in the septum compared to the lateral wall was observed in the group with mechanical dyssynchrony (SUVmean: 5.6±2.7 vs 11.2±4.1, respectively, $p<0.0001$), while in the group without dyssynchrony, ^{18}F-FDG distribution did not differ between septal and lateral wall (SUVmean: 7.3±2.9 vs 8.3±2.5, respectively, $p=0.3$) (Figure 1A). ^{18}F-FDG uptake in the lateral wall in patients with mechanical dyssynchrony was higher compared to those without, albeit not significantly ($p=0.1$). Even though septal ^{18}F-FDG uptake was lower in patients with mechanical dyssynchrony compared to patients without mechanical dyssynchrony, here was no statistically significant difference between both groups ($p=0.22$).

Table 1. Clinical characteristics of patients

Parameter	All patients (n=30)	With mechanical dyssynchrony (n=23)	Without mechanical dyssynchrony (n=7)	P value
Clinical characteristics:				
Male (% of total)	16 (53%)	10 (43%)	6 (86%)	0.05
Age (years)	68±10	68±9	68±12	0.94
Diabetes mellitus (% of total)	4 (13%)	3 (13%)	1 (14%)	0.93
Systolic blood pressure (mmHg)	134±22	134±21	120±28	0.18
Diastolic blood pressure (mmHg)	69±15	70±14	65±17	0.47
NYHA class II/III:	17(57%)/13(43%)	12(52%)/11(48%)	5(71%)/2(29%)	0.42
Electrocardiographic parameters				
QRS width (ms)	161±16	161±15	163±21	0.73
LBBB (Strauss)	25(83%)	21 (91%)	4(57%)	**0.03**
RV pacing	1(3%)	0(0%)	1(14%)	0.23
NS-IVCD	4(10%)	2(9%)	2(29%)	0.21
Echocardiographic parameters (pre-CRT):				
EDV (ml)	142 [133;193]	142 [126;203]	164 [116;202]	0.88
ESV (ml)	100 [91;138]	98 [85;147]	101 [76;138]	0.74
EF (%)	32±8	32±9	32±5	0.99
Heart failure therapy:				
β-blockers	26(87%)	19(83%)	7(100%)	0.54
ACEi/ARB	27(90%)	21(91%)	6(86%)	0.66
Aldosterone antagonists	17(57%)	13(57%)	4(57%)	0.9

ACEi - angiotensin converting enzyme inhibitors; ARB - angiotensin-receptor blockers; EDV – end-diastolic volume; ESV – end-systolic volume, LBBB *– left bundle branch block, RV – right ventricle, NS-IVCD - non-specific intraventricular conduction delay.*

Regional MBF

A significantly lower MBF in the septum compared to the lateral wall was observed in the group with mechanical dyssynchrony (0.6±0.1 ml/g/min vs 0.9±0.2 ml/g/min, respectively, p<0.0001), while in the group without dyssynchrony there was no statistical difference in the MBF between both walls (0.6±0.2 ml/g/min vs 0.8±0.2 ml/g/min, respectively, p=0.16). No difference in regional MBF between both patient groups was observed (Figure 1B).

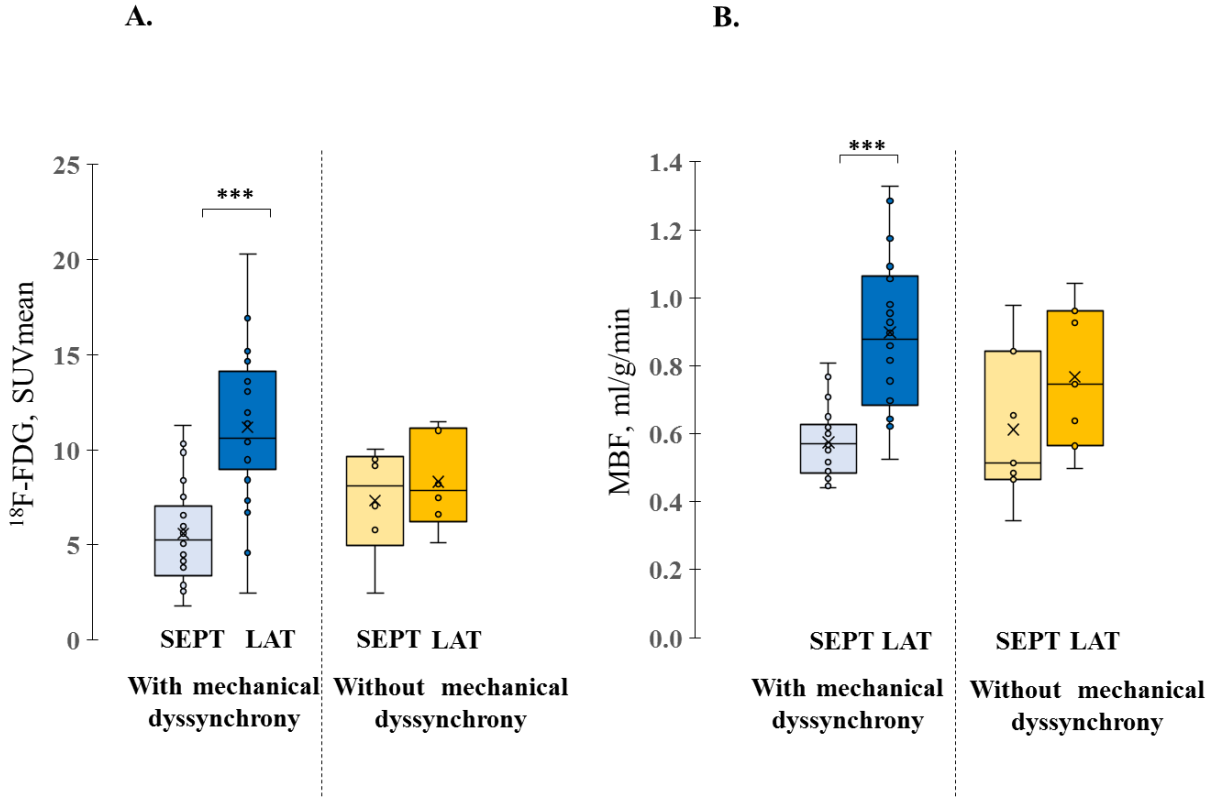

Figure 1. Regional glucose metabolism and myocardial blood flow (MBF). *Regional glucose metabolism (^{18}F-FDG uptake) (A) and MBF (B) in patients with and without mechanical dyssynchrony. SEPT-septum, LAT-lateral wall. *** p≤0.0001.*

Relation between regional metabolism, MBF and myocardial work

In the group with mechanical dyssynchrony, a significantly lower myocardial work was observed in the septum compared to the lateral wall (370±816 mmHg*% vs 3174±1033 mmHg*%, respectively, p<0.0001), whereas no regional differences in myocardial work were observed in the group without mechanical dyssynchrony (2017±685 mmHg*% vs 2267±572 mmHg*%, respectively, p=0.26). There was significantly less work performed by the septum in the group of dyssynchrony compared to the non-dyssynchrony group (370±816 mmHg*% vs 2017±685 mmHg*%, respectively, p=0.0007). Additionally, negative (wasted) work was

observed in the septum of 40% of patients with mechanical dyssynchrony, but never in patients without dyssynchrony. The work performed by the lateral wall was borderline significantly higher (p=0.05) in the group with dyssynchrony compared to the group without dyssynchrony (3174±1033 mmHg*% vs 2267±572 mmHg*%, respectively).

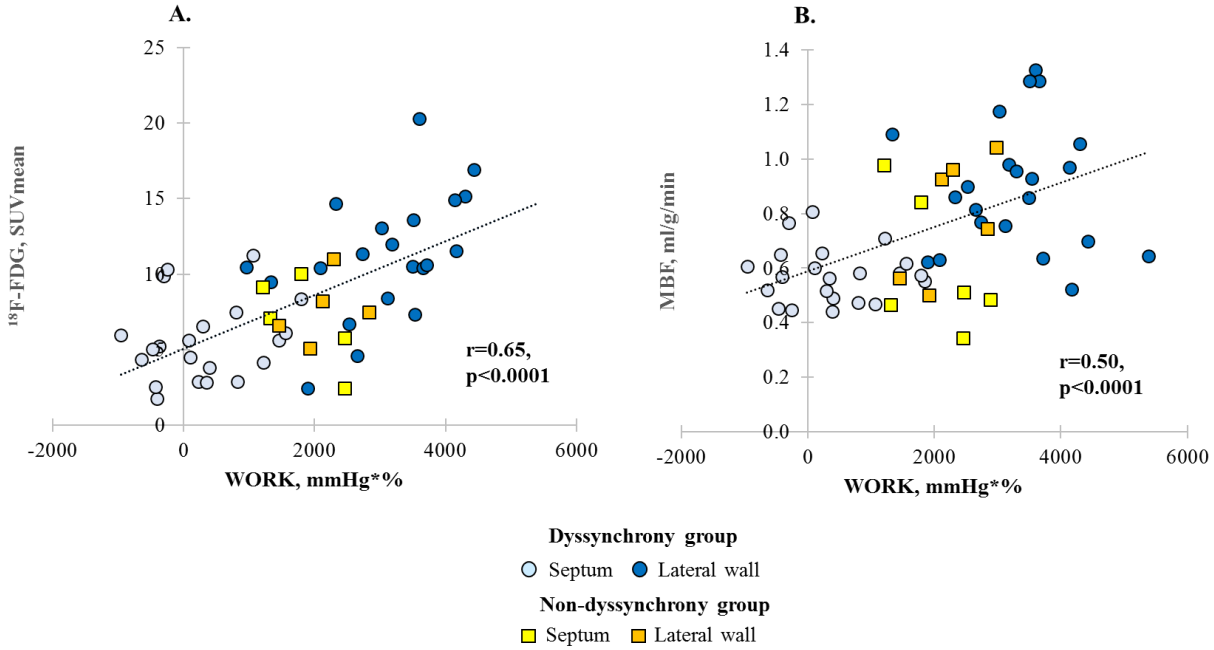

Figure 2. Correlation plots between myocardial work versus glucose metabolism and perfusion. *Correlation between myocardial work and glucose metabolism (^{18}F-FDG) (A) and myocardial work and MBF (B), measured in the septum and lateral wall in patients with and without mechanical dyssynchrony.*

Both regional glucose metabolism and MBF linearly correlated with regional myocardial work (r=0.65 and r=0.5, respectively, p<0.0001) (Figure 2A-B).

A representative example of the distribution of metabolism, perfusion and work between septal and lateral wall in patients with and without mechanical dyssynchrony is shown in Figure 3.

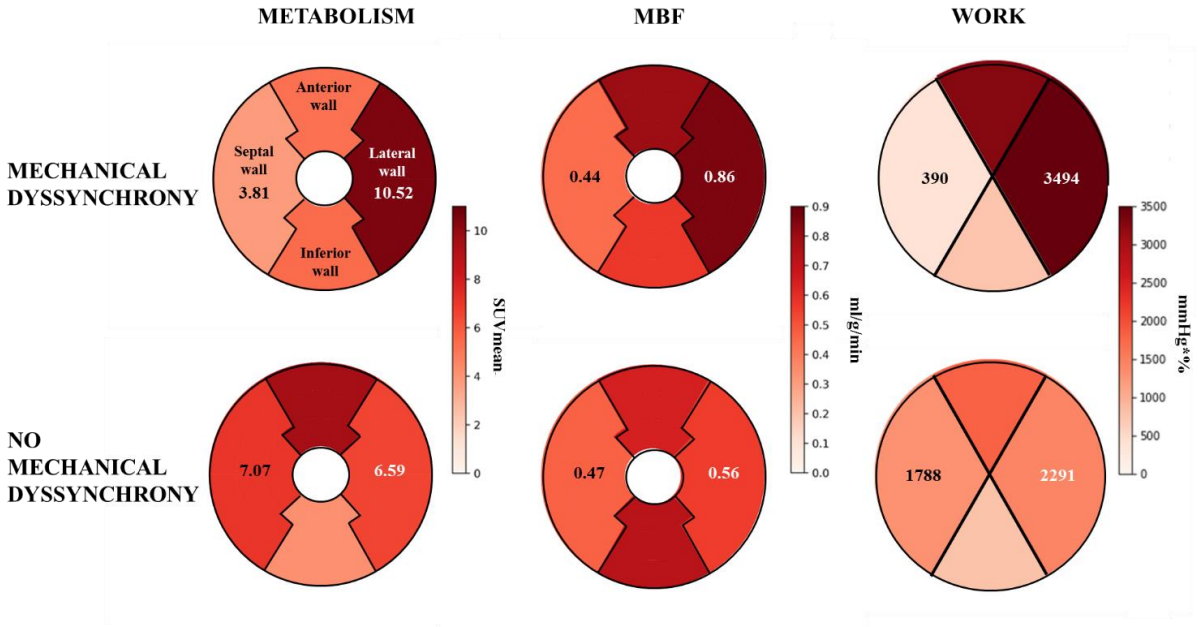

Figure 3. Representative example of the regional glucose metabolism, MBF and workload. *The figure shows lower septal compared to the lateral wall glucose metabolism, MBF and workload in a patient with mechanical dyssynchrony and relatively homogeneous glucose metabolism, MBF and workload in a patient without mechanical dyssynchrony.*

Effect of mechanical dyssynchrony on ^{18}F-FDG and MBF SLR and its relation to volumetric reverse remodelling

Patients with mechanical dyssynchrony demonstrated larger volumetric reverse remodelling 12 months after CRT compared to patients without mechanical dyssynchrony (Δ LV ESV 47±14% vs -3±20%, p<0.0001).

Patients with mechanical dyssynchrony compared to patients without mechanical dyssynchrony had a significantly lower ^{18}F-FDG SLR (0.5±0.1 vs 0.9±0.2, respectively, p=0.02). However, no differences between both groups were observed in MBF SLR (0.7±0.2 vs 0.8±0.2, respectively, p=0.2). Pre-CRT ^{18}F-FDG SLR showed a significant linear correlation with volumetric reverse remodelling 12 months after CRT (r=0.62, p=0.001) (Figure 4A). Pre-CRT MBF SLR did not show a significant correlation with volumetric reverse remodelling (r=-0.02, p=0.3) (Figure 4B).

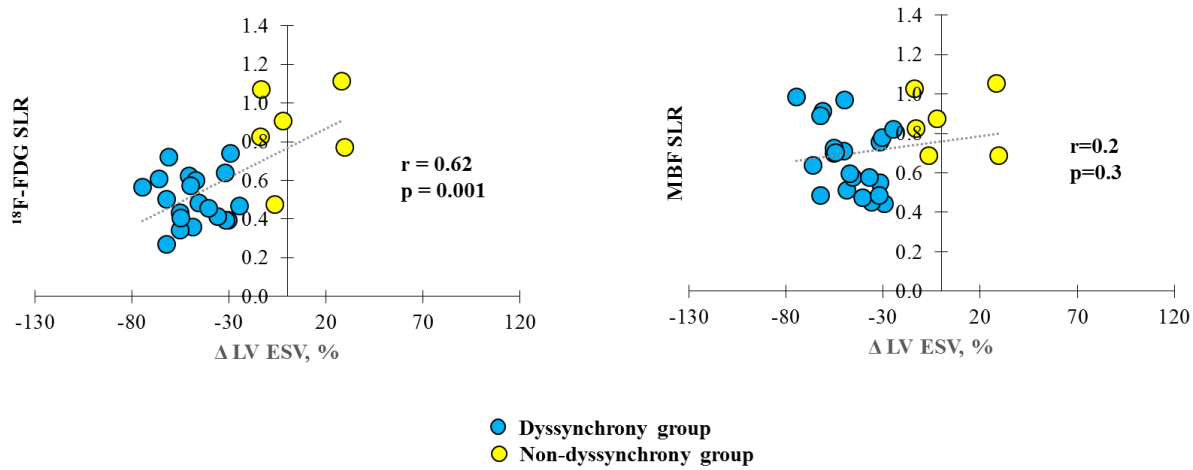

Figure 4. Correlation plots between volumetric reverse remodelling versus ^{18}F-FDG and MBF SLRs. *Correlation plot between ^{18}F-FDG SLR versus Δ LV ESV (A) and MBF SLR versus Δ LV ESV (B) in patients with and without mechanical dyssynchrony.*

Reproducibility of assessment of mechanical dyssynchrony

Echocardiographic assessment of the presence of mechanical dyssynchrony demonstrated good intraobserver ($\kappa = 0.85$ (95% CI, 0.70-0.99), $p < 0.0001$) and interobserver ($\kappa = 0.81$ (95% CI, 0.64-0.98), $p < 0.0001$) agreement.

DISCUSSION

The main finding of our study in non-ischemic CRT-candidates is the regional heterogeneity of myocardial glucose metabolism and perfusion in the presence of LV mechanical dyssynchrony, which can be attributed to the regional differences in myocardial loading conditions. Low ^{18}F-FDG SLR appeared to be highly associated with the presence of mechanical dyssynchrony and showed a significant linear correlation with volumetric reverse remodelling after CRT.

Regional myocardial ^{18}F-FDG uptake

Our study showed that non-ischemic HF patients eligible for CRT, who present with mechanical dyssynchrony, have heterogeneous regional glucose metabolism with a two-fold higher ^{18}F-FDG uptake in the lateral wall compared to septum. In contrast, patients without mechanical dyssynchrony revealed an almost homogeneous metabolism.

Previous studies have demonstrated regional ^{18}F-FDG uptake heterogeneity in the presence of ventricular conduction abnormalities. An experimental study of Ono et al. showed a significantly higher ^{18}F-FDG uptake in the lateral wall compared to the septum (88.0 ± 5.2% versus 67.4 ± 12.1%) in right ventricular pacing[38]. Similar findings in patients with dilated cardiomyopathy and LBBB were reported by Nowak et al.[39]. However, regional glucose metabolism in the presence of mechanical dyssynchrony was not investigated in these studies, hence a direct comparison to our findings cannot be performed.

Furthermore, Castro et al showed marked overall LV ^{18}F-FDG uptake heterogeneity in non-ischemic HF patients with mechanical dyssynchrony as evaluated by SPECT phase analysis[108]. This is in line with our findings, where patients with mechanical dyssynchrony showed pronounced differences in ^{18}F-FDG uptake between septal and lateral wall, hence also overall LV heterogeneity. While in the study of Castro et al, all patients without mechanical dyssynchrony also demonstrated heterogeneity in LV metabolism, even though less pronounced, we could not confirm these findings in our study cohort. This discrepancy can be due to the small number of participants (n=7) in our group of patients without dyssynchrony. However, our study population (23% without mechanical dyssynchrony) comes close to the real world situation where about 30-35% CRT-candidates do not present neither AR nor SF on echocardiography[31]. Additionally, the effect of using different modalities (SPECT vs. echocardiography) and approaches (automatic vs visual) for the assessment of mechanical dyssynchrony should not be neglected when comparing the results. Unfortunately, a more detailed comparison between both studies cannot be performed, as the study of Castro et al. did not explore LV metabolism per region.

Regional absolute MBF

Similar to ^{18}F-FDG findings, regional differences in MBF were pronounced only in the dyssynchrony patients while no differences were observed in the group without mechanical dyssynchrony.

There is a lot of controversy on regional myocardial perfusion in patients with ventricular conduction abnormalities, which may be attributed to the use of different imaging modalities, radiopharmaceuticals, study protocols and approaches for flow assessment. The study by Baller et al. showed a low absolute MBF in the septal and high MBF in the lateral wall using ^{11}C-acetate, while the study of Koepfli et al. showed a more homogeneous perfusion at rest using ^{15}O-water[96,97]. In the latter study, regional perfusion inhomogeneity was observed only during stress imaging which could be explained by the fact that 'stress' increases the imbalance in regional mechanical work resulting in higher regional perfusion changes[98]. Masci et al. reported a homogeneous ^{13}N-NH_3 MBF between LV walls in patients with LBBB and dilated cardiomyopathy, which may be explained by the inclusion of patients without advanced disease when LV dyssynchrony was not pronounced enough to induce perfusion heterogeneities as well as by the simplified approach of myocardial perfusion assessment [40].

However, also here, a direct comparison with our results cannot be performed, as abovementioned studies were not focusing on MBF in the presence of mechanical dyssynchrony, but rather analyzed an overall population with ventricular conduction abnormalities irrespective of mechanical dyssynchrony. On the other hand, findings in the literature should be mainly driven by patients with mechanical dyssynchrony, as about 65% of patients with ventricular conduction abnormalities have at least one echocardiographic sign of mechanical dyssynchrony (AR or SF)[31]. Hence, decreased perfusion in the septum compared to lateral wall as described by aforementioned studies is in line with the heterogeneous regional perfusion in the dyssynchrony group reported in our study.

Relation between regional metabolism, MBF and myocardial work

Linear correlation between workload vs metabolism and workload vs MBF, demonstrated in our study, explains the different regional distribution patterns of both parameters between patients with and without mechanical dyssynchrony.

The patient group without mechanical dyssynchrony did not present any regional heterogeneity neither in myocardial work, nor in metabolism or MBF, suggesting that despite electrical dyssynchrony on ECG, all myocardial walls equally contribute to LV contraction, requiring comparable amount of energy and oxygen. In contrast, patients with mechanical dyssynchrony showed a pronounced regional heterogeneity in all three mentioned parameters with a clear

shift of the septal values to the lower end and lateral wall towards the higher end of the spectrum. In this group of patients, septum does not significantly contribute to LV contraction, but rather wastes energy, being stretched by the opposite segments, whereas the lateral wall is the region which contributes the most to LV performance. The lateral wall, which is pre-stretched by the early activated septum, contracts with a greater force (according to Frank-Starling law), and compensates for the zero external work of the septum. Such a redistribution of myocardial work, with unloading of the early-activated septum and a higher load in the late-activated lateral wall, causes a respective adaptation of regional energy and oxygen demand which explains the high metabolism and perfusion in the lateral wall and the low values in the septum observed in our study.

Effect of mechanical dyssynchrony on SLRs and its relation to volumetric reverse remodelling

Despite the regional differences in both glucose metabolism and perfusion in patients with mechanical dyssynchrony, only ^{18}F-FDG SLR and not MBF SLR was associated with the presence of mechanical dyssynchrony.

Several studies have demonstrated that the presence of mechanical dyssynchrony is favorable for volumetric CRT response[31,34,109]. However, the inconsistent results in the literature, controversy around the definition of mechanical dyssynchrony and the lack of randomized trials have so far prevented the general acceptance and inclusion of mechanical dyssynchrony in CRT guidelines. On the other hand, relatively simple markers of mechanical dyssynchrony, such as AR and SF, used in our study and validated earlier, have been shown to be reliable and reproducible as surrogates for mechanical dyssynchrony[110]. Interestingly, in our study almost all patients with SF and/or AR had LBBB QRS morphology on surface ECG, while QRS patterns of non-dyssynchrony patients were more diverse and consisted of LBBB, right ventricular pacing and nonspecific intraventricular conduction delay. These findings demonstrate that LBBB is often, but not always associated with mechanical dyssynchrony. This might be one of the reasons why not all patients fulfilling the current criteria for CRT implantation successfully respond to this therapy and highlights the need to define other parameters that may better identify patients who will most likely benefit from CRT.

In contrast, low ^{18}F-FDG SLR is associated with the presence of at least one of these echocardiographic markers of mechanical dyssynchrony. Furthermore, ^{18}F-FDG SLR showed a good linear correlation with volumetric reverse remodelling 12 months after CRT implantation. Interestingly, the majority of patients with good reverse remodelling belonged to the group of mechanical dyssynchrony. Our findings highlight the existing relation between

mechanical dyssynchrony, ^{18}F-FDG SLR and volumetric reverse remodelling and may indicate a place for nuclear imaging in prediction of CRT response. Further studies are needed to explore this assumption further, especially in ischemic patients or patients with a QRS duration between 120-150 ms, who still remain a major challenge to improve the response rate to CRT.

Study limitations

Although ischemia was excluded in our patient cohort based on late gadolinium enhancement CMR and/or coronary angiography 3 months prior to CRT implantation and/or thorough clinical evaluation of patient history and complaints, one cannot completely rule out ischemia at the time of CRT implantation, however these chances are negligible.

In the current study, clinically used reconstruction algorithms and software programs were applied without correcting for partial volume effect, which may lead to a slight underestimation of the true tracer concentration in the thinned LV walls.

We did not perform absolute quantification of cardiac glucose metabolism, but only glucose uptake defined by SUVmean was used in the current study. Quantification of glucose consumption as well as using other metabolic PET tracers such as ^{11}C-acetate could help to better understand the pathophysiological mechanisms and metabolic adaptations during abnormal LV activation patterns.

Another limitation is the difference in LV segmentation models used for perfusion/metabolism (17 AHA model) and regional myocardial work (18 segment model). However, since regional values were represented as averages of corresponding segments and since the difference between both segmentation models is only the exclusion of the small apical region, we believe that the influence on the correlation between SLRs and work is negligible.

CONCLUSIONS

Non-ischemic HF patients with mechanical dyssynchrony demonstrate heterogeneous regional glucose metabolism and MBF, while patients without mechanical dyssynchorny do not, which can be attributed to alterations in regional myocardial workload between both groups. ^{18}F-FDG-SLR appeared to be highly associated with the presence of mechanical dyssynchrony and should be explored as a possible predictor for favorable CRT response.

CHAPTER III

Left ventricular regional glucose metabolism in combination with septal scar extent identifies CRT responders

Submitted to JACC - CVI

Ganna Degtiarova, MD[a,b], Piet Claus, PhD[c], Jürgen Duchenne, PhD[c,d], Jan Bogaert, MD, PhD[e], Johan Nuyts, PhD[a], Camilla Kjellstad Larsen, MD[f], John M. Aalen, MD[f,] Jan Gunnar Fjeld, MD, PhD[g], Caroline Stokke, MD, PhD[g], Einar Hopp, MD, PhD[g], Otto Armin Smiseth, MD, PhD[f], Jens-Uwe Voigt, MD, PhD[c,d], Olivier Gheysens, MD, PhD[a,b]

a) Nuclear Medicine and Molecular Imaging, Department of Imaging and Pathology, KU Leuven, Leuven, Belgium
b) Nuclear Medicine, University Hospitals Leuven, Belgium
c) Department of Cardiovascular Sciences, KU Leuven, Leuven, Belgium
d) Department of Cardiovascular Diseases, University Hospitals Leuven, Leuven, Belgium
e) Department of Radiology, University Hospitals Leuven, Leuven, Belgium
f) Department of Cardiology, Oslo University Hospital, Oslo, Norway
g) Division of Radiology and Nuclear Medicine, Oslo University Hospital, Oslo, Norway.

This chapter addresses the following research questions:

- Can ^{18}F-FDG PET reliably guide the therapy of HF patients**?**

ABSTRACT

Objectives: We investigated if regional left ventricular (LV) glucose metabolism in combination with myocardial scar could predict response to cardiac resynchronization therapy (CRT).

Background: CRT is effective in selective heart failure (HF) patients, but non-response rate remains high. Positron emission tomography (PET) may provide a better insight into the pathophysiology of LV remodelling, however, its role for evaluating and selecting patients for CRT remains uncertain.

Methods: Consecutive CRT eligible HF patients underwent echocardiography, cardiac magnetic resonance (CMR) and ^{18}F-fluorodeoxyglucose (FDG) PET within 1 week before CRT implantation. Echocardiography was additionally performed 12 months after CRT and end-systolic volume reduction ≥15% was defined as CRT response. Septal-to-lateral wall (SLR) FDG uptake ratio was calculated from static FDG images. Late gadolinium enhancement (LGE) CMR was analyzed semi-quantitatively to define scar extent.

Results: We evaluated 88 patients (67±10y, 72% males). ^{18}F-FDG SLR showed a linear correlation with volumetric reverse remodelling 12 months after CRT (r=0.41, p=0.0001). In non-ischemic HF patients, low FDG SLR alone predicted CRT response with sensitivity and specificity of more than 80%, however in ischemic HF patients specificity decreased to 46%, suggesting that in this cohort low SLR can also be caused by the presence of septal scar. In the multivariate logistic regression model, including low FDG SLR, extent of septal scar and current CRT guideline parameters, only low FDG SLR and septal scar remained associated with CRT response. Their combination could predict CRT response with sensitivity and specificity of 80% and 83%, respectively.

Conclusions: FDG SLR can be used as a predictor of CRT response and combined with septal scar extent CRT responders can be distinguished from non-responders with high diagnostic accuracy. Further studies are needed to verify whether this imaging approach can prospectively be used to optimize patient selection.

INTRODUCTION

Ventricular conduction disturbances are associated with adverse cardiac remodelling and severely impaired left ventricular (LV) function, resulting in low quality of life and increased cardiovascular morbidity and mortality[111]. Cardiac resynchronization therapy (CRT) has emerged as a promising therapy for these patients, however, the non-response rate of up to 40% warrants an optimization of selection criteria for CRT candidates and remains an active area of investigation[26]. In search of novel hallmarks for successful CRT response, an emphasis is put on non-invasive cardiac imaging modalities, such as cardiac magnetic resonance (CMR) and nuclear imaging. The latter can provide deeper insight into the pathophysiology of LV remodelling, and may play a role in the selection of HF patients, who will most likely benefit from CRT**.**

We have demonstrated in previous work that non-ischemic patients with left bundle branch block (LBBB) have a typical pattern of low septal and high lateral wall glucose metabolism, as assessed with ^{18}F-fluorodeoxyglucose positron emission tomography/computed tomography (FDG PET/CT) before CRT implantation [112]. These regional metabolic alterations were most pronounced in the presence of mechanical dyssynchrony and correlated with regional and temporal inhomogeneity of myocardial work, consistent with a reduced early systolic loading of the septum versus an increased loading of the late activated lateral wall[106,113]. We and other investigators have shown, that this typical pattern of differential regional glucose metabolism before CRT implantation immediately normalizes after CRT, suggesting that FDG uptake might be a promising marker to optimize patient selection for CRT[37,39]. Furthermore, in a subgroup of non-ischemic HF patients, we have demonstrated that low FDG SLR before CRT implantation is associated with favorable volumetric reverse remodelling 12 months after CRT implantation [113]. However, in ischemic HF patients low FDG SLR can also be caused by the presence of septal scar. In general, the presence and extent of myocardial scar in CRT candidates, assessed with late-gadolinium enhancement (LGE) CMR, has been advocated to be an important predictor of negative CRT response, making scar assessment before CRT implantation of paramount importance [114].

Therefore, in a prospective multicenter study we aimed to investigate whether regional glucose metabolism, derived from FDG-PET, together with septal scar, assessed by LGE-CMR, could be used to distinguish CRT responders from non-responders.

MATERIAL AND METHODS

Study Population

Patients referred for CRT implantation between August 2015 and November 2017 were prospectively recruited at the University Hospitals Leuven, Leuven, Belgium and Oslo University Hospital, Oslo, Norway. Inclusion for CRT was based on the 2013 ESC guidelines[8]. The main exclusion criteria were presence of right bundle branch block, recent myocardial infarction, valve surgery within 90 days prior to enrolment, history of heart transplantation or listed for heart transplantation, implanted LV assist device, severe aortic stenosis and uncorrected congenital heart disease. The study was approved by the local institutional ethics committees and all patients gave written and informed consent prior to inclusion. The WORK-CRT study was registered at ClinicalTrials.gov (NCT02537782).

Clinical and physical evaluation

The medical history as well as clinical and laboratory data of all patients were thoroughly collected before CRT implantation. The underlying cause of HF was established based on coronary angiography, nuclear imaging, CMR or patient's medical history. Each patient underwent 12-lead ECG recording to evaluate QRS width and the presence of LBBB was defined according to ESC 2013 criteria[8].

Echocardiography

All patients underwent a standard two-dimensional echocardiography within 1 week before and 12 months after CRT implantation using commercially available systems (Vivid E9 and E95, GE Vingmed Ultrasound, Horten, Norway). Acquired data were stored digitally and analysed off-line using an EchoPAC workstation (version 202, GE Vingmed Ultrasound). LV end-diastolic volume (EDV), end-systolic volume (ESV) and LV ejection fraction (LVEF) were measured using the modified biplane Simpson's method. Volumetric remodelling after CRT was defined as the relative reduction in LV ESV between baseline and 12 months post-CRT (Δ LV ESV,% = (ESV 12M – ESV baseline) / ESV baseline) and an ESV reduction $\geq$ 15% was considered as CRT response. All echocardiographic analyses were performed in Leuven, Belgium.

FDG-PET/CT

Static FDG-PET was performed 1 week before CRT implantation on a Biograph HiRez 40 or 16 PET/CT (Siemens, Erlangen, Germany) or Discovery MI PET/CT (GE Healthcare, Chicago, IL, USA). A scout acquisition followed by a low-dose CT (80 kVp, 11 mAs) was performed for optimal patient positioning and subsequent attenuation correction of PET emission data. In order to facilitate myocardial glucose consumption over fatty acid uptake, patient preparation consisted of an intravenous hyperinsulinemic euglycemic clamping approach in Leuven, while an oral glucose loading method was applied in Oslo, as previously described[86]. After reaching a steady state plasma glucose level, 4.25 MBq/kg FDG was administered intravenously and a 40-minute acquisition was performed approximately 45 minutes after tracer administration.

All PET images were reconstructed using ordered-subsets expectation maximization algorithms (4 iterations and 8 subsets), matrix size 256x256 and a 5.0 mm Gaussian filter.

FDG static images were generated from the whole 40 min acquisition and were analyzed in Leuven, using in-house developed software as previously published [88]. FDG uptake was calculated per segment, using a 17 segment polar map, and expressed as mean standardized uptake value (SUVmean). Septal and lateral wall FDG uptake was calculated as the averaged SUVmean of the five corresponding segments respectively. FDG SLR was calculated by dividing mean FDG uptake in the septum by mean uptake in the lateral wall.

CMR and scar analysis

CMR was performed prior to CRT implantation using a 1.5 Tesla Ingenia in Leuven (Philips Healthcare, Best, the Netherlands) or Aera in Oslo (Siemens, Erlangen, Germany). LGE images were acquired during steady state after intravenous injection of 0.15 mmol/kg gadoterate meglumine (Doteram™, Guerbet, Villepinte, France) and were analyzed visually by an experienced radiologist to determine the presence of scar, both of ischemic and non-ischemic origin, and semiquantitatively to calculate scar extent. Scar analysis was performed on stacks of multiple short axis images on magnitude reconstructed LGE using the *Segment software v2.0 R5270* and a 17 segment model was generated[115]. Manual correction of non-pathological LGE areas was applied when deemed necessary by the investigator. The total scar extent and scar extent in each of the LV walls, with the main focus on the septum, was calculated and reported as percentage of total LV myocardial volume in the diastolic phase.

Cardiac resynchronization therapy

CRT implantation was performed according to the 2013 ESC guidelines[107]. Pacing electrodes were placed in the right atrium, right ventricle and LV with LV pacing leads preferably positioned in the lateral and postero-lateral venous branches, guided by coronary venography. After implantation, the device was set to bi-ventricular pacing in all patients.

Statistical Analysis

Statistical analysis was performed using MedCalc ® v.10.3.0 Software. Shapiro-Wilk test was used to check the normality of data distribution. Normally distributed continuous variables were expressed as mean ± standard deviation, otherwise median and interquartile range were used. Categorical variables were represented as percentages. Paired and unpaired t-tests were used for comparison of normally distributed continuous variables, Mann-Whitney U test was applied for not normally distributed variables, while χ^2 test was used for categorical variables. The correlation between parameters was assessed with Pearson correlation coefficients. To determine independent predictors of LV ESV changes ≥15%, multivariate stepwise logistic regression analysis was performed. ROC analysis was applied on continuous parameters to identify the optimal cut-off values, while area under the curve (AUC) was used to assess the overall model performance. To assess the diagnostic performance of categorical parameters, a 2x2 contingency table was used. All statistical tests were 2-tailed. A p-value of less than 0.05 was considered statistically significant.

RESULTS

A total of 88 patients meeting the eligibility criteria were included in the study. Patient characteristics are summarized in Table 1.

Table 1. Baseline patients characteristics

Parameter	**All patients (n=88)**	**Responders (n=48)**	**Non-responders (n=40)**
Male (% of total)	63 (72%)	28 (58%)	35 (88%)*
Age (years)	67±10	68±10	64±11
Weight, kg	80±16	77±14	83±16
Diabetes mellitus (% of total)	14 (16%)	8 (17%)	6 (15%)
Systolic blood pressure (mmHg)	125±20	129±18	120±20*
Diastolic blood pressure (mmHg)	69±11	72±12	66±10*
NYHA class:	2.47±0.6	2.44±0.5	2.50±0.7
Heart failure etiology: -ischemic -non-ischemic	 41 (47%) 47 (53%)	 13(27%) 35(73%)	 28(70%)* 12(30%)*
Electrocardiographic parameters			
QRS width (ms)	168±23	167±21	168±26
LBBB (ESC 2013)	76 (86%)	45 (94%)	31 (78%)*
Echocardiographic parameters (pre-CRT):			
EDV (ml)	188±85	172±65	208±101
ESV (ml)	134±69	123±53	148±84
EF (%)	30±8	31±8	29±8
Echocardiographic parameters (post-CRT):			
EDV (ml)	154±78#	122±54#	197±86*
ESV (ml)	101±67#	71±39#	141±76*
EF (%)	38±10#	43±9#	31±8*
Heart failure therapy:			
β-blockers	80 (91%)	42 (88%)	38 (95%)
ACEi/ARB	82 (93%)	46 (96%)	36 (90%)
Aldosterone antagonists	42 (48%)	23 (48%)	19 (48%)

**p<0.01 compared to responders; #p<0.0001 compared to the baseline*

LV volumes at 12 months follow-up were available in 84 patients, 4 patients did not have echocardiography after 1 year due to HF deterioration (n=2), LV assist device implantation (n=1) and heart transplantation (n=1). FDG-PET/CT was performed in all 88 patients, out of whom 53 patients also underwent LGE CMR.

Forty-eight (55%) patients were considered responders, while 40 (45%) patients including those who did not complete the study protocol were non-responders.

Responders were more often female, had more often LBBB pattern, had less often ischemic cardiomyopathy and had less dilated hearts compared to non-responders.

FDG septal-to-lateral wall ratio

Among patients who underwent FDG-PET/CT, 45 patients received an euglycemic hyperinsulinemic clamping protocol and 43 patients underwent an oral glucose loading protocol, with an equal distribution of both methods between responders and non-responders (p=0.5 for the difference between groups). Regional FDG SUVmean values in the septum and lateral wall were significantly higher whereas FDG SLR values were significantly lower in the group with euglycemic hyperinsulinemic clamping compared to the oral glucose loading group (all p<0.01) (Figure 1, Table 2).

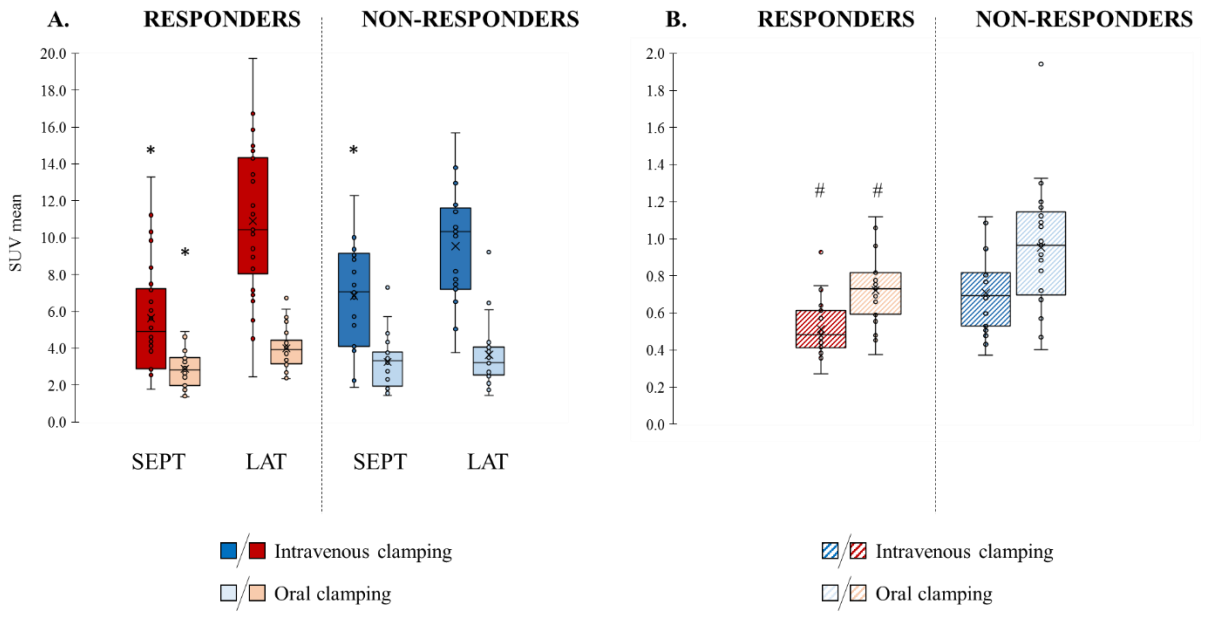

Figure 1. Glucose metabolism. *Regional FDG uptake (A) and FDG septal-to-lateral wall uptake ratio (B), shown for CRT responders and non-responders and both clamping approaches. * p<0.001 compared to lateral wall, # p<0.0001 compared to non-responders.*

Table 2. ^{18}F-FDG PET results for responders and non-responders and both clamping approaches. FDG uptake is represented as mean standardized uptake value (SUVmean)

	Responders (n=48)			Non-responders (n=40)		
	All patients (n=48)	**IV clamping (n=26)**	**Oral glucose loading (n=22)**	**All patients (n=40)**	**IV clamping (n=19)**	**Oral glucose loading (n=21)**
^{18}F-FDG septum, SUV	4.4±2.7	5.6±3.0$^{\&}$	2.9±1.0	5.0±2.9	6.8±2.9$^{\&}$	3.3±1.5
^{18}F-FDG lateral wall, SUV	7.7±4.6*	10.9±4.0* $^{\&}$	4.0±1.2*	6.4±3.9*	9.5±3.2*$^{\&}$	3.6±1.8
^{18}F-FDG SLR	0.6±0.2$^{\#}$	0.5±0.1$^{\&\#}$	0.7±0.2$^{\#}$	0.8±0.3	0.7±0.2$^{\&}$	1±0.3

*SLR: septal to lateral wall ratio of FDG SUVmean; $^{\#}p<0.0001$ compared to non-responders; *p<0.001 compared to the septum; $^{\&}p<0.01$ compared to oral loading.*

Overall, septal glucose uptake was significantly lower compared to the lateral wall in both responders (n=48, 4.4±2.7 vs 7.7±4.6, p<0.0001) and non-responders (n=40, 5.0±2.9 vs 6.4±3.9, p=<0.001), but the difference was more pronounced among responders (Table 2). FDG SLR was also significantly lower in CRT responders compared to non-responders (0.6±0.2 vs 0.8±0.3, p<0.0001) (Table 2).

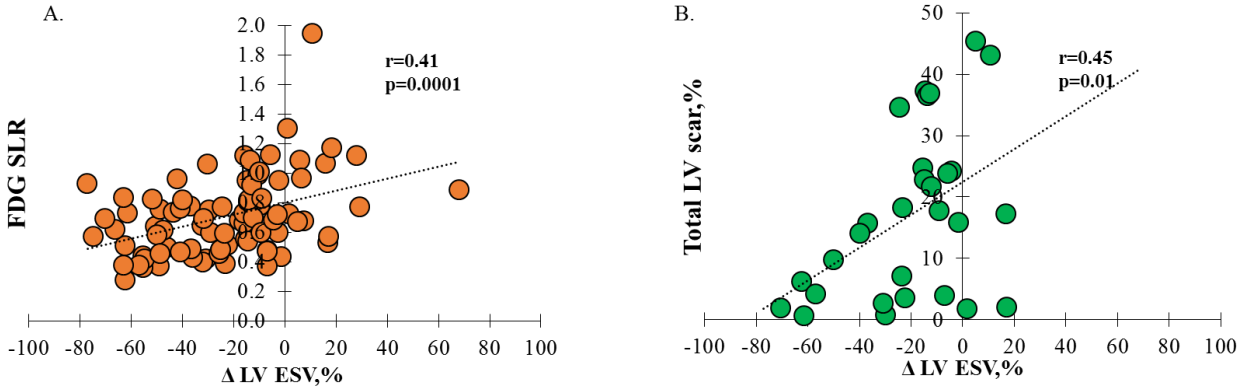

Figure 2. Correlation plots between volumetric reverse remodelling post CRT versus FDG SLR (A) and the total amount of LV scar (B), assessed with PET and CMR, respectively, before CRT. *Note that scar extent is expressed as a percentage of total LV volume.*

FDG SLR significantly and linearly correlated with volumetric reverse remodelling 12 months after CRT (r=0.41, p=0.0001) and showed a high overall performance for the prediction of CRT response (AUC 0.73 [0.62-0.84], p=0.0001) (Figure 2A, 3A). In non-ischemic HF patients, FDG SLR ≤0.75 and ≤0.82 for respectively euglycemic hyperinsulinemic clamping and oral glucose loading protocol, could predict CRT response with sensitivity and specificity of more than 80% (Figure 3B, C). Applying these thresholds to the ischemic HF population resulted in a sensitivity of 85%, but a decrease in specificity to 46%.

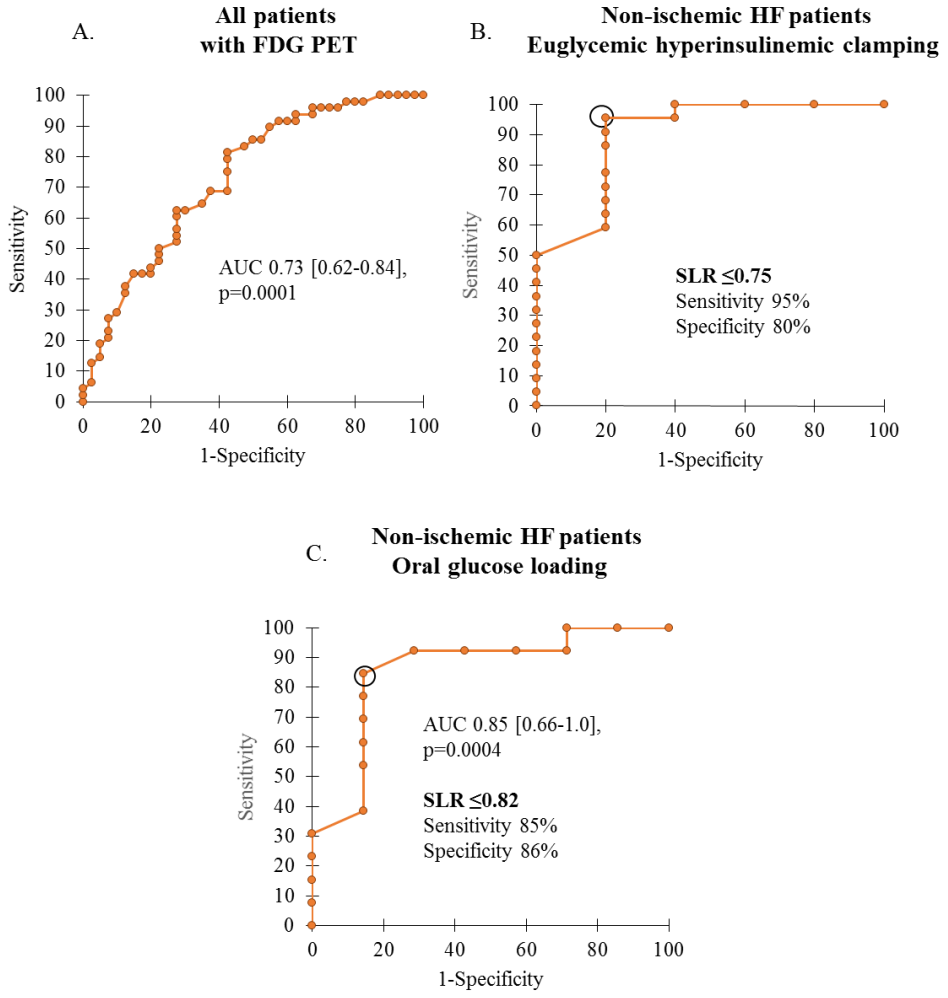

Figure 3. Association of FDG SLR with CRT response in different groups of patients. *ROC curve analysis for FDG SLR to predict CRT response, shown in all patients (A), in non-ischemic patients with euglycemic hyperinsulinemic clamping (B) and non-ischemic patients with an oral glucose loading (C).*

Scar assessment LGE-CMR

In patients with available LGE CMR scans, scar was observed in 33 patients, among whom 20 patients had scar of ischemic origin, 9 patients had non-ischemic scar and 4 patients had evidence for both ischemic and non-ischemic scar. The remaining patients (n=20) did not have any evidence for scar. Scar was mainly present in the septum (n=25), followed by the inferior (n=19), anterior (n=18) and lateral (n=17) wall and was larger and more often encountered in non-responders compared to responders (Table 3).

There was a significant linear correlation between the total amount of LV scar and 12 months reverse remodelling after CRT (r=0.45, p=0.01) with a lower total scar extent being associated with more pronounced reverse remodelling (Figure 2B).

Table 3. CMR LGE findings represented for different patient groups

Scar characteristics	**All patients (n=53)**	**Responders (n=35)**	**Non-responders (n=18)**
Scar extent, % of the LV volume	2.02 [0-17.8]	0 [0-4.0]	20.2 [3.9-36.5]*
Absence of scar, patients	20 53%)	19 (54%)	1 (6%)*
Presence of scar, patients:	33 (62%)	16 (46%)	17 (95%)*
- Ischemic scar, patients	20 (38%)	8(23%)	12 (67%)*
- Non-ischemic scar, patients	9(17%)	7(20%)	2(11%)
- Combined scar, patients	4 (8%)	1(3%)	3 (17%)
Scar location:			
- Septum, patients	25 (47%)	12(34%)	13 (72%)*
- Lateral wall, patients	17 (32%)	6 (17%)	11 (61%)*
- Anterior wall, patients	18 (34%)	7 (20%)	11 (61%)*
- Inferior wall, patients	19 (36%)	9 (26%)	10 (56%)*

**p<0.05 compared to responders*

Combined assessment of FDG SLR and LV scar for predicting CRT response

In the multivariate logistic regression model with FDG SLR cut-offs, extent of septal scar and current parameters listed in CRT guidelines, including the presence of LBBB, LVEF and QRS width, FDG SLR (p=0.004) and the extent of septal scar (p=0.004) were the only

significant independent predictors for CRT response (Table 4). The combination of FDG-SLR and septal scar could predict CRT response with a sensitivity, specificity and AUC of 80%, 83% and 0.88 [0.78-0.98], respectively (Figure 4).

Table 4. Multivariate logistic regression with a stepwise approach with ESV reduction≥15% as dependent variable

Parameter	P-value
FDG SLR cut-off*	**0.004**
Septal ischemic scar, %#	**0.004**
LBBB	NS
LV EF, %	NS
QRS width, ms	NS

** - SLR ≤0.75 for euglycemic hyperinsulinemic clamping and SLR ≤0.82 for an oral glucose loading; # - scar presented as a percentage of the whole LV volume*

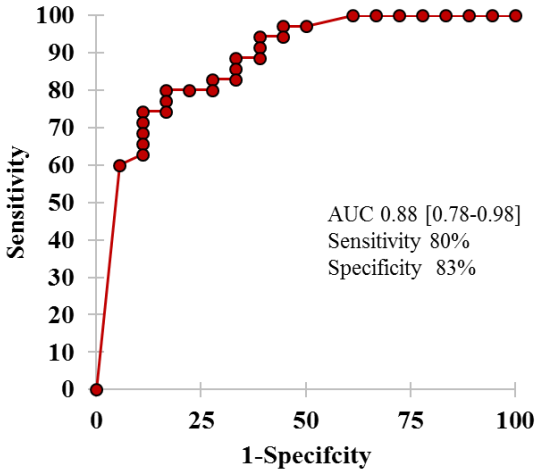

y =-1.4 – 0.23 x septal scar (%) + 3.4 x ^{18}F-FDG SLR cut-off (1)

Figure 4. Performance of the combined assessment of FDG SLR and septal scar for the prediction of CRT response. *Note that extent of septal scar is represented as percentage of total LV myocardial volume, while FDG SLR cut-off implies SLR ≤0.75 for euglycemic hyperinsulinemic clamping and SLR ≤0.82 for an oral glucose loading. In the logistic regression equation, represented below the graph, the coefficient for FDG SLR equal to 1 should be used when FDG SLR is below the mentioned cut-off, otherwise 0 should be used as a coefficient.*

DISCUSSION

This is the first study to investigate whether FDG SLR together with LV scar analysis could be used to predict CRT response. The main findings were that (i) low FDG SLR and septal scar were independent predictors of CRT response and (ii) a combination of both parameters can separate CRT responders from non-responders with high diagnostic accuracy.

In previous work focusing on non-ischemic CRT candidates, we have demonstrated that FDG SLR reflects regional differences in glucose metabolism that are proportional to regional myocardial work. We have also shown, that in non-ischemic HF patients low FDG SLR is highly associated with the presence of mechanical dyssynchrony and significantly correlates with volumetric reverse remodelling 12 months after CRT [112,113]. In these patients, the lower the SLR, the larger is the contribution of lateral wall to LV contraction and output, and the lower is the contribution of the septum, which might even waste work by being stretched from the opposing lateral segments. When SLR is close to one, both walls contribute equally to LV contraction, leaving little room for functional improvement after CRT.

In the current study we explored the predictive value of ^{18}F-FDG SLR in a larger group of HF patients, with both ischemic and non-ischemic origin. In this cohort, we have also shown a linear correlation between FDG SLR and volumetric remodelling 12 months after CRT, with a lower SLR being associated with more favorable remodelling.

The different patient preparation protocols for FDG-PET in both centers resulted in more pronounced differences in regional glucose metabolism with the euglycemic hyperinsulinemic clamping method, as compared to oral glucose load. The latter was reflected in a different range of SLRs, necessitating two separate FDG SLR cut-off values for CRT prediction, depending on the method used. In our study, FDG SLR cut-off values were defined in the non-ischemic subgroup, where differences in regional glucose metabolism are mainly attributed to regional changes in myocardial work and not to the presence of scar. As expected, high specificity of defined cut-off values in non-ischemic HF patients, decreased significantly when applied to the ischemic population, in whom a low SLR can also be caused by the presence of septal scar, hence limiting the potential of regional functional recovery. Therefore, a low SLR remains always sensitive, but is less specific in the presence of ischemic disease, and should therefore be accompanied with septal scar assessment before CRT implantation.

The impact of septal scar on FDG SLR was clearly demonstrated when comparing regional glucose metabolism between responders and non-responders. Low FDG SLR in non-responders

was mainly driven by more frequently encountered septal wall scar, hence severely impaired glucose uptake, while low FDG SLR among responders, represented by predominantly non-ischemic HF patients, was mainly caused by differences in regional work.

The negative influence of scar on CRT response previously described by others, has been confirmed in our study by the linear correlation between total amount of LV scar and volumetric reverse remodelling after CRT [114]. This confirms the hypothesis, that successful CRT requires not only the presence of correctable dyssynchrony, but also enough viable myocardium to restore LV function. Not only the presence, but also the location of scar has been advocated to be another important predictor of CRT response with septal and lateral wall scar being associated with a lack of CRT response [116,117]. The latter is not surprising as both septal and lateral wall are regions which are affected by a LBBB-like conduction delay and which are the target of resynchronization therapy. In our study, the absence of lateral scar in CRT candidates is already incorporated in the definition of low SLR, as the presence of lateral scar would only increase FDG SLR. Therefore, only septal scar needs to be distinguished as it can lead to a low FDG SLR.

Multivariate logistic regression analysis, including the extent of scar in septal wall and FDG SLR cut-offs in combination with parameters currently listed in CRT guideline (presence of LBBB, QRS duration and LVEF), revealed that only FDG SLR and septal scar extent were independent parameters of CRT response. Patients with low SLR and smaller septal scar extent had a higher chance of favorable CRT response. The fact that the remaining parameters, were not withheld is somewhat expected, because presence of LBBB and wide QRS are more often encountered in patients with low SLR.

The importance of combining FDG SLR and septal scar, is highlighted by two representative patient cases in Figure 5. Both patients have similar low FDG SLRs below the cut-off value and are considered possible responders. However, the low FDG SLR in the first patient (left) is mainly driven by a large septal scar, unlikely to respond to CRT, while the low FDG SLR in the second patient (right) is solely attributed to a difference in regional myocardial work, hence suggestive for favorable response. Therefore, FDG SLR analysis should be accompanied by scar recognition in order to optimize selection of patients, who will most likely benefit from CRT.

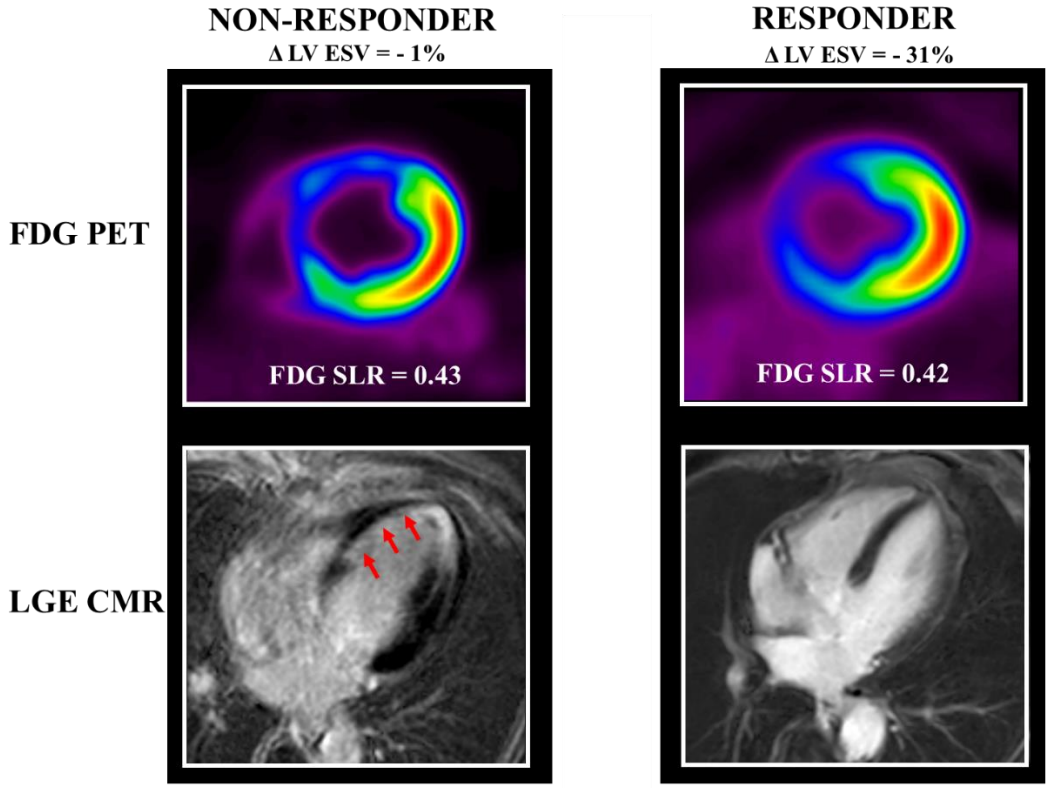

Figure 5. A representative example of a CRT responder and a non-responder highlighting the need to combine FDG SLR with septal scar assessment. *Both patients have similar low SLR below the predefined cut-off value and are considered to be potential responders. However, careful analysis of LGE CMR demonstrates, that the low SLR in one patient (left) is mainly driven by a septal scar that decreases the potential for regional reverse remodelling, making the patient unlikely to respond to CRT. In contrast, the low SLR in the other patient (right) is solely attributed to the difference in regional myocardial work, suggestive of a responder.*

Limitations:

In the current study we propose low FDG SLR as reliable marker of CRT response, but one should be aware of the radiation burden and the dedicated patient preparation protocol for FDG-PET. In non-ischemic HF patients, who usually do not have indications for nuclear imaging, risks and benefits should be assessed individually and search for other CRT predictors might be considered [31].

In our study, definition of CRT response was based only on the magnitude of volumetric reverse-remodelling which has been shown to correlate with clinical improvement and survival during long-term follow-up. It is, however, by no means an ideal surrogate parameter and an outcome analysis will have to confirm our conclusions in the future[118].

CMR was not feasible in 40% of patients due to the presence of implantable devices or poor renal function. It would be interesting to explore the feasibility to reliably assess septal scar with alternative modalities, such as echocardiography or nuclear imaging in patients with contra-indications for CMR or in centers with low CMR availability or expertise.

CONCLUSIONS

Low FDG SLR predicts CRT response with high sensitivity and specificity, especially in non-ischemic heart failure patients. Combination of low FDG SLR with septal scar further increases the diagnostic accuracy to reliably separate CRT responders from non-responders. Further studies are needed to verify whether this imaging approach can prospectively be used to better identify patients who will most likely respond to CRT.

CHAPTER IV

Assessment of myocardial perfusion with ^{99m}Tc-Teboroxime using a dedicated cardiac SPECT camera

[Manuscript in preparation]

This chapter addresses the following research questions:

- Are the characteristics of ^{99m}Tc-Teboroxime suitable for perfusion assessment?
- Is it feasible to image and quantify myocardial perfusion with ^{99m}Tc-Teboroxime using a dedicated cardiac camera in a pig model?

ABSTARCT

Aim: Absolute myocardial blood flow (MBF) and myocardial flow reserve (MFR) provide additional diagnostic and prognostic information compared to relative perfusion in patients with coronary artery disease (CAD). The introduction of dedicated cardiac cadmium-zinc-telluride *(*CZT) SPECT cameras enables dynamic imaging and makes perfusion quantification feasible. However currently used ^{99m}Tc-based tracers suffer from non-linear extraction at higher flow rates. Here, we aim to assess MBF and MFR in a pig model using a CZT SPECT and ^{99m}Tc-Teboroxime, a radiotracer with linear myocardial uptake and rapid myocardial clearance.

Materials and methods: Healthy (n=5) and infarcted (n=3) pigs underwent a two-day rest-adenosine stress imaging protocol. A 30-min dynamic acquisition (Discovery NM530c) was performed after administration of 370 MBq ^{99m}Tc-Teboroxime. Since no kinetic model for ^{99m}Tc-Teboroxime is commercially available, MBF quantification was performed using different commercially available and validated models for ^{99m}Tc-tetrofosmin, ^{99m}Tc-sestamibi and ^{201}Tl. In healthy pigs SPECT-derived MBF values, obtained with each of the algorithms, were correlated with microspheres-derived MBF (a gold standard), in order to evaluate the algorithm that best fitted the results of ^{99m}Tc-Teboroxime. This algorithm was further applied for the quantification of SPECT MBF in infarcted pigs.

Results: ^{99m}Tc-Teboroxime was successfully synthesized and demonstrated a fast wash-out from the myocardium. Segmental SPECT- and microspheres-derived MBF was homogeneous across the heart in healthy pigs. However, among 2 healthy animals with completed rest-stress imaging protocol, increased flow at stress was only observed in one case, while in another animal MFR was around 1. None of the kinetic models perfectly reflected the kinetics of ^{99m}Tc-Teboroxime, but the lowest bias with microspheres-derived MBF values was observed with 1CM ^{99m}Tc-sestamibi model (0.32 ml/g/min). However, the limits of agreement were high (LOA: -0.30 – 1.95 ml/g/min). This model was further applied for perfusion quantification in infarcted pigs, where a heterogeneous MBF was observed, with a lower perfusion in the infarcted region.

Conclusion: Non-invasive imaging and assessment of absolute MBF and MFR with ^{99m}Tc-Teboroxime is feasible using a dedicated cardiac SPECT camera. Our study demonstrated the fast myocardial wash-out that could enable rapid serial studies, but further optimization of kinetic models specifically developed for ^{99m}Tc-Teboroxime and comparison to routinely used ^{99m}Tc- tracers is warranted to evaluate possible clinical applications.

INTRODUCTION

Coronary artery disease (CAD) is the leading cause of morbidity and mortality in the United States, Europe and developed countries. Moreover, as the population ages and life expectancy increases, cardiovascular diseases will have an even bigger socio-economic impact and therefore multimodal imaging of CAD still remains of major clinical and research interest [119,120].

Radionuclide myocardial perfusion imaging (MPI), represented by single photon emission tomography (SPECT) and positron emission tomography (PET), has been widely implemented in the work-up of stable patients with suspected or known CAD for several decades. MPI has proven its value to assess myocardial ischemia, treatment choice and prognosis [67,68,121]. SPECT MPI is limited to only visual or semi-quantitative assessment of myocardial perfusion, which may cause an underestimation of the extent of atherosclerotic burden and ischemia, especially in patients with multi-vessel or main stem disease [69,70]. In contrast to SPECT, PET allows dynamic imaging with subsequent computation of quantitative information on myocardial blood flow (MBF) and myocardial flow reserve (MFR), hereby overcoming the shortcomings of SPECT. Despite obvious advantages for PET MPI, wide implementation of PET imaging is currently hampered by a relatively high cost, limited availability and requirement of an on-site cyclotron or generator. As consequence, the majority of MPI (especially in Europe) is still performed on conventional SPECT cameras, acknowledging the limitations of the technique.

However, the advent of new cardiac dedicated SPECT cameras with either multi-pinhole or multi-parallel hole solid state cadmium-zinc-telluride collimators (CZT), represented by Discovery NM 530c (GE Healthcare, Haifa, Israel) and D-SPECT (Spectrum-Dynamics, Cesarea, Israel), respectively, revolutionized the field of nuclear cardiology, enabling for the first time dynamic SPECT acquisition. Indeed, recent preclinical and clinical studies have demonstrated a good correlation between MBF/MFR values, derived from different perfusion tracers (^{99m} Tc-sestamibi, ^{99m}Tc-tetrofosmin and ^{201}Tl-thallium), and either microspheres or ^{15}O-H_20 as reference standard [76,78]. Nevertheless, the ^{99m}Tc-labeled radiotracers are suboptimal for an accurate perfusion assessment due to their relatively low extraction fraction, especially at high flow rates, that may underestimate the apparent flow increase at stress [79–81]. On the other hand, ^{201}Tl has a higher and more linear extraction fraction, but has worse image quality due to low photon energy and exposes patients to a higher radiation. With the advent of dedicated cardiac cameras and limitations of current SPECT tracers, the interest in a

previously developed imaging agent ^{99m}Tc-Teboroxime has been renewed. ^{99m}Tc-Teboroxime has a high and linear extraction fraction at high flow rates and fast myocardial kinetics[81–83]. The latter impeded its wide use with conventional Anger cameras, but can be a valuable hallmark in the era of cardiac-dedicated SPECT systems.

Therefore, the aim of our study was to assess the feasibility to image myocardial perfusion and quantify MBF and MFR with ^{99m}Tc-Teboroxime using a dedicated cardiac camera in a pig model in comparison to colored microspheres serving as reference.

METHODS

Radiosynthesis

Cold kits for radiosynthesis of ^{99m}Tc-Teboroxime were made and supplied in lyophilized form by the radiopharmacy unit of KU Leuven according to previously published reports (US patent 4,705,849 (1987) and 6,056,941 (2000) by A. Nunn and E. Schramm). Radiosynthesis was performed according to the protocol described by Zheng et al. [122]. In brief, ^{99m}Tc-Teboroxime was synthesized by adding 740 MBq of ^{99m}Tc-pertechnetate to the vial. The vial was heated for 5 minutes in a boiling water bath and then cooled to room temperature before adding 9 ml of 20% propyleneglycol solution. Radiochemical purity of the prepared radiotracer was determined by radio high pressure liquid chromatography on a XBridge C18 column (Jana, 4.6 mm x 150 mm, 5µm).

Biodistribution

Ex vivo biodistribution studies with ^{99m}Tc-Teboroxime were performed in 12 wild type mice (n = 3 per time point, weight 26-34 g). Mice were anesthetized with 2.5% isoflurane in oxygen at a flow rate of 1L/min and 37 kBq was injected via the tail vein. At specific time points (2, 15, 30 and 60 minutes) after tracer administration, mice were sacrificed by decapitation and blood and major organs were collected in tared tubes and weighed. Radioactivity in blood and organs was counted using an automated γ-counter (Wallac 2480 Wizard 3q, Perkin Elmer, Waltham, USA). Obtained values were expressed as percentage of injected dose per gram tissue (% ID/g).

Large animal study

Eight female domestic cross-bred pigs weighing 25–30 kg (n = 5 healthy controls and n = 3 infarcted pigs) were included in the experiment. A schematic representation of the experimental protocol is shown in Figure 1.

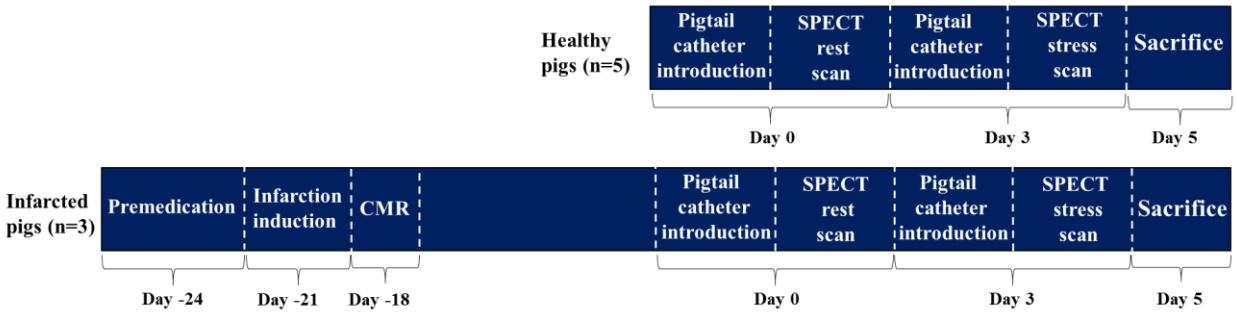

Figure 1. Schematic overview of the experimental study protocol. *CMR -cardiac magnetic resonance, SPECT - single photon emission tomography.*

Induction of myocardial infarction was performed according to the established protocol in our laboratory. To prevent life-threatening arrhythmia during the percutaneous intracoronary intervention, animals were pretreated with 200 mg amiodarone (Cordarone, Sanofi, Diegem, Belgium) 2x/d for 3 days before myocardial infarction induction. One day before and on the day of myocardial infarction animals received 300 mg clopidogrel (Plavix, Sanofi, Paris, France) and 100 mg aspirin (Dispril, Reckitt Benckiser, Brussels, Belgium). The day of the procedure, pigs were sedated with 2.5 mg/kg Xylazine (Vexylan, CEVA Sante Animale, Brussels, Belgium) and Telazol (tiletamine 4 mg/kg and zolazepam 4 mg/kg (Zoletil100, Virbac Animal Health, Carros, France)). After intubation, anesthesia was induced with an intravenous bolus injection of 3 mg/kg propofol (Diprivan, AstraZeneca, Brussels, Belgium) and maintained with a continuous infusion of 10 mg/kg/hr propofol and 18 μg/kg/hr remifentanil (Ultiva, GSK, Genval, Belgium). Mechanical ventilation was started immediately after anaesthesia induction. Coronary arteries for angiography were reached through the intra-arterial sheath, inserted into the carotid artery (8fr). To prevent thromboembolism a bolus of 10,000 IU heparin (Heparine Leo, Leo Pharma, Wilrijk, Belgium) and 500 mg acetylsalicylic acid (Aspegic, Sanofi, Diegem, Belgium) were injected through the sheath. A guide wire was introduced in the left anterior descending artery (LAD) under fluoroscopic guidance and myocardial infarction was induced by 90 min balloon inflation (2.5610 mm Maverick balloon at 6 atm), distal to the second diagonal branch of LAD. Acute ischemia was followed by 2 h of reperfusion. Invasive monitoring of blood pressure and 3-lead electrocardiographic monitoring was performed during the entire experimental procedure. To prevent infection of the cervical wound 2.5 mg kg^{-1} enrofloxacin (Baytril, Bayer, Brussels, Belgium) was administered intramuscularly at the end of experiment. Subsequent analgesia was achieved with 0,3 mg of Buprenorphine (Temgesic, 2 mg/ml), that was intramuscularly injected every 8 h during 48 h after myocardial infarction induction. Clopidogrel (Plavix, Sanofi, Paris, France) 75 mg/day and aspirin (Dispril, Reckitt Benckiser, Brussels, Belgium) 100 mg/day were orally administered till the pig was euthanized. On day 3 after myocardial infarction all animals received cardiac magnetic resonance (CMR) (TRIO-Tim, Siemens, Erlangen) after intravenous infusion of gadolinium (gadoterate meglumine 0.2 mmol kg^{-1}) for assessing the presence, extent and location of myocardial scar.

For each SPECT scan, all animals underwent the same sedation, intubation, general anesthesia and mechanical ventilation, as described above. Additionally, a pigtail catheter (6fr) was advanced into the left ventricle (LV) through an intra-arterial sheath inserted into the carotid artery (8fr). To prevent thromboembolism a bolus of 10,000 IU heparin (Heparine Leo, Leo Pharma, Wilrijk, Belgium) was injected through the sheath. To prevent wound infection 2.5

mg/kg enrofloxacin (Baytril, Bayer, Brussels, Belgium) was administered intramuscularly at the end of each experiment. Each pig was euthanized at day 5 after the first SPECT scan using an in-house protocol with propofol and saturated KCl.

Ethical approval

Both animal experiments were approved by the in-house ethical committee (Ethische Commissie Dierproeven, KU Leuven), with permit numbers P011/2016 and P021/2016. Animals were housed and treated according to the Guide for the Care and Use of Laboratory Animals (National Institute of Health, USA), and the European Directive 2010/63/EU and the Belgian Royal Decree of 29 May 2013.

SPECT acquisition

All cardiac images were acquired on a Discovery NM 530c (GE Healthcare, Haifa, Israel). SPECT acquisitions included a two-day rest-adenosine stress imaging protocol with ^{99m}Tc-Teboroxime and were performed at day 0 and day 3 in the group of healthy animals, while acquisition in the infarcted group were performed on day 21 and 24 after induction of myocardial infarction (Figure 1). A CT-scan (120 kVp, 1.0mA, 2.0 rmp) was acquired on Discovery NM/CT 670 (GE Healthcare, Haifa, Israel) prior to each SPECT imaging for subsequent attenuation correction (AC) of the emission data.

Pigs were positioned in left lateral decubitus and fixed in a box for all imaging modalities. To allow accurate positioning of the heart in the center of the CZT camera, a small activity of ^{201}TI (20 MBq) was injected followed by a 10-min acquisition (Figure 2).

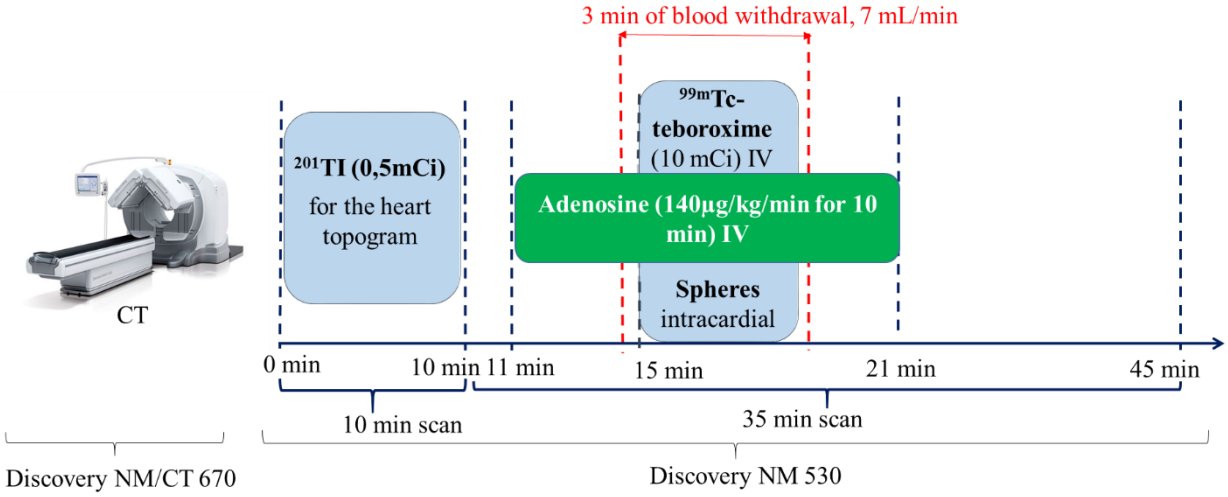

Figure 2. Schematic overview of the SPECT and microspheres stress protocol. *Note that the rest protocol was identical to stress, except for the adenosine injection. Co-injection of colored microspheres with ^{99m}Tc-Teboroxime was performed only in healthy pigs.*

Upon positioning the heart in the center of the field-of-view, a dynamic 35-min list-mode acquisition was started together with intravenous injection of 370 MBq ^{99m}Tc-Teboroxime. ^{99m}Tc-Teboroxime was injected using an infusion pump (Nemoto Sonic Shot GX**)** at a rate of 9 ml over 20 s, followed by a 9 ml saline flush over 20 seconds [78]. A pharmacological stress examination was performed using intravenous adenosine (140 µg/kg/min) for 10 minutes, starting 4 minutes prior to tracer and microsphere injection (Figure 2).

SPECT image reconstruction and analysis

All images were reconstructed with and without CT-based AC on a standard workstation (Xeleris, GE Healthcare, Haifa, Israel) using a manufacturer-supplied iterative reconstruction algorithm with 50 iterations. AC was performed by manual co-registration of the acquired SPECT and CT images.

List-mode data of all animals were re-binned into 100 frames of 20 sec, that were subsequently used to generate time-activity curves (TAC) of different regions. For this, regions of interest (ROIs) were manually drawn on a reference image using dynamic analysis tool (Xeleris 4.0, GE Healthcare, Haifa, Israel) and were automatically copied to all 100 reconstructed frames. The reference image was chosen visually and corresponded to the image with good visualization of the heart (Figure 3). At least 3 ellipsoidal ROIs were drawn in the LV myocardial wall, one ROI was placed in the LV cavity for blood pool activity and one ROI was placed in the liver – organ of major ^{99m}Tc-Teboroxime excretion (Figure 3). All ROIs were normalized and per injected activity.

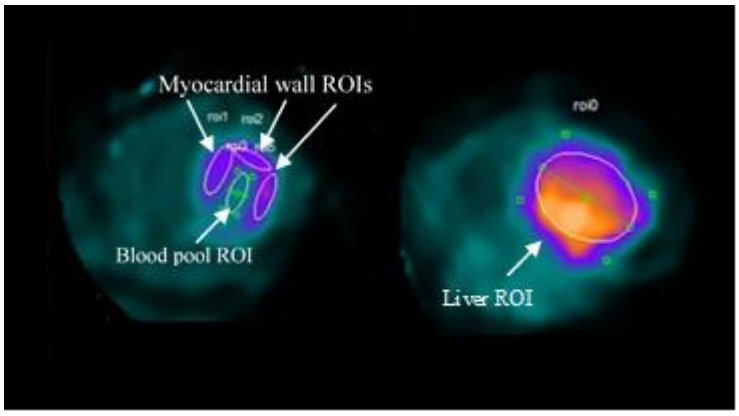

Figure 3. Representative example of ROIs placed in the blood pool, LV myocardial wall and liver in a healthy animal. *Shown ROIs are drawn on the reference image and will be subsequently automatically copied to 100 dynamic frames.*

Changes in the myocardium/liver and myocardium/blood pool ratios during rest and stress SPECT acquisitions were used to determine the optimal time window to generate static images. Perfusion scans were displayed in conventional short axis (SA), vertical long axis (VLA), horizontal long axis (HLA) and as polar maps. Image quality was assessed visually, taking into account liver interference with the inferior wall, contrast between structures, and sharpness of the myocardial edges.

For absolute quantification of MBF, list-mode data were re-binned in 18 frames of 10 sec and 4 frames of 120 sec, and analyzed with 4DM Reserve software (Xeleris 4.0, GE Healthcare, Haifa, Israel). Because of the lack of a well-validated and available kinetic model for ^{99m}Tc-Teboroxime in 4DM, in healthy animals quantification of MBF was performed using available 1-tissue compartment (1CM) and net-retention (NR) models for ^{99m}Tc-labeled radiotracers, ^{13}N-NH_3 and ^{201}Tl. Perfusion was quantified per segment using the 17 segment American Heart Association heart model[89]. Segmental MBF values, obtained with each of the algorithms, were correlated with segmental microspheres-derived MBF (a gold standard), in order to evaluate the algorithm that best fitted the kinetics of ^{99m}Tc-Teboroxime. This algorithm was further applied for the quantification of SPECT MBF in infarcted pigs. Additionally, SPECT MBF was calculated per coronary artery territory (LAD, left circumflex (LCX), right coronary artery (RCA)), as mean perfusion of the corresponding segments, and for the whole myocardium (global), as mean perfusion of the 17 segments. MFR was calculated per segment, per vascular territory and for the whole myocardium, as a ratio of the corresponding stress and rest MBF values.

Microspheres protocol and analysis

Microspheres were only administered in healthy animals. Simultaneously with radiotracer injection, 2 million eosin or yellow 15 μm dye extraction Dye-Trak microspheres (Triton Technologies, San Diego, USA), diluted in 10 ml of saline, were injected in the LV cavity during rest and stress respectively. Injection was done over 20 sec followed by a 20 mL saline flush. Reference blood samples were withdrawn from the carotid artery for 3 minutes at a speed of 7 mL/min starting 20 sec prior to microsphere administration (Figure 2).

After sacrificing the animals, the whole heart was excised and 17 small samples (max 1 gram of tissue) were harvested, corresponding to the 17 segments of the AHA model [89]. In order to evaluate the homogeneity of microsphere distribution, tissue samples from both

kidneys were also collected. The difference in perfusion between the kidneys ≤15% was considered within the acceptable limit.

Microsphere processing and MBF quantification was performed according to the manufacturer's protocol (User`s Manual for Dye-track and Dye-track VII+, Triton Technology Inc., San-Diego, USA). MBF was calculated for each kidney and for each of the 17 segments of the heart [89]. MBF per coronary artery territory was represented as an average MBF of the corresponding segments, while global MBF was calculated as an average of the 17 segments. MFR was calculated per segment, per vascular territory and for the whole myocardium as a ratio of the corresponding stress and rest MBF values.

Statistical analysis

Statistical analysis was performed using SPSS Statistics 20 (IBM, Chicago, IL, USA). The normality of data distribution was evaluated using the Wilk-Shapiro test. Continuous variables were presented as mean±standard deviation and compared using a t-test. The correlation microspheres-derived and SPECT-derived MBF was assessed with Pearson correlation coefficients. The agreement between two methods was assessed with a Bland-Altman test. A value of $p<0.05$ was considered statistically significant.

RESULTS

Radiosynthesis of ^{99m}Tc-Teboroxime

^{99m}Tc-Teboroxime was successfully synthesized with a radiochemical purity of > 95 % in all cases as determined by radio high pressure liquid choromatography.

Biodistribution of ^{99m}Tc-Teboroxime

The results of the biodistribution studies in mice at different time points are shown in Figure 4.

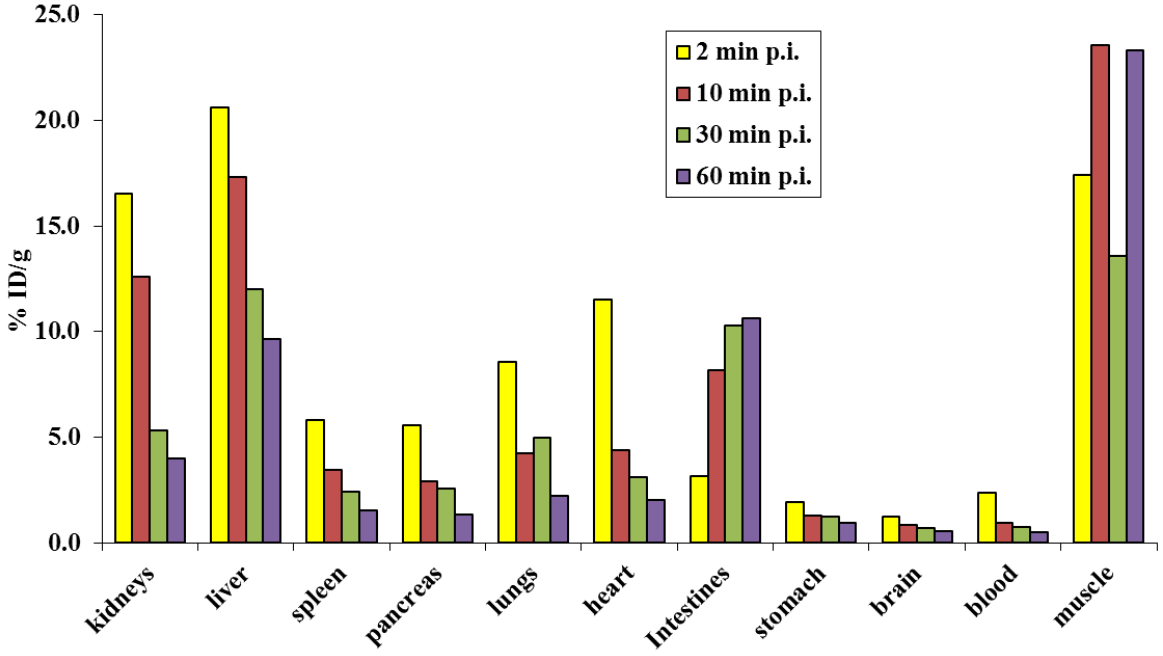

Figure 4. Biodistribution results of ^{99m}Tc-Teboroxime in mice. *Values are represented as percentage of injected dose per gram tissue (%ID/g), averaged for 3 mice per each time point.*

A high myocardial uptake of ^{99m}Tc-Teboroxime at 2 minutes post injection (11.52±0.41 ID%/g) decreased very rapidly, with only 4.42±0.94 ID%/g of injected dose left in the heart 10 min post injection and 2.04±0.12 ID%/g of injected dose 60 minutes post injection.

In contrast to the myocardium, radiotracer uptake in other organs was limited, except for the liver, intestines and kidneys, suggesting a predominant hepatobiliary excretion of ^{99m}Tc-Teboroxime in combination with a renal clearance.

^{99m}Tc-Teboroxime was cleared quite rapidly from the blood with less than 1 % of the injected dose left in the blood after 10 minutes post injection. Interestingly, a high muscular uptake was observed and remained quite constant over a 60-min period.

Large animal experiment

SPECT study

Out of 8 included animals, only 2 healthy and 3 infarcted pigs successfully completed the full protocol with both rest and stress SPECT acquisitions. In the other three healthy pigs, only a resting study without CT (n=1) and a stress study (n=1) were performed because of technical problems, whereas in another pig only 1 CT scan was acquired, that has been used for attenuation correction of both stress and rest images. In total, 7 AC (3 rest and 4 stress scans) images in the healthy pigs and 6 AC images (3 rest and 3 stress scans) in the infarcted pigs were obtained and analysed.

Kinetics of ^{99m}Tc-Teboroxime in large animals

The ^{99m}Tc-Teboroxime kinetics were analyzed on the 7 AC images obtained in control animals. A representative example of the TAC in the LV cavity, LV wall and liver is shown in Figure 5.

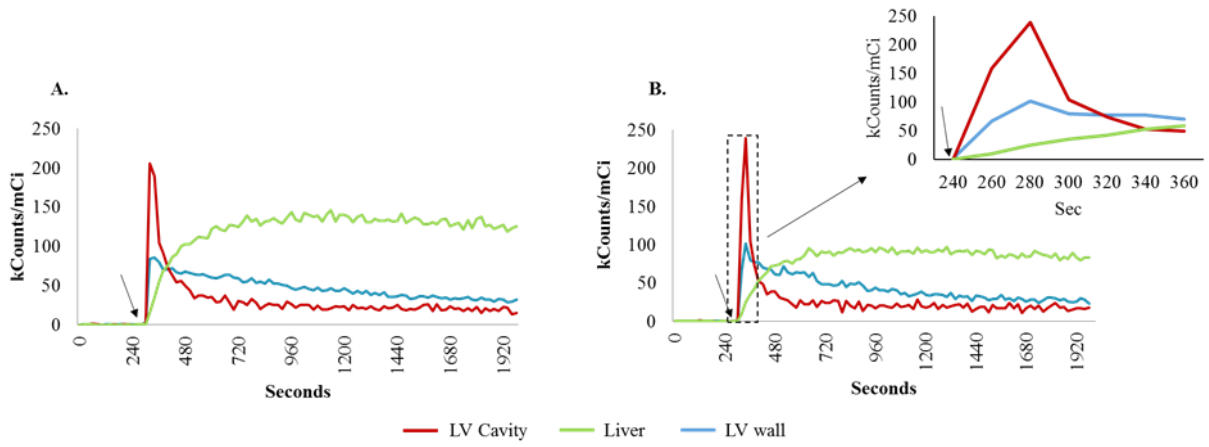

Figure 5. Representative example of ^{99m}Tc-Teboroxime kinetics in LV cavity, LV wall and liver, demonstrated for rest (A) and pharmacological stress (B) SPECT acquisitions. *A zoomed image demonstrates the first pass of the tracer in the LV cavity, that is immediately followed by rapid increase in tracer uptake in the LV wall and to the less extent in the liver. Note the fast tracer wash out from the blood pool and myocardium in contrast to its continuous accumulation in the liver during both rest and stress scans. Time of tracer injection is indicated by the black arrow.*

The TAC of the LV cavity (blood pool) showed a high first pass followed by a rapid decrease of ^{99m}Tc-Teboroxime concentration in the blood pool, suggesting a fast clearance of the tracer from the circulation.

The TAC of the LV myocardial wall demonstrated a fast tracer uptake by the heart immediately following the first pass. Afterwards, a decrease of tracer concentration in the heart was observed, reaching 50% of maximal uptake already at 502±167sec post-injection, corresponding to a fast myocardial wash-out of ^{99m}Tc-Teboroxime. There was a trend towards faster myocardial clearance during stress (427±60sec) compared to rest (588±212sec), however the difference was not significant ($p>0.05$).

In contrast to the LV cavity and wall, there was a quite rapid and constant accumulation of radiotracer in the liver, reaching a maximum uptake at 629±255 sec, that remained relatively constant during the exam. There was no significant difference in liver kinetics between rest and stress studies.

The dynamic changes in LV wall/ LV cavity as well as LV wall/liver ratios were similar between rest and stress acquisitions and an optimal time window for static reconstructions was defined between 100-400 sec after tracer injection (Figure 6).

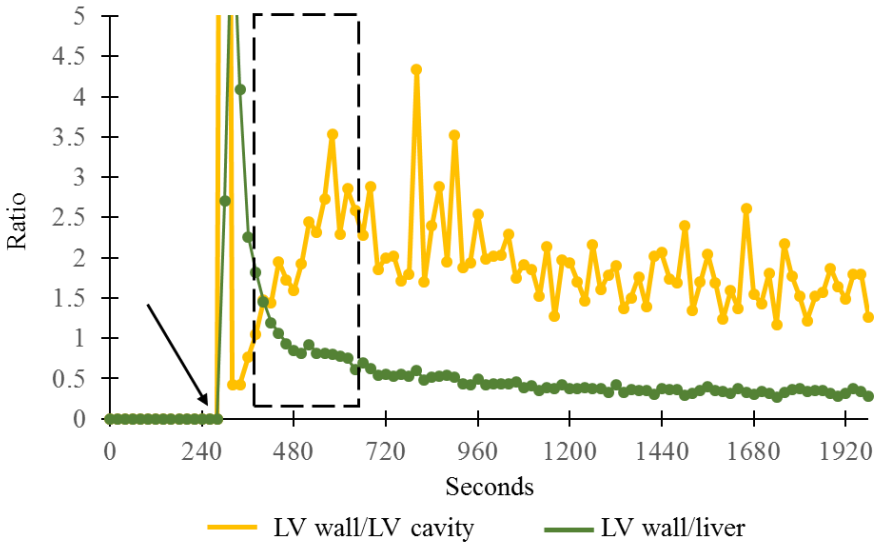

Figure 6. A representative example of the changes of LV wall/LV cavity and LV wall/liver count ratios in a healthy pig during rest SPECT acquisition. *This example illustrates how the 5 min optimal time-window (black dashed box, 100-400sec after tracer injection) was selected for subsequent visual assessment of myocardial images. Time of tracer injection is indicated by the black arrow.*

Visual assessment of myocardial perfusion images

All static 5-min (100-400 sec pi) SPECT AC scans of healthy and infarcted pigs demonstrated high contrast between myocardium and LV cavity and good delineation of the LV wall. Increased liver uptake was observed in all images but did not affect the diagnostic quality of the images except for one case (Figure 7,8).

In contrast to a homogenous tracer distribution in healthy pigs, a clear apical perfusion defect corresponding to the LAD territory was observed in infarcted animals. The perfusion defect at stress exceeded the defect at rest, indicating the presence of inducible ischemia. The location and extent of the perfusion defect perfectly corresponded to the regions of late gadolinium enhancement (LGE) on CMR scans (Figure 7,8).

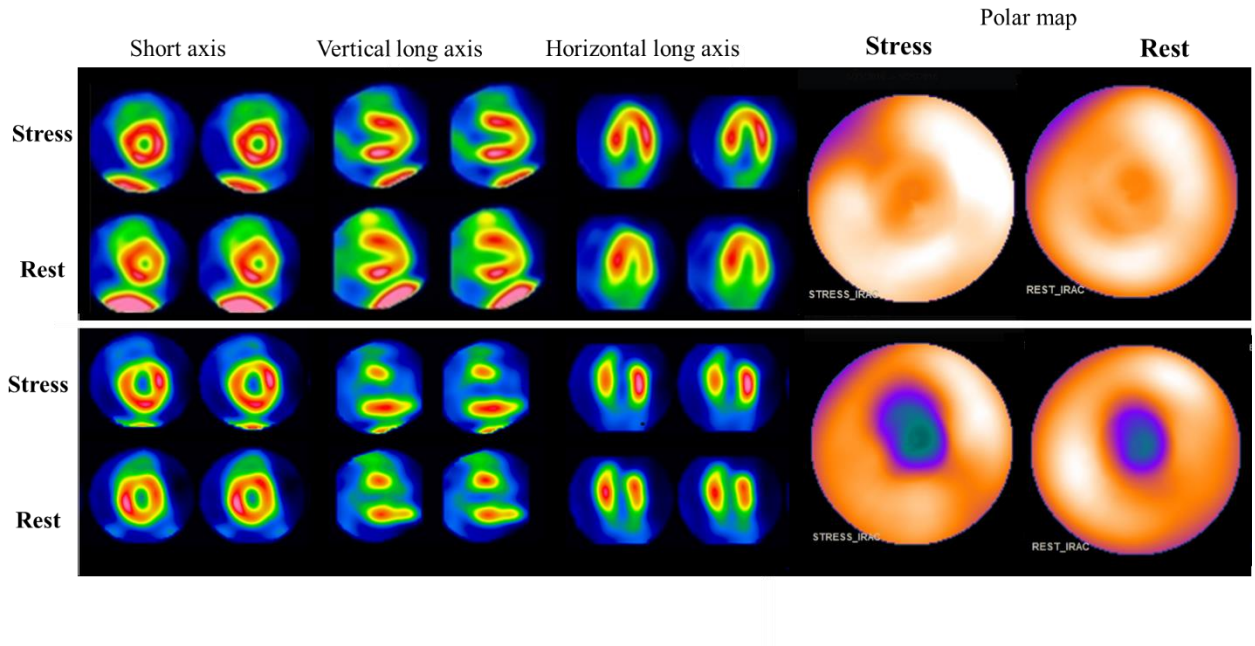

Figure 7. Representative 5-min static AC reconstructions, showing a homogeneous tracer uptake in the myocardium in the healthy pig (upper raw) and a perfusion defect in the anterior wall in the infarcted pig (lower raw). *Perfusion defect is larger at stress compared to rest, being indicative of inducible ischemia in the peri-infarct area. Note the high tracer uptake in the liver that does not influence image interpretation.*

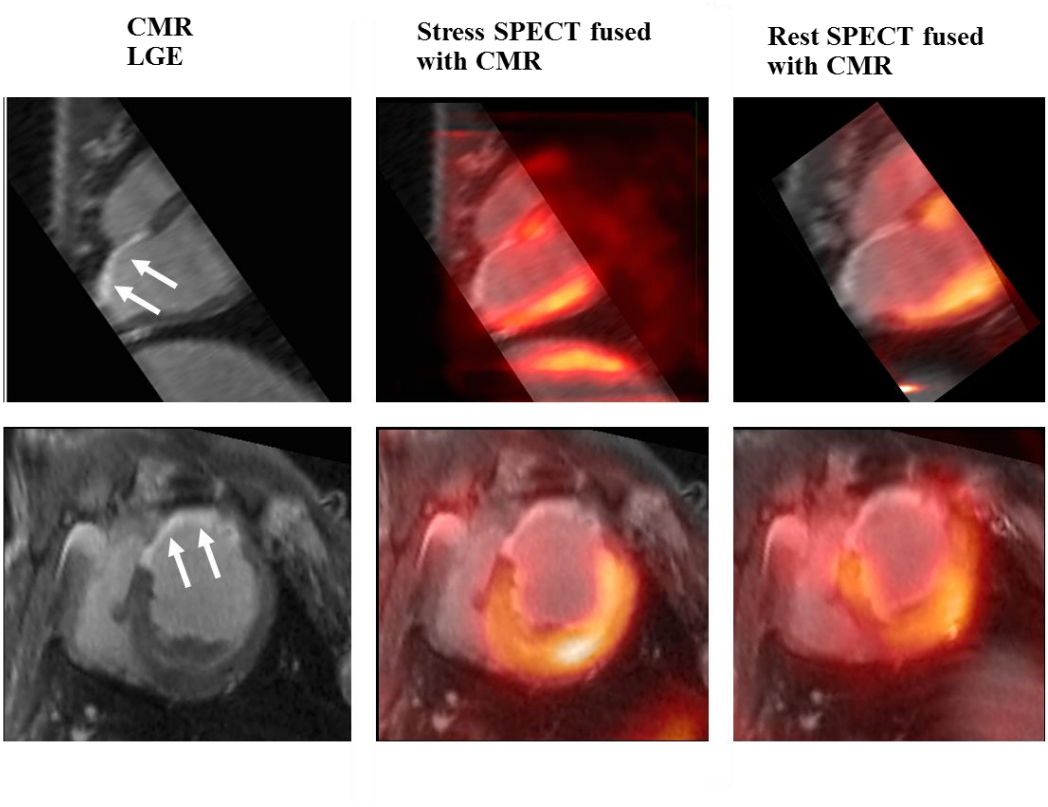

Figure 8. Representative example of CMR and SPECT scan of the infarcted animal. *Note the match between the perfusion defect on CZT SPECT scans with the region of LGE on CMR.*

Microsphere-derived MBF

For the analysis of microsphere-derived MBF, we focused only on the 2 healthy pigs with complete rest and stress imaging protocols. In both pigs, segmental analysis demonstrated a relatively homogenous MBF across the myocardium, both during rest and stress. Segmental perfusion values at rest were similar among both animals and corresponded to 1.08±0.2 ml/min/g and 1.05±0.18 ml/min/g, respectively. However, while segmental MBF significantly increased at stress in one animal (2.97±0.53 ml/min/g), stress MBF of another animal was similar to values at rest (1.02±0.14 ml/min/g). Similarly to segmental analysis, stress MBF per vascular territory and for the whole myocardium was increased only in one animal, resulting in a global MFR of 2.8. Another animal did not respond to adenosine stress and had global MFR around 1.0.

The difference in perfusion between the kidneys during the same experiment varied between 1 and 15%.

Kinetic model for ^{99m}Tc-Teboroxime

Segmental and regional analysis of SPECT-derived MBF in both healthy pigs that completed the full protocol demonstrated a relatively homogenous perfusion across the heart during rest and stress, independently of the applied algorithm. In analogy to the microsphere results, stress induced hyperemia was only observed in one animal. Despite the similar patterns of perfusion distribution between applied algorithms, the differences in absolute MBF and MFR values was pronounced, with the highest stress MBF observed with Tc 1CM algorithm (Figure 9).

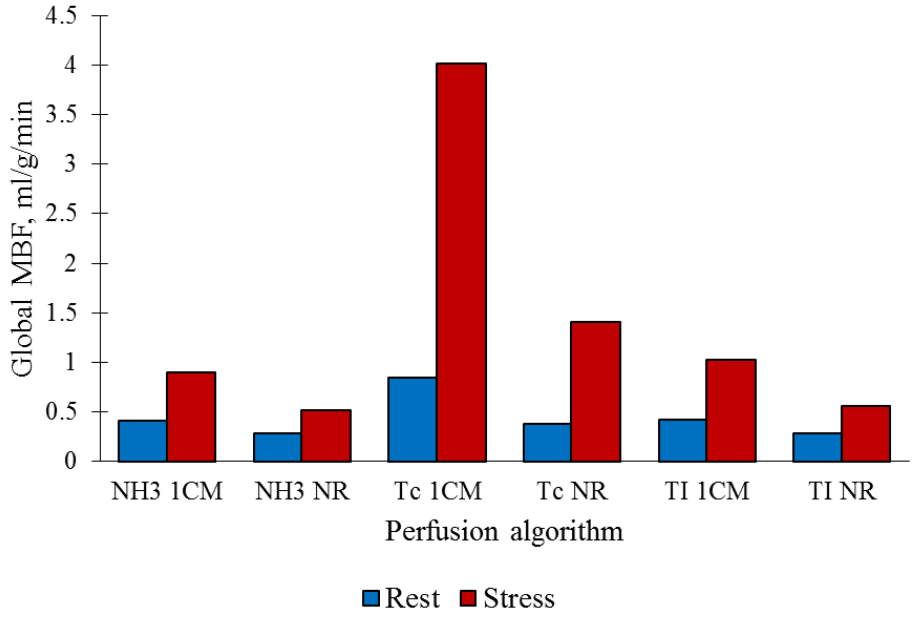

Figure 9. Representative example of global rest and stress SPECT-derived MBF of a healthy pig, quantified using different available commercial algorithms. *Note similar perfusion pattern but the pronounced difference in the absolute MBF values between the algorithms. The pig demonstrated a response to adenosine injection, with the most pronounced increase in stress flow, observed with Tc 1CM model. 1CM – 1-tissue compartment kinetic model; NR - net-retention model. Tc – Technetium sestamibi, Tl – Thallium, NH3 – Ammonia.*

Segmental SPECT-derived MBF correlated well with corresponding microsphere measurements, independently of the applied perfusion algorithm (all $r>0.56$, $p\leq0.03$) (Figure 10). The lowest bias between microspheres and SPECT-derived MBF values was obtained when Tc algorithm, based on 1CM kinetic model was used (-0,32 ml/g/min), however at the expense of wide limits of agreement (LOA from -1,83 to 1,19 ml/g/min). All kinetic models, except for the Tc 1CM model, underestimated the absolute flow derived from SPECT in comparison to the microsphere measurements.

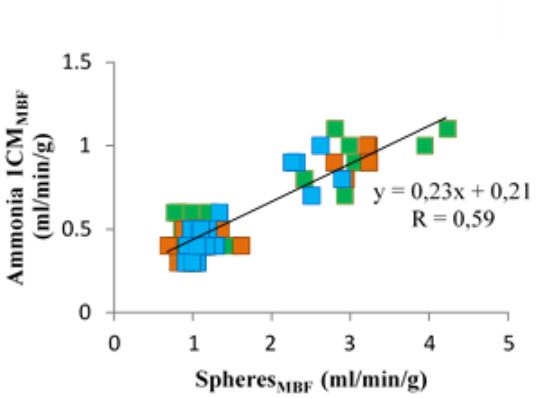
Ammonia 1CM$_{MBF}$ (ml/min/g)
y = 0,23x + 0,21
R = 0,59
Spheres$_{MBF}$ (ml/min/g)

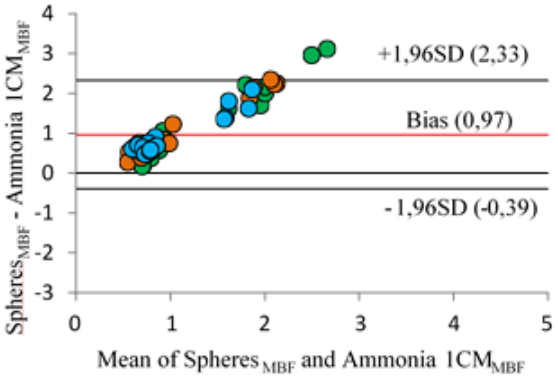
+1,96SD (2,33)
Bias (0,97)
-1,96SD (-0,39)
Spheres$_{MBF}$ - Ammonia 1CM$_{MBF}$
Mean of Spheres$_{MBF}$ and Ammonia 1CM$_{MBF}$

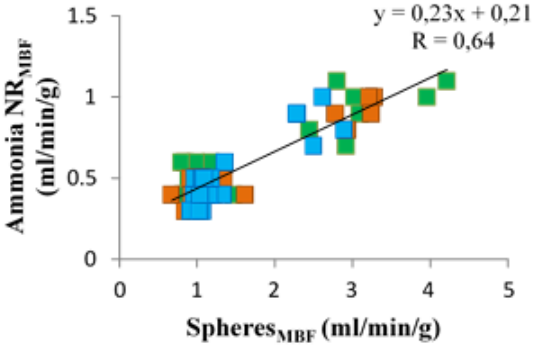
Ammonia NR$_{MBF}$ (ml/min/g)
y = 0,23x + 0,21
R = 0,64
Spheres$_{MBF}$ (ml/min/g)

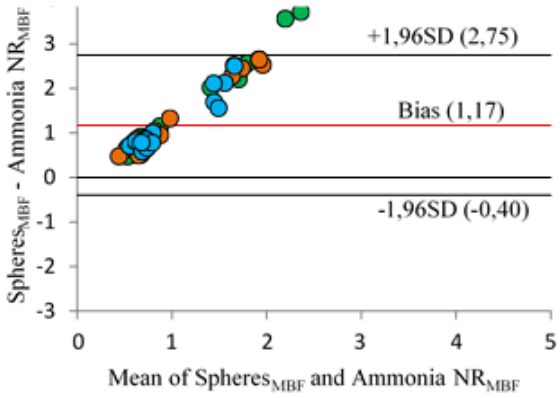
+1,96SD (2,75)
Bias (1,17)
-1,96SD (-0,40)
Spheres$_{MBF}$ - Ammonia NR$_{MBF}$
Mean of Spheres$_{MBF}$ and Ammonia NR$_{MBF}$

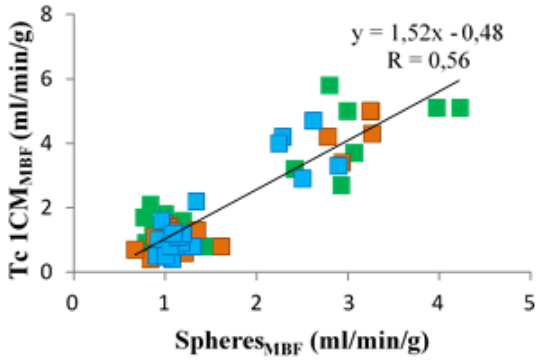
Tc 1CM$_{MBF}$ (ml/min/g)
y = 1,52x - 0,48
R = 0,56
Spheres$_{MBF}$ (ml/min/g)

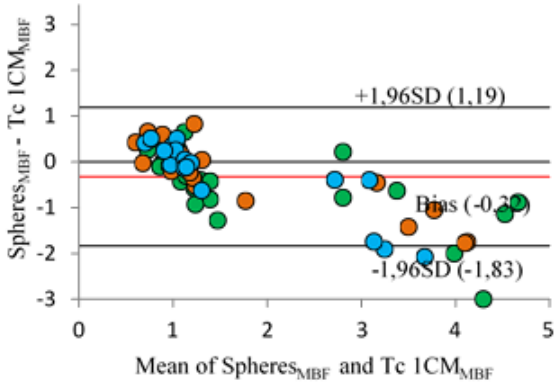
+1,96SD (1,19)
-1,96SD (-1,83)
Spheres$_{MBF}$ - Tc 1CM$_{MBF}$
Mean of Spheres$_{MBF}$ and Tc 1CM$_{MBF}$

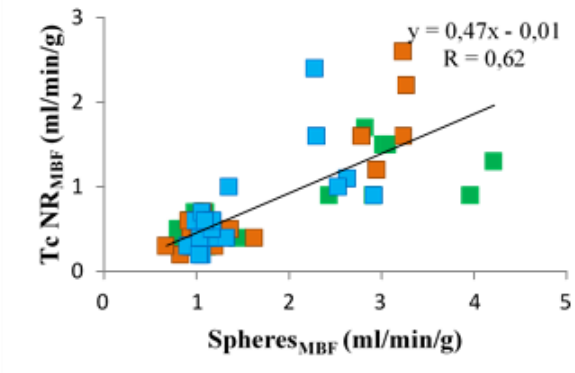
Tc NR$_{MBF}$ (ml/min/g)
y = 0,47x - 0,01
R = 0,62
Spheres$_{MBF}$ (ml/min/g)

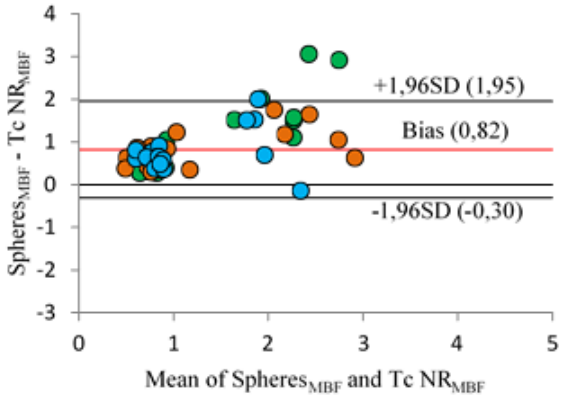
+1,96SD (1,95)
Bias (0,82)
-1,96SD (-0,30)
Spheres$_{MBF}$ - Tc NR$_{MBF}$
Mean of Spheres$_{MBF}$ and Tc NR$_{MBF}$

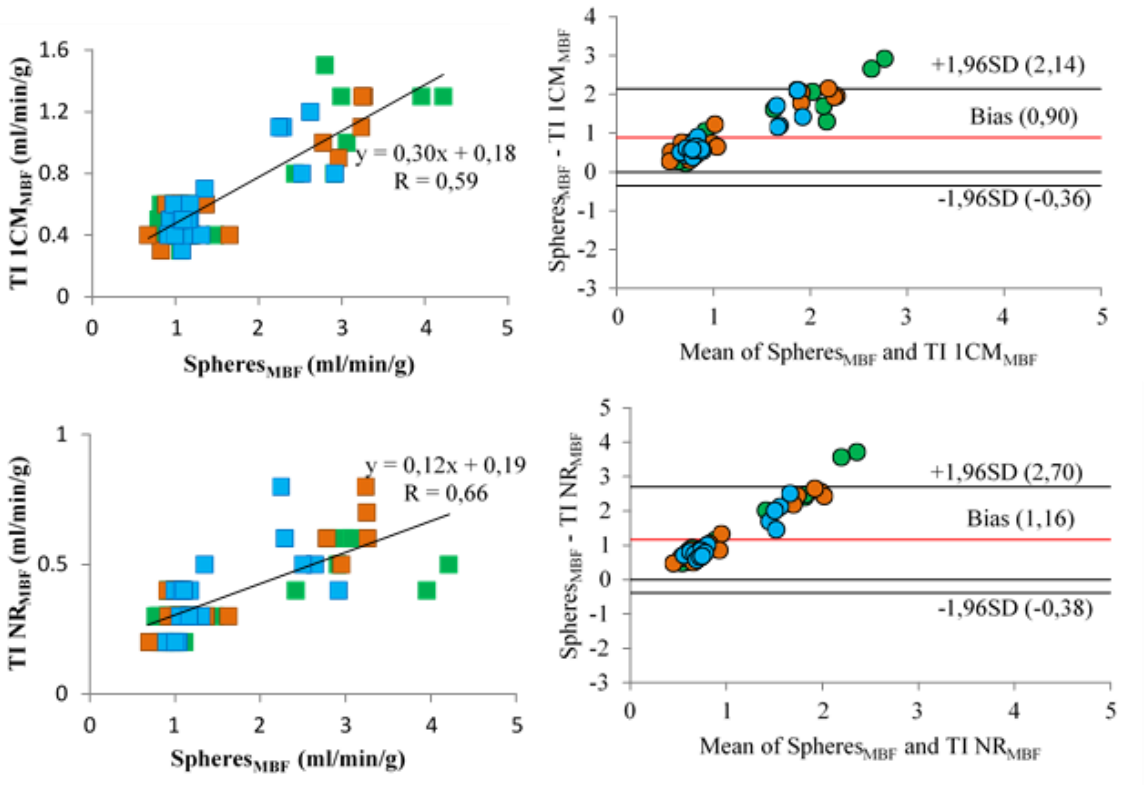

Figure 10. Correlation plots (left) and Bland-Altman plots (right) between microspheres-derived MBF and SPECT MBF, derived from different algorithms for perfusion quantification. *All data points correspond to MBF calculated per segments of both pigs with completed rest – stress protocol. Data points are colored according to the corresponding coronary territory (LAD – green, LCX – orange, RCA –blue). 1CM – 1 tissue compartment kinetic model; NR - net-retention kinetic model.*

SPECT-derived MBF in infarcted animals

In the group of 3 infarcted animals with the completed rest and stress SPECT imaging protocols, SPECT MBF was quantified using Tc 1CM model. In this group of animals, a heterogeneous MBF was observed, with a lower stress MBF and MFR values in the area of LAD, corresponding to the infarcted region.

An overview of SPECT MBF, quantified with Tc algorithm, based on 1CM kinetic model, for every infarcted pig is shown in Figure 11.

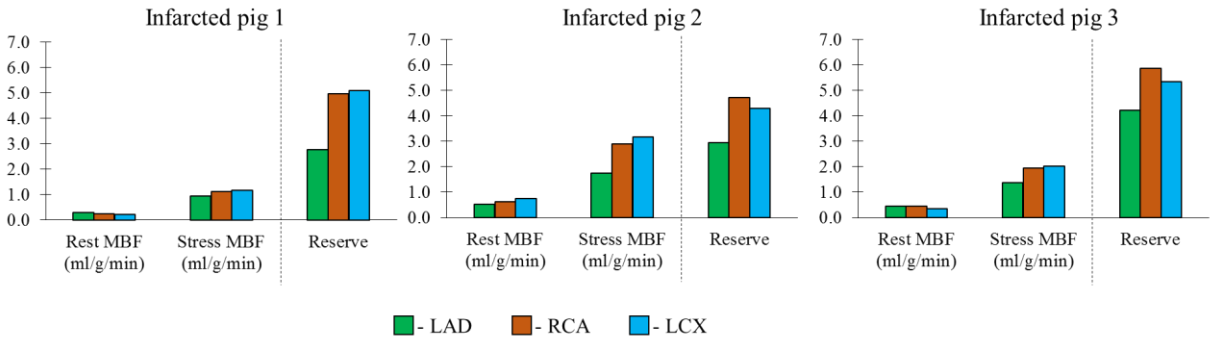

Figure 11. An overview of regional SPECT-derived MBF and MFR per each infarcted animal, participated in the experiment. *MBF was calculated based on the Tc-sestamibi 1CM model. Note lower stress MBF and MFR in LAD territory, corresponding to the area of myocardial infarction.*

DISCUSSION

This study demonstrates the feasibility to image myocardial perfusion and quantify MBF and MFR with ^{99m}Tc-Teboroxime using a cardiac-dedicated CZT SPECT camera in a large animal model.

^{99m}Tc-Teboroxime was successfully synthesized and *ex vivo* biodistribution studies in mice showed a high and specific myocardial uptake, along with a fast myocardial wash-out. Our findings are in agreement with previously published studies showing 70% myocardial clearance of ^{99m}Tc-Teboroxime within 15 minutes after administration [122,123]. The excretion of ^{99m}Tc-Teboroxime occurs mainly through the hepatobiliary system and to a lesser extent via the urinary system which is also in line with previous studies [123]. However, absolute values of biodistribution studies were significantly higher in our study, compared to the study by Zheng et al [122]. In his paper the reported radioactivity in the heart and blood at 2 min post injection were respectively 11.52±0.41 %ID/g and 2.38±0.25 %ID/g versus 3±0.37%ID/g and 0.47±0.05%ID/g, observed in our study, though the myocardium/blood ratio were quite similar. This discrepancy can be at least partially explained by the animal model used in both studies - mice vs rats.

In our study, *in vivo* kinetics of ^{99m}Tc-Teboroxime was investigated only in healthy animals, in which there is a minimal influence of external factors (ischemia, scar) on tracer behavior in the heart. Similar to the *ex vivo* biodistribution studies, *in vivo* images revealed fast myocardial kinetics with $T_{1/2}$ of respectively 9 and 7 minutes at rest and during stress. These values correspond well to reported myocardial half-lives, with somewhat faster myocardial wash out at stress [124–126].

In vivo biodistribution revealed a high liver uptake, which has been already described in several other studies [122,124,126]. This could interfere with myocardial activity in the inferior wall, resulting in suboptimal image quality and difficulties to reliable interpret perfusion studies. Therefore we defined an optimal 5-minute time window between 100 and 400 sec post injection to allow adequate visual assessment while minimizing liver interference. Even though liver activity is always present, in our study image interpretation was only hampered in one case but nevertheless this could be a potential drawback for clinical applications. Our optimal time window is within the window recommended by the study of Li et al., who suggested that acquisition within the first 15 min after ^{99m}Tc-Teboroxime injection provides good image quality with a conventional Anger camera [124].

Visual analysis of static images demonstrated a homogeneous ^{99m}Tc-Teboroxime distribution in the heart of healthy pigs, while in infarcted animals a clear perfusion defect was observed in the territory of LAD. This perfusion defect was larger at stress, indicating the presence of a border zone ischemia, which perfectly matched the location of the infarct on LGE CMR serving as gold standard.

Microspheres-derived MBF was used as a reference standard in healthy animals. Obtained MBF values at rest were similar to the values previously reported in pigs, ranging between 0.9 and 1.2 ml/min/g [127,128]. Furthermore, MFR observed in one pig with successful induced coronary vasodilation was also within the range of reported values in previous studies (MFR of 1.6-5) [128–130], corroborating that microsphere-derived values, obtained in our study, could serve as a standard for perfusion and flow reserve quantification. In another animal, stress MBF values were similar to rest MBF values, indicating that the pig did not adequately respond to the pharmacological stress agent. The latter can be explained by a suboptimal dose of adenosine used to induce maximal coronary vasodilation. Indeed, some studies have shown that the evident effect of adenosine infusion on coronary vasodilation in pigs was only observed with higher doses of adenosine ranging from 240 µg/kg/min to 500 µg/kg/min [131,132].

Due to the lack of a well-validated kinetic model for ^{99m}Tc-Teboroxime, SPECT-derived MBF and MFR were calculated using validated algorithms and models for routinely used perfusion tracers. We observed a moderate correlation between SPECT-derived and microsphere-derived MBF, independently of the perfusion algorithm applied, but imaging derived absolute values were underestimated by all approaches except for the ^{99m}Tc 1CM. This flow quantification algorithm demonstrated the lowest bias between SPECT-derived and microspheres-derived MBF, but the limits of agreement on Bland-Altman plot were rather wide, pointing out that even this model is not perfectly suited to assess to quantify flow with ^{99m}Tc-Teboroxime. Nevertheless, the ^{99m}Tc perfusion protocol was further applied in infarcted animals, where perfusion heterogeneity in segmental and regional MBF and MFR was observed, with lowest values in the LAD territory corresponding to the infarcted area.

Despite the observed correlation between microspheres- and SPECT-derived parameters, none of the kinetic models demonstrated a perfect line of identity between both methods. The latter can be, at least partially, explained by the peculiar mechanism of ^{99m}Tc-Teboroxime uptake and wash out from the myocardium that is different from other ^{99m}Tc-labeled compounds or PET perfusion tracers[133]. However, despite the difference in absolute

values between microsphere-derived and SPECT-derived MBF and MFR, a similar trend between these values was observed in the pigs.

Our study has several limitations. First, there is currently no well-validated kinetic model for ^{99m}Tc-Teboroxime available in commercial software packages. Therefore, in the current study, we applied different available kinetic models for ^{99m}Tc, ^{201}TI, and ^{13}N-Ammonia for flow and flow reserve quantification, however none of these models perfectly reflect the myocardial kinetics of ^{99m}Tc-Teboroxime. Secondly, we observed a variable response to adenosine among the animals with only 5 animals completing the experimental protocol of which 4 responded to adenosine stress. Finally, in the current study we have only evaluated the feasibility of using ^{99m}Tc-Teboroxime in a large animal model but the performance of this tracer has not been compared to routinely used radiotracers for MPI.

CONCLUSIONS

The results of our proof-of-concept study demonstrate the feasibility to non-invasively assess and quantify myocardial perfusion and flow reserve with ^{99m}Tc-Teboroxime using a dedicated cardiac CZT camera. However, development and validation of kinetic models dedicated for ^{99m}Tc-Teboroxime are needed for accurate quantification of absolute MBF.

PART IV

DISCUSSION

DISCUSSION

In the first part of the thesis manuscript, we explained the pathophysiology of LV remodelling in the presence of prominent markers of successful CRT response (LBBB, mechanical dyssynchrony) and found a potential application for nuclear imaging in selection of patients, who will most likely benefit from CRT implantation. The main findings and conclusions of this part are:

1. LBBB causes heterogeneity in regional cardiac perfusion and metabolism

In the group of non-ischemic HF CRT-candidates, we have demonstrated, that the presence of LBBB causes a redistribution of regional absolute myocardial perfusion and metabolism, as assessed with ^{13}N-NH3 and ^{18}F-FDG PET-CT, respectively. More specifically, highest ^{18}F-FDG uptake and absolute MBF were observed in the lateral wall, lowest values in the septum and intermediate values for both perfusion and metabolism in the anterior and inferior walls (**Chapter I, Figure 1** and **Figure 2A**). Since these findings were observed in a group of patients with non-ischemic cardiomyopathy, the influence of scar/ischemia on the obtained results can be almost completely excluded. We therefore assume that regional redistribution of myocardial perfusion and metabolism in LBBB patients represents an adaptation to the differences in regional workload in an asynchronously contracting ventricle. Indeed, it has been demonstrated that septum of LBBB heart contracts early against the low LV pressure and relaxed lateral wall, losing its contribution to the cardiac output, but rather displacing the blood towards the lateral wall and stretching lateral segments. In contrast, the lateral wall has to compensate for the low septal contribution to cardiac output. Being pre-stretched by the septum, it contracts with the greater force, thus bearing an excessive workload[37]. This discoordinated myocardial contraction with the differential regional workload distribution results in a physiological adaptation of energetic and oxygen demands, causing regional perfusion and metabolism heterogeneity, as observed in our study. The strong linear correlation between ^{18}F-FDG glucose metabolism and amount of myocardial work has been already demonstrated earlier by our group in a preclinical sheep LBBB model, and only further strengthens and supports our hypothesis[37].

Our results are in line with previous studies that explored cardiac metabolism with ^{18}F-FDG PET in LBBB patients [38,39]. ^{18}F-FDG SLRs, obtained in our study also perfectly matched the range presented by other authors in a similar patient cohort [39,94]. In contrast to concordant

results for metabolic activity, results on myocardial perfusion have rather been conflicting. While some studies showed similar to our results septal hypoperfusion, other studies reported homogeneous perfusion across the heart in patients with LBBB[39,57]. In order to try to explain the differences across the studies, we evaluated and compared different approaches of perfusion assessment (see below).

2. The different approaches of perfusion assessment with ^{13}N-NH3 PET influence the perfusion results in patients with LBBB

In order to find at least a partial explanation for the controversial myocardial perfusion results in LBBB patients, described in the literature, we compared different approaches of perfusion assessment with ^{13}N-NH_3 PET/CT in the same cohort of non-ischemic HF patients. More specifically, absolute quantification of perfusion in ml/g/min, calculated using different kinetic models, was compared to a semi-quantitative approach, that implies assessment of tracer concentration (SUV), derived from "late" static images. We have demonstrated that absolute quantification of myocardial perfusion results in a lower perfusion in the septal and a higher perfusion in the lateral wall, independently of the applied kinetic model, while no significant differences were observed between both walls using the semi-quantitative approach **(Chapter I, Figure 2)**. The latter can be explained by the metabolization of ^{13}N-NH_3 in myocardial tissue. It is well known that upon entering the intracellular compartment, ^{13}N-NH_3 is metabolically trapped, and takes part into the amino acid metabolism[48]. The differences in regional (amino acid) metabolism, present in LBBB patients, may differently influence regional tracer retention and wash out (**Chapter I, Figure 3A**). The latter may explain why tracer concentration on the late (10-30 min after tracer injection) static ^{13}N-NH3 images is not proportional to regional absolute perfusion. This is further supported by the lack of a correlation between absolute flow values (ml/g/min) and late tracer uptake (SUV). Thus, in contrast to absolute perfusion quantification, derived from images immediately after tracer injection, late (10-30 min) static images do not represent a pure perfusion alone, but are rather a composite of regional perfusion and metabolism. These observations may be an explanation for the conflicting results on ^{13}N-NH_3 PET perfusion in literature [40,134]. They further indicate that in patients with LBBB myocardial perfusion assessed with ^{13}N-NH_3 PET should be quantified based on tracer kinetic modelling.

3. Reliable assessment of viability with PET can be challenging in patients with LBBB

We have demonstrated that a significant number of non-ischemic HF patients with LBBB present the areas of perfusion/metabolism reverse mismatch in the septum and mismatch in the lateral wall, when evaluated with the clinical algorithm using static 'late' ^{13}N-NH_3/^{18}F-FDG PET images (**Chapter I, Figure V**). As mentioned above, the presence of these patterns is most likely explained by a physiological adaptation of regional oxygen and energy demands in the dyssynchronous heart. Our study has clearly demonstrated that even in the absence of ischemia, these mismatch patterns typical for hibernation in an ischemic population, can be observed in LBBB patients. Our findings rise the important question and awareness about the accuracy of this method to evaluate myocardial viability or hibernating myocardium in ischemic patients with LBBB, where it might be challenging to distinguish hibernation from physiological adaptations in a dyssynchronous heart.

4. Presence of mechanical dyssynchrony causes heterogeneity in regional cardiac perfusion and metabolism

As one of the steps towards a better understanding of the pathophysiology of LV remodelling in dyssynchronous heart, we explored the regional changes of absolute cardiac perfusion and metabolism in the presence of mechanical dyssynchrony, that have recently emerged as a reliable marker of successful CRT response. In this chapter we focused mainly on the septal and lateral wall, as earlier work had shown that those are affected the most by dyssynchrony (**Chapter I Figure 1 and Figure 2A**).

We have demonstrated that the presence of mechanical dyssynchrony, represented by the presence of either SF or AR or both on echocardiography, causes the heterogeneous regional absolute perfusion and metabolism. In contrast, patients without mechanical dyssynchrony, present a more homogeneous perfusion and metabolism across both walls **(Chapter II, Figure 1).** We could also demonstrate that the regional alterations in both glucose metabolism and MBF linearly correlated with regional myocardial work. The latter supports the notion that observed perfusion and metabolism changes reflect a physiological adaptation of the heart to the altered workload, and as a consequence to the regional oxygen and energy demands **(Chapter II, Figure 2)** [37,38,100]. It was further interesting to note that in patients with mechanical dyssynchrony, the septum can even waste energy, when being stretched by the

opposite segments. This is reflected by the negative work that was observed in the septum, when assessed with echocardiography strain technique **(Chapter II, Figure 2).** Interesting, that while ^{18}F-FDG PET metabolism also represents a surrogate of myocardial work, in contrast to echocardiography, it cannot reliably distinguish its wasted portion. The reason behind is that ^{18}F-FDG uptake provides the information on both the metabolism, needed to perform external work, and the basic metabolism of the cell. Even when the septum wastes energy, a minimum of ^{18}F-FDG uptake will still be observed, representing in this case the basic metabolic needs of the region. On the other hand, echocardiography stress-strain loops provide information on external myocardial work, both positive and negative, but lacks the information about the basic-metabolism of the cell.

5. **Regional cardiac metabolism, but not cardiac perfusion, assessed with PET before CRT implantation, is associated with the extent of volumetric reverse remodelling after CRT implantation**

In the non-ischemic HF CRT candidates we have demonstrated that ^{18}F-FDG SLR assessed with PET before CRT implantation correlated linearly with the extent of volumetric reverse remodelling after CRT implantation, with the lower SLR associated with more pronounced reverse remodelling. When these findings were put in perspective to regional work, it was concluded that a very low SLR, reflecting very little contribution of the septum and high contribution of the lateral wall to LV function was associated with better functional improvement 12 months after CRT implantation. It is interesting to note that only ^{18}F-FDG SLR and not ^{13}N-NH_3 MBF SLR was associated with volumetric reverse remodelling after CRT **(Chapter II, Figure 4)**. This can be partially explained by more pronounced difference in regional ^{18}F-FDG uptake than in regional MBF, observed in CRT candidates **(Chapter I Figure 4).**

6. **^{18}F-FDG PET can be used to guide the therapy of HF patients**

After observing in **Chapter II, Figure 4** a linear correlation between ^{18}F-FDG SLR before CRT implantation and the extent of volumetric reverse remodelling after CRT in non-ischemic HF patients, we hypothesized that low ^{18}F-FDG SLR can find its place in the reliable differentiation of CRT responders from non-responders.

Before testing ^{18}F-FDG SLR as a predictive parameters, we first wanted to confirm that the linear correlation between ^{18}F-FDG SLR and the extent of volumetric reverse remodelling

persisted in a HF population with both ischemic and non-ischemic origin (**Chapter III, Figure 2A)**. We were able to demonstrate a statistically significant correlation between both parameters in the whole patient cohort, albeit slightly weaker (r=0.41) compared to the non-ischemic cohort alone (r=0.62) (**Chapter II, Figure 4)**.

In **Chapter III Figure 3** we have demonstrated that ^{18}F-FDG SLR has a high overall performance to predict CRT response. It is important to mention that the cut-off values for ^{18}F-FDG SLR were highly dependent on the type of patient preparation protocol for ^{18}F-FDG acquisition. When using preparation specific cut-off values, ^{18}F-FDG SLR could predict CRT response with high sensitivity and specificity in non-ischemic HF patients. However, specificity dropped significantly when the same thresholds were applied on the ischemic population. The latter can be explained by the fact that a low SLR can also be caused by the presence of septal scar that decreases the potential of regional functional recovery, hence is unfavorable for CRT response. Low ^{18}F-FDG SLR is a very sensitive, but relatively unspecific marker in the presence of ischemic disease, and should therefore always be accompanied with septal scar assessment before CRT implantation.

Multivariate analysis, including ^{18}F-FDG SLR, extent of septal scar and currently used guideline criteria for CRT implantation, represented by LBBB, QRS width and LVEF, revealed that ^{18}F-FDG SLR and the extent of septal scar were the only significant determinants of successful CRT response. Combination of both can reliably differentiate CRT responders from non-responders with high sensitivity and specificity, independently of HF etiology (**Chapter III, Figure 4)**. Patients with low SLR and smaller septal scar extent had a higher chance to become CRT responders. The principle finding of this chapter is illustrated in **Chapter III Figure 5**, where two patients with similar ^{18}F-FDG SLRs below the cut-off value at first sight are considered possible responders. However, low ^{18}F-FDG SLR in one patient was caused by a septal scar, whereas in the other patient it was solely attributed to regional changes in myocardial work. Therefore only the last patient responded to CRT implantation, highlighting the need to accompany ^{18}F-FDG SLR with the scar assessment in ischemic patients.

In the second part of the manuscript, that was devoted to improve the management of patients with CAD, we have demonstrated the possibility to quantify absolute myocardial perfusion with ^{99m}Tc-Teboroxime using a novel cardiac-dedicated CZT SPECT camera. The main findings and conclusions of this part are:

7. ^{99m}Tc-Teboroxime characteristics are suitable for perfusion assessment

Before *in vivo* evaluation, biodistribution studies in mice confirmed several important characteristics of ^{99m}Tc-Teboroxime (**Chapter IV, Figure 4**). The tracer has high myocardial tracer uptake with fast myocardial wash-out, limited tracer accumulation in non-excreting organs as well as high tracer accumulation in the liver. The latter might compromise the reliable assessment of tracer uptake in the inferior wall, therefore requires to look for the optimal acquisition window. Our biodistirubution findings are in line with the earlier biodistribution studies, confirming fast tracer myocardial kinetics of ^{99m}Tc-Teboroxime, that limits tracer application with the conventional SPECT cameras, but may serve as an advantage for novel fast cardiac dedicated SPECT cameras.

8. It is feasible to quantify myocardial flow reserve with ^{99m}Tc-Teboroxime using a dedicated cardiac camera in a pig model

Our proof-of-concept experiments in a large animal model showed the feasibility to image myocardial perfusion. We could demonstrate that the good image quality scans can be obtained during a 5 min-static acquisition, starting 100 sec after tracer administration (**Chapter IV, Figure 7**). Furthermore, we have also shown the possibility to quantify myocardial perfusion and flow reserve with ^{99m}Tc-Teboroxime using a dedicated cardiac camera. Even though the kinetic models used in our study were suboptimal to reflect the kinetics of ^{99m}Tc-Teboroxime, we were able to demonstrate regional changes in absolute perfusion in the infarcted animals. Further optimization of kinetic models specifically developed for ^{99m}Tc-Teboroxime and comparison to routinely used ^{99m}Tc-tracers is warranted to evaluate possible clinical applications and advantages over currently used protocols.

PART V

CONCLUSIONS AND FUTURE PERSPECTIVES

Conclusions

The first part of PhD project could shed some light on the pathophysiology of LV remodelling in the presence of promising markers of CRT response, such as LBBB and mechanical dyssynchrony, and resulted in the following conclusions:

- Presence of LBBB or mechanical dyssynchrony is associated with the low myocardial perfusion and metabolism values in the LV septum and higher values in the LV lateral wall;

- Regional redistribution of perfusion and metabolism in dyssynchronous heart follow the similar redistribution of regional myocardial work and represent the physiological adaptation of oxygen and energy supply to the regional heart demands;

- The larger is the difference in regional glucose metabolism, expressed as septal-to-lateral wall metabolism ratio, before CRT implantation, the more beneficial it is for a patient after CRT implantation;

- The predefined septal-to-lateral wall glucose metabolism ratio in combination with septal scar extent can reliably differentiate CRT responders from non-responders, independently of HF etiology, for the first time listing ^{18}F-FDG septal-to-lateral wall ratio among the tools for CRT prediction.

The second part of PhD project brought to light the possibility to improve the management of patients with CAD and led to the following conclusions:

- ^{99m}Tc-Teboroxime possesses properties favourable for the quantification of myocardial perfusion with recently introduced ultrafast cardiac-dedicated SPECT CZT cameras.

- It is feasible to non-invasively visualize and quantify myocardial perfusion and flow reserve with ^{99m}Tc-Teboroxime using a dedicated cardiac CZT SPECT camera, however, a development and validation of kinetic model dedicated for this tracer is further required.

Future perspectives

While our experimental and clinical studies allowed us to address the predefined research questions presented in this thesis, some questions and findings should be further unravelled.

Are the changes in perfusion and metabolism related to LV dyssynchrony absolute or relative?

In order to comprehensively understand the pathophysiological changes that accompany LV dyssynchrony, presented in Chapter I and Chapter II, we would like to explore whether the alterations observed in myocardial perfusion and metabolism in non-ischemic LBBB patients are absolute or rather relative, by comparing our results to findings in 'healthy volunteers'.

Is the different regional kinetics of ^{13}N-NH_3 attributed only to abnormal LV activation?

It would be interesting to explore the regional temporal kinetics of ^{13}N-NH_3 in different patient groups such as healthy controls and a CAD cohort. This will help us to understand whether the different regional temporal kinetics of ^{13}N-NH_3 is attributed only to abnormal LV activation, as was demonstrated in Chapter I, or whether this can also be caused by other conditions.

Is combined assessment of glucose metabolism and viability superior to other imaging-derived markers of CRT response, such as regional myocardial work and septal flash/apical rocking?

Although combined assessment of glucose metabolism with PET and viability with CMR demonstrated a high overall performance to predict CRT response (Chapter III), PET is associated with a radiation burden for the patient and requires a dedicated patient preparation. Therefore, we plan to compare the predictive value of PET to other non-invasive imaging-derived markers of CRT response, such as regional myocardial work, and SF/AR, in order to see whether glucose metabolism is superior and therefore PET imaging, especially in non-ischemic HF patients, is justified.

Can septal scar be reliably assessed with nuclear imaging or echocardiography as compared to the gold standard LGE CMR?

Presence of implantable devices and poor renal function has prevented us from performing CMR in about 40% of the recruited patients. Therefore, the prediction model developed in our study could not be applied in patients lacking information on viability/scar. Therefore we plan

to explore the feasibility of other modalities, such as echocardiography or nuclear imaging, to reliably assess the myocardial scar, what can be especially important in patients with contra-indications for CMR or in centers with low CMR availability or expertise.

Is the performance of ^{99m}Tc-Teboroxime at least non-inferior to routinely used clinical tracers?

Whereas our experimental findings in Chapter IV provided evidence for good image quality and possible perfusion quantification with ^{99m}Tc-Teboroxime using a cardiac SPECT CZT camera, further optimization/development of a ^{99m}Tc-Teboroxime-specific kinetic model and comparison to routinely used ^{99m}Tc-labeled tracers should be performed before pursuing this path.

REFERENCES

1. Auricchio A, Fantoni C, Regoli F, Carbucicchio C, Goette A, Geller C, et al. Characterization of Left Ventricular Activation in Patients with Heart Failure and Left Bundle-Branch Block. Circulation. 2004;109:1133–9.

2. Vassallo JA, Cassidy DM, Marchlinski FE, Buxton AE, Waxman HL, Doherty JU, et al. Endocardial activation of left bundle branch block. Circulation [Internet]. 1984;69:914–23. Available from: http://www.ncbi.nlm.nih.gov/pubmed/6705167

3. Vaillant C, Martins RP, Donal E, Leclercq C, Thébault C, Behar N, et al. Resolution of Left Bundle Branch Block–Induced Cardiomyopathy by Cardiac Resynchronization Therapy. J Am Coll Cardiol [Internet]. 2013;61:1089–95. Available from: https://linkinghub.elsevier.com/retrieve/pii/S0735109712059955

4. Duchenne J. Regional myocardial work characterisation in the remodelled left ventricle. KU Leuven-University Leuven, PhD Thesis. 2018;3.

5. Derval N, Duchateau J, Mahida S, Eschalier R, Sacher F, Lumens J, et al. Distinctive Left Ventricular Activations Associated With ECG Pattern in Heart Failure Patients. Circ Arrhythm Electrophysiol [Internet]. 2017;10. Available from: http://www.ncbi.nlm.nih.gov/pubmed/28630171

6. Lieberman R, Padeletti L, Schreuder J, Jackson K, Michelucci A, Colella A, et al. Ventricular pacing lead location alters systemic hemodynamics and left ventricular function in patients with and without reduced ejection fraction. J Am Coll Cardiol [Internet]. 2006;48:1634–41. Available from: http://www.ncbi.nlm.nih.gov/pubmed/17045900

7. Aro AL, Anttonen O, Tikkanen JT, Junttila MJ, Kerola T, Rissanen HA, et al. Intraventricular conduction delay in a standard 12-lead electrocardiogram as a predictor of mortality in the general population. Circ Arrhythm Electrophysiol [Internet]. 2011;4:704–10. Available from: http://www.ncbi.nlm.nih.gov/pubmed/21841194

8. Brignole M, Auricchio A, Baron-Esquivias G, Bordachar P, Boriani G, Breithardt O-A, et al. 2013 ESC Guidelines on cardiac pacing and cardiac resynchronization therapy: The Task Force on cardiac pacing and resynchronization therapy of the European Society of Cardiology (ESC). Developed in collaboration with the European Heart Rhythm Association (EHRA). Europace [Internet]. Narnia; 2013 [cited 2019 Mar 26];15:1070–118. Available from: https://academic.oup.com/europace/article-lookup/doi/10.1093/europace/eut206

9. Saba S, Marek J, Schwartzman D, Jain S, Adelstein E, White P, et al. Echocardiography-Guided Left Ventricular Lead Placement for Cardiac Resynchronization Therapy. Circ Hear Fail [Internet]. 2013;6:427–34. Available from: https://www.ahajournals.org/doi/10.1161/CIRCHEARTFAILURE.112.000078

10. Khan FZ, Virdee MS, Palmer CR, Pugh PJ, O'Halloran D, Elsik M, et al. Targeted Left Ventricular Lead Placement to Guide Cardiac Resynchronization Therapy. J Am Coll Cardiol [Internet].

2012;59:1509–18. Available from: https://linkinghub.elsevier.com/retrieve/pii/S0735109712003725
11. Ponikowski P, Voors AA, Anker SD, Bueno H, Cleland JGF, Coats AJS, et al. 2016 ESC Guidelines for the diagnosis and treatment of acute and chronic heart failure: The Task Force for the diagnosis and treatment of acute and chronic heart failure of the European Society of Cardiology (ESC). Developed with the special contribution. Eur J Heart Fail [Internet]. 2016;18:891–975. Available from: http://www.ncbi.nlm.nih.gov/pubmed/27207191
12. Ruschitzka F, Abraham WT, Singh JP, Bax JJ, Borer JS, Brugada J, et al. Cardiac-Resynchronization Therapy in Heart Failure with a Narrow QRS Complex. N Engl J Med [Internet]. Massachusetts Medical Society ; 2013 [cited 2019 Feb 11];369:1395–405. Available from: http://www.nejm.org/doi/10.1056/NEJMoa1306687
13. Abraham WT, Fisher WG, Smith AL, Delurgio DB, Leon AR, Loh E, et al. Cardiac Resynchronization in Chronic Heart Failure. N Engl J Med [Internet]. 2002;346:1845–53. Available from: http://www.nejm.org/doi/abs/10.1056/NEJMoa013168
14. Francia P, Balla C, Paneni F, Volpe M. Left bundle-branch block--pathophysiology, prognosis, and clinical management. Clin Cardiol [Internet]. 2007;30:110–5. Available from: http://www.ncbi.nlm.nih.gov/pubmed/17385703
15. Baldasseroni S, Opasich C, Gorini M, Lucci D, Marchionni N, Marini M, et al. Left bundle-branch block is associated with increased 1-year sudden and total mortality rate in 5517 outpatients with congestive heart failure: a report from the Italian network on congestive heart failure. Am Heart J [Internet]. 2002;143:398–405. Available from: http://www.ncbi.nlm.nih.gov/pubmed/11868043
16. Kumar V, Venkataraman R, Aljaroudi W, Osorio J, Heo J, Iskandrian AE, et al. Implications of left bundle branch block in patient treatment. Am J Cardiol [Internet]. 2013;111:291–300. Available from: http://www.ncbi.nlm.nih.gov/pubmed/23111137
17. Lund LH, Jurga J, Edner M, Benson L, Dahlström U, Linde C, et al. Prevalence, correlates, and prognostic significance of QRS prolongation in heart failure with reduced and preserved ejection fraction. Eur Heart J [Internet]. 2013;34:529–39. Available from: http://www.ncbi.nlm.nih.gov/pubmed/23041499
18. Strauss DG, Selvester RH, Wagner GS. Defining left bundle branch block in the era of cardiac resynchronization therapy. Am J Cardiol [Internet]. Elsevier Inc.; 2011;107:927–34. Available from: http://dx.doi.org/10.1016/j.amjcard.2010.11.010
19. Risum N, Strauss D, Sogaard P, Loring Z, Hansen TF, Bruun NE, et al. Left bundle-branch block: The relationship between electrocardiogram electrical activation and echocardiography mechanical contraction. Am Heart J [Internet]. 2013;166:340–8. Available from: https://linkinghub.elsevier.com/retrieve/pii/S0002870313002949
20. Yu C-M, Lin H, Zhang Q, Sanderson JE. High prevalence of left ventricular systolic and diastolic asynchrony in patients with congestive heart failure and normal QRS duration. Heart [Internet]. 2003;89:54–60. Available from: http://www.ncbi.nlm.nih.gov/pubmed/12482792

21. Perry R, De Pasquale CG, Chew DP, Aylward PE, Joseph MX. QRS Duration Alone Misses Cardiac Dyssynchrony in a Substantial Proportion of Patients with Chronic Heart Failure. J Am Soc Echocardiogr [Internet]. 2006;19:1257–63. Available from: https://linkinghub.elsevier.com/retrieve/pii/S089473170600472X

22. Yu C-M, Chan Y-S, Zhang Q, Yip GWK, Chan C-K, Kum LCC, et al. Benefits of cardiac resynchronization therapy for heart failure patients with narrow QRS complexes and coexisting systolic asynchrony by echocardiography. J Am Coll Cardiol [Internet]. 2006;48:2251–7. Available from: http://www.ncbi.nlm.nih.gov/pubmed/17161255

23. Bleeker GB, Holman ER, Steendijk P, Boersma E, van der Wall EE, Schalij MJ, et al. Cardiac resynchronization therapy in patients with a narrow QRS complex. J Am Coll Cardiol [Internet]. 2006;48:2243–50. Available from: http://www.ncbi.nlm.nih.gov/pubmed/17161254

24. Bax JJ, Bleeker GB, Marwick TH, Molhoek SG, Boersma E, Steendijk P, et al. Left ventricular dyssynchrony predicts response and prognosis after cardiac resynchronization therapy. J Am Coll Cardiol [Internet]. 2004;44:1834–40. Available from: http://www.ncbi.nlm.nih.gov/pubmed/15519016

25. Yu C-M, Fung W-H, Lin H, Zhang Q, Sanderson JE, Lau C-P. Predictors of left ventricular reverse remodeling after cardiac resynchronization therapy for heart failure secondary to idiopathic dilated or ischemic cardiomyopathy. Am J Cardiol [Internet]. 2003;91:684–8. Available from: https://linkinghub.elsevier.com/retrieve/pii/S0002914902034045

26. Cleland JGF, Daubert J-C, Erdmann E, Freemantle N, Gras D, Kappenberger L, et al. The Effect of Cardiac Resynchronization on Morbidity and Mortality in Heart Failure. N Engl J Med [Internet]. 2005;352:1539–49. Available from: http://www.nejm.org/doi/abs/10.1056/NEJMoa050496

27. Chung ES, Leon AR, Tavazzi L, Sun J-P, Nihoyannopoulos P, Merlino J, et al. Results of the Predictors of Response to CRT (PROSPECT) trial. Circulation [Internet]. 2008;117:2608–16. Available from: http://www.ncbi.nlm.nih.gov/pubmed/18458170

28. Gorcsan J, Sogaard P, Bax JJ, Singh JP, Abraham WT, Borer JS, et al. Association of persistent or worsened echocardiographic dyssynchrony with unfavourable clinical outcomes in heart failure patients with narrow QRS width: a subgroup analysis of the EchoCRT trial. Eur Heart J [Internet]. 2016;37:49–59. Available from: https://academic.oup.com/eurheartj/article-lookup/doi/10.1093/eurheartj/ehv418

29. Parsai C, Bijnens B, Sutherland GR, Baltabaeva A, Claus P, Marciniak M, et al. Toward understanding response to cardiac resynchronization therapy: left ventricular dyssynchrony is only one of multiple mechanisms. Eur Heart J [Internet]. 2009;30:940–9. Available from: http://www.ncbi.nlm.nih.gov/pubmed/19004844

30. Ghani A, Delnoy PPH, Ottervanger JP, Misier ARR, Smit JJJ, Adiyaman A, et al. Apical rocking is predictive of response to cardiac resynchronization therapy. Int J Cardiovasc Imaging [Internet]. 2015;31:717–25. Available from: http://link.springer.com/10.1007/s10554-015-0607-0

31. Stankovic I, Prinz C, Ciarka A, Daraban AM, Kotrc M, Aarones M, et al. Relationship of visually assessed apical rocking and septal flash to response and long-term survival following cardiac

resynchronization therapy (PREDICT-CRT). Eur Heart J Cardiovasc Imaging. 2016;17:262–9.
32. Chen J, Garcia E V, Folks RD, Cooke CD, Faber TL, Tauxe EL, et al. Onset of left ventricular mechanical contraction as determined by phase analysis of ECG-gated myocardial perfusion SPECT imaging: development of a diagnostic tool for assessment of cardiac mechanical dyssynchrony. J Nucl Cardiol [Internet]. 12:687–95. Available from: http://www.ncbi.nlm.nih.gov/pubmed/16344231
33. Henneman MM, Chen J, Dibbets-Schneider P, Stokkel MP, Bleeker GB, Ypenburg C, et al. Can LV dyssynchrony as assessed with phase analysis on gated myocardial perfusion SPECT predict response to CRT? J Nucl Med [Internet]. 2007;48:1104–11. Available from: http://www.ncbi.nlm.nih.gov/pubmed/17574987
34. Tao N, Qiu Y, Tang H, Qian Z, Wu H, Zhu R, et al. Assessment of left ventricular contraction patterns using gated SPECT MPI to predict cardiac resynchronization therapy response. J Nucl Cardiol [Internet]. Springer US; 2018 [cited 2019 Jun 24];25:2029–38. Available from: http://link.springer.com/10.1007/s12350-017-0949-1
35. Bilchick KC, Dimaano V, Wu KC, Helm RH, Weiss RG, Lima JA, et al. Cardiac Magnetic Resonance Assessment of Dyssynchrony and Myocardial Scar Predicts Function Class Improvement Following Cardiac Resynchronization Therapy. JACC Cardiovasc Imaging [Internet]. 2008;1:561–8. Available from: https://linkinghub.elsevier.com/retrieve/pii/S1936878X08002623
36. COCHET H, DENIS A, PLOUX S, LUMENS J, AMRAOUI S, DERVAL N, et al. Pre- and Intra-Procedural Predictors of Reverse Remodeling After Cardiac Resynchronization Therapy: An MRI Study. J Cardiovasc Electrophysiol [Internet]. 2013;24:682–91. Available from: http://doi.wiley.com/10.1111/jce.12101
37. Duchenne J, Turco A, Ünlü S, Pagourelias ED, Vunckx K, Degtiarova G, et al. Left Ventricular Remodeling Results in Homogenization of Myocardial Work Distribution. Circ Arrhythmia Electrophysiol [Internet]. 2019;12:1–14. Available from: https://www.ahajournals.org/doi/10.1161/CIRCEP.118.007224
38. Ono S, Nohara R, Kambara H, Okuda K, Kawai C. Regional myocardial perfusion and glucose metabolism in experimental left bundle branch block. Circulation [Internet]. 1992;85:1125–31. Available from: http://www.ncbi.nlm.nih.gov/pubmed/1537110
39. Nowak B, Sinha AM, Schaefer WM, Koch KC, Kaiser HJ, Hanrath P, et al. Cardiac resynchronization therapy homogenizes myocardial glucose metabolism and perfusion in dilated cardiomyopathy and left bundle branch block. J Am Coll Cardiol. 2003;41:1523–8.
40. Masci PG, Marinelli M, Piacenti M, Lorenzoni V, Positano V, Lombardi M, et al. Myocardial structural, perfusion, and metabolic correlates of left bundle branch block mechanical derangement in patients with dilated cardiomyopathy: A tagged cardiac magnetic resonance and positron emission tomography study. Circ Cardiovasc Imaging. 2010;3:482–90.
41. Stanley WC, Recchia FA, Lopaschuk GD. Myocardial substrate metabolism in the normal and failing heart. Physiol Rev [Internet]. 2005;85:1093–129. Available from:

http://www.ncbi.nlm.nih.gov/pubmed/15987803
42. Depre C, Vanoverschelde JL, Taegtmeyer H. Glucose for the heart. Circulation [Internet]. 1999;99:578–88. Available from: http://www.ncbi.nlm.nih.gov/pubmed/9927407
43. Mochizuki T, Tsukamoto E, Kuge Y, Kanegae K, Zhao S, Hikosaka K, et al. FDG uptake and glucose transporter subtype expressions in experimental tumor and inflammation models. J Nucl Med [Internet]. 2001;42:1551–5. Available from: http://www.ncbi.nlm.nih.gov/pubmed/11585872
44. Knuuti MJ, Nuutila P, Ruotsalainen U, Saraste M, Härkönen R, Ahonen A, et al. Euglycemic hyperinsulinemic clamp and oral glucose load in stimulating myocardial glucose utilization during positron emission tomography. J Nucl Med [Internet]. 1992;33:1255–62. Available from: http://www.ncbi.nlm.nih.gov/pubmed/1613561
45. Knaapen P, Lubberink M. Cardiac positron emission tomography: myocardial perfusion and metabolism in clinical practice. Clin Res Cardiol [Internet]. 2008;97:791–6. Available from: http://www.ncbi.nlm.nih.gov/pubmed/18432394
46. Murthy VL, Naya M, Foster CR, Hainer J, Gaber M, Di Carli G, Blankstein R, Dorbala S, Sitek A, Pencina MJ DCM. Improved cardiac risk assessment with noninvasive measures of coronary flow reserve. Circulation. 2014;54:873–9.
47. Huang SC, Williams BA, Krivokapich J, Araujo L, Phelps ME, Schelbert HR. Rabbit myocardial 82Rb kinetics and a compartmental model for blood flow estimation. Am J Physiol [Internet]. 1989;256:H1156-64. Available from: http://www.ncbi.nlm.nih.gov/pubmed/2784945
48. Schelbert HR, Phelps ME, Huang SC, MacDonald NS, Hansen H, Selin C, et al. N-13 ammonia as an indicator of myocardial blood flow. Circulation [Internet]. 1981;63:1259–72. Available from: http://www.ncbi.nlm.nih.gov/pubmed/7226473
49. Khorsand A, Graf S, Eidherr H, Wadsak W, Kletter K, Sochor H, et al. Gated cardiac 13N-NH3 PET for assessment of left ventricular volumes, mass, and ejection fraction: comparison with electrocardiography-gated 18F-FDG PET. J Nucl Med [Internet]. 2005;46:2009–13. Available from: http://www.ncbi.nlm.nih.gov/pubmed/16330564
50. Bengel FM, Higuchi T, Javadi MS, Lautamäki R. Cardiac Positron Emission Tomography. J Am Coll Cardiol [Internet]. 2009;54:1–15. Available from: https://linkinghub.elsevier.com/retrieve/pii/S0735109709011723
51. Huisman MC, Higuchi T, Reder S, Nekolla SG, Poethko T, Wester H-J, et al. Initial characterization of an 18F-labeled myocardial perfusion tracer. J Nucl Med [Internet]. 2008;49:630–6. Available from: http://www.ncbi.nlm.nih.gov/pubmed/18344426
52. Yu M, Guaraldi MT, Mistry M, Kagan M, McDonald JL, Drew K, et al. BMS-747158-02: a novel PET myocardial perfusion imaging agent. J Nucl Cardiol [Internet]. 14:789–98. Available from: http://www.ncbi.nlm.nih.gov/pubmed/18022105
53. Jødal L, Le Loirec C, Champion C. Positron range in PET imaging: an alternative approach for assessing and correcting the blurring. Phys Med Biol [Internet]. 2012;57:3931–43. Available from:

http://www.ncbi.nlm.nih.gov/pubmed/22643300
54. Maddahi J, Czernin J, Lazewatsky J, Huang S-C, Dahlbom M, Schelbert H, et al. Phase I, first-in-human study of BMS747158, a novel 18F-labeled tracer for myocardial perfusion PET: dosimetry, biodistribution, safety, and imaging characteristics after a single injection at rest. J Nucl Med [Internet]. 2011;52:1490–8. Available from: http://www.ncbi.nlm.nih.gov/pubmed/21849402
55. Berman DS, Maddahi J, Tamarappoo BK, Czernin J, Taillefer R, Udelson JE, et al. Phase II safety and clinical comparison with single-photon emission computed tomography myocardial perfusion imaging for detection of coronary artery disease: flurpiridaz F 18 positron emission tomography. J Am Coll Cardiol [Internet]. 2013;61:469–77. Available from: http://www.ncbi.nlm.nih.gov/pubmed/23265345
56. van den Hoff J, Burchert W, Börner AR, Fricke H, Kühnel G, Meyer GJ, et al. [1-(11)C]Acetate as a quantitative perfusion tracer in myocardial PET. J Nucl Med [Internet]. 2001;42:1174–82. Available from: http://www.ncbi.nlm.nih.gov/pubmed/11483676
57. Vernooy K, Verbeek XAAM, Peschar M, Crijns HJGM, Arts T, Cornelussen RNM, et al. Left bundle branch block induces ventricular remodelling and functional septal hypoperfusion. Eur Heart J [Internet]. 2005;26:91–8. Available from: http://www.ncbi.nlm.nih.gov/pubmed/15615805
58. Rohatgi R, Epstein S, Henriquez J, Ababneh AA, Hickey KT, Pinsky D, et al. Utility of positron emission tomography in predicting cardiac events and survival in patients with coronary artery disease and severe left ventricular dysfunction. Am J Cardiol [Internet]. 2001;87:1096–9. Available from: https://linkinghub.elsevier.com/retrieve/pii/S0002914901014680
59. Neumann F-J, Sousa-Uva M, Ahlsson A, Alfonso F, Banning AP, Benedetto U, et al. [2018 ESC/EACTS Guidelines on myocardial revascularization. The Task Force on myocardial revascularization of the European Society of Cardiology (ESC) and European Association for Cardio-Thoracic Surgery (EACTS)]. G Ital Cardiol (Rome) [Internet]. 20:1S–61S. Available from: http://www.ncbi.nlm.nih.gov/pubmed/31379378
60. Eitzman D, Al-Aouar Z, Kanter HL, vom Dahl J, Kirsh M, Deeb GM, et al. Clinical outcome of patients with advanced coronary artery disease after viability studies with positron emission tomography. J Am Coll Cardiol [Internet]. 1992;20:559–65. Available from: https://linkinghub.elsevier.com/retrieve/pii/073510979290008B
61. Inoue N, Takahashi N, Ishikawa T, Sumita S, Kobayashi T, Matsushita K, et al. Reverse perfusion-metabolism mismatch predicts good prognosis in patients undergoing cardiac resynchronization therapy: a pilot study. Circ J [Internet]. 2007;71:126–31. Available from: http://www.ncbi.nlm.nih.gov/pubmed/17186990
62. Birnie D, de Kemp RA, Tang AS, Ruddy TD, Gollob MH, Guo A, et al. Reduced septal glucose metabolism predicts response to cardiac resynchronization therapy. J Nucl Cardiol [Internet]. 2012;19:73–83. Available from: http://link.springer.com/10.1007/s12350-011-9483-8
63. Mangiavacchi M, Gasparini M, Faletra F, Klersy C, Morenghi E, Galimberti P, et al. Clinical

predictors of marked improvement in left ventricular performance after cardiac resynchronization therapy in patients with chronic heart failure. Am Heart J [Internet]. 2006;151:477.e1-477.e6. Available from: http://www.ncbi.nlm.nih.gov/pubmed/16442917

64. Knuuti J, Wijns W, Saraste A, Capodanno D, Barbato E, Funck-Brentano C, et al. 2019 ESC Guidelines for the diagnosis and management of chronic coronary syndromes. Eur Heart J [Internet]. 2020;41:407–77. Available from: http://www.ncbi.nlm.nih.gov/pubmed/31504439

65. Taqueti VR, Di Carli MF. Radionuclide Myocardial Perfusion Imaging for the Evaluation of Patients with Known or Suspected Coronary Artery Disease in the Era of Multimodality Cardiovascular Imaging. Prog Cardiovasc Dis [Internet]. Elsevier Inc.; 2015;57:644–53. Available from: http://www.ncbi.nlm.nih.gov/pubmed/25770849

66. Knuuti J, Ballo H, Juarez-Orozco LE, Saraste A, Kolh P, Rutjes AWS, et al. The performance of non-invasive tests to rule-in and rule-out significant coronary artery stenosis in patients with stable angina: a meta-analysis focused on post-test disease probability. Eur Heart J [Internet]. 2018;39:3322–30. Available from: http://www.ncbi.nlm.nih.gov/pubmed/29850808

67. Cremer P, Hachamovitch R, Tamarappoo B. Clinical decision making with myocardial perfusion imaging in patients with known or suspected coronary artery disease. Semin Nucl Med. 2015;44:320–9.

68. Shaw LJ, Iskandrian AE. Prognostic value of gated myocardial perfusion SPECT. J Nucl Cardiol. 2004;11:171–85.

69. Lima RSL, Watson DD, Goode AR, Siadaty MS, Ragosta M, Beller GA, et al. Incremental value of combined perfusion and function over perfusion alone by gated SPECT myocardial perfusion imaging for detection of severe three-vessel coronary artery disease. J Am Coll Cardiol. Elsevier Masson SAS; 2003;42:64–70.

70. Ragosta M, Bishop AH, Lipson LC, Watson DD, Gimple LW, Sarembock IJ, et al. Comparison Between Angiography and Fractional Flow Reserve Versus Single-Photon Emission Computed Tomographic Myocardial Perfusion Imaging for Determining Lesion Significance in Patients With Multivessel Coronary Disease. Am J Cardiol. 2007;99:896–902.

71. Parkash R, DeKemp RA, Ruddy TD, Kitsikis A, Hart R, Beauchesne L, et al. Potential utility of rubidium 82 PET quantification in patients with 3-vessel coronary artery disease. J Nucl Cardiol [Internet]. 11:440–9. Available from: http://www.ncbi.nlm.nih.gov/pubmed/15295413

72. Ziadi MC, Dekemp RA, Williams K, Guo A, Renaud JM, Chow BJW, et al. Does quantification of myocardial flow reserve using rubidium-82 positron emission tomography facilitate detection of multivessel coronary artery disease? J Nucl Cardiol [Internet]. 2012;19:670–80. Available from: http://www.ncbi.nlm.nih.gov/pubmed/22415819

73. Saraste A, Kajander S, Han C, Nesterov SV KJ. PET: is myocardial flow quantification a clinical reality? J Nucl Cardiol. 2012;19:1044–59.

74. Hesse B, Tägil K, Cuocolo A, Anagnostopoulos C, Bardiés M, Bax J, et al. EANM/ESC procedural

guidelines for myocardial perfusion imaging in nuclear cardiology. Eur J Nucl Med Mol Imaging [Internet]. 2005;32:855–97. Available from: http://www.ncbi.nlm.nih.gov/pubmed/15909197

75. Danad I, Raijmakers PG, Driessen RS, Leipsic J, Raju R, Naoum C, et al. Comparison of Coronary CT Angiography, SPECT, PET, and Hybrid Imaging for Diagnosis of Ischemic Heart Disease Determined by Fractional Flow Reserve. JAMA Cardiol [Internet]. 2017;2:1100. Available from: http://cardiology.jamanetwork.com/article.aspx?doi=10.1001/jamacardio.2017.2471

76. Agostini D, Roule V, Nganoa C, Roth N, Baavour R, Parienti J-J, et al. First validation of myocardial flow reserve assessed by dynamic 99mTc-sestamibi CZT-SPECT camera: head to head comparison with 15O-water PET and fractional flow reserve in patients with suspected coronary artery disease. The WATERDAY study. Eur J Nucl Med Mol Imaging [Internet]. 2018;45:1079–90. Available from: http://link.springer.com/10.1007/s00259-018-3958-7

77. Nakazato R, Berman DS, Hayes SW, Fish M, Padgett R, Xu Y, et al. Myocardial perfusion imaging with a solid-state camera: simulation of a very low dose imaging protocol. J Nucl Med [Internet]. 2013;54:373–9. Available from: http://www.ncbi.nlm.nih.gov/pubmed/23321457

78. Wells RG, Timmins R, Klein R, Lockwood J, Marvin B, deKemp R a., et al. Dynamic SPECT Measurement of Absolute Myocardial Blood Flow in a Porcine Model. J Nucl Med [Internet]. 2014;55:1685–91. Available from: http://jnm.snmjournals.org/cgi/doi/10.2967/jnumed.114.139782%5Cnhttp://jnm.snmjournals.org/content/55/10/1685.long

79. Salerno M, Beller GA. Noninvasive assessment of myocardial perfusion. Circ Cardiovasc Imaging. 2009;2:412–24.

80. Baggish AL, Boucher CA. Radiopharmaceutical agents for myocardial perfusion imaging. Circulation. 2008;118:1668–74.

81. Kailasnath P, Sinusas AJ. Comparison of TI-201 with Tc-99m-labeled myocardial perfusion agents: Technical, physiologic, and clinical issues. J Nucl Cardiol. 2001;8:482–98.

82. Stewart RE, Schwaiger M, Hutchins GD, Chiao P, Gallagher KP, Petry NA, et al. Myocardial Clearance Kinetics of Technetium 99m-SQ30217: A Marker of Regional Myocardial Blood Flow. J Nucl Med. 1990;31:1183–90.

83. Marshall RC, Leidholdt EM, Barnett CA. The effect of flow on technetium-99m-Teboroxime (SQ30217) and thallium-201 extraction and retention in rabbit heart. J Nucl Med. 1991;32:1979–88.

84. Sogbein OO, Pelletier-Galarneau M, Schindler TH, Wei L, Wells RG, Ruddy TD. New SPECT and PET Radiopharmaceuticals for Imaging Cardiovascular Disease. Biomed Res Int [Internet]. 2014;2014:1–24. Available from: http://www.hindawi.com/journals/bmri/2014/942960/

85. Hesse B, Diaz LA, Snader CE, Blackstone EH, Lauer MS. Complete bundle branch block as an independent predictor of all-cause mortality: report of 7,073 patients referred for nuclear exercise testing. Am J Med [Internet]. 2001;110:253–9. Available from: http://www.ncbi.nlm.nih.gov/pubmed/11239842

86. Lewis P, Nunan T, Dynes A, Maisey M. The use of low-dose intravenous insulin in clinical myocardial F-18 FDG PET scanning. Clin Nucl Med [Internet]. 1996;21:15–8. Available from: http://www.ncbi.nlm.nih.gov/pubmed/8741883
87. Turco A, Gheysens O, Duchenne J, Nuyts J, Rega F, Voigt JU, et al. Partial volume and motion correction in cardiac PET: First results from an in vs ex vivo comparison using animal datasets. J Nucl Cardiol [Internet]. 2019; Available from: http://www.ncbi.nlm.nih.gov/pubmed/30644052
88. Nuyts J, Suetens P, Oosterlinck A, De Roo M, Mortelmans L. Delineation of ECT images using global constraints and dynamic programming. IEEE Trans Med Imaging [Internet]. 1991;10:489–98. Available from: http://www.ncbi.nlm.nih.gov/pubmed/18222853
89. Cerqueira MD, Weissman NJ, Dilsizian V, Jacobs AK, Kaul S, Laskey WK, et al. Standardized myocardial segmentation and nomenclature for tomographic imaging of the heart. A statement for healthcare professionals from the Cardiac Imaging Committee of the Council on Clinical Cardiology of the American Heart Association. Circulation. 2002;105:539–42.
90. Hutchins GD, Schwaiger M, Rosenspire KC, Krivokapich J, Schelbert H, Kuhl DE. Noninvasive quantification of regional blood flow in the human heart using N-13 ammonia and dynamic positron emission tomographic imaging. J Am Coll Cardiol [Internet]. 1990;15:1032–42. Available from: http://www.ncbi.nlm.nih.gov/pubmed/2312957
91. DeGrado TR, Hanson MW, Turkington TG, Delong DM, Brezinski DA, Vallée JP, et al. Estimation of myocardial blood flow for longitudinal studies with 13N-labeled ammonia and positron emission tomography. J Nucl Cardiol [Internet]. 3:494–507. Available from: http://www.ncbi.nlm.nih.gov/pubmed/8989674
92. Bormans G, Maes A, Langendries W, Nuyts J, Vrolix M, Vanhaecke J, et al. Metabolism of nitrogen-13 labelled ammonia in different conditions in dogs, human volunteers and transplant patients. Eur J Nucl Med [Internet]. 1995;22:116–21. Available from: http://www.ncbi.nlm.nih.gov/pubmed/7758497
93. Flameng WJ, Shivalkar B, Spiessens B, Maes A, Nuyts J, VanHaecke J, et al. PET scan predicts recovery of left ventricular function after coronary artery bypass operation. Ann Thorac Surg [Internet]. 1997;64:1694–701. Available from: http://www.ncbi.nlm.nih.gov/pubmed/9436557
94. Neri G, Zanco P, Zanon F, Buchberger R. Effect of biventricular pacing on metabolism and perfusion in patients affected by dilated cardiomyopathy and left bundle branch block: Evaluation by positron emission tomography. Europace. 2003;5:111–5.
95. Nowak B, Stellbrink C, Schaefer WM, Sinha AM, Breithardt OA, Kaiser H-J, et al. Comparison of regional myocardial blood flow and perfusion in dilated cardiomyopathy and left bundle branch block: role of wall thickening. J Nucl Med [Internet]. 2004;45:414–8. Available from: http://www.ncbi.nlm.nih.gov/pubmed/15001681
96. Baller D, Vogt J, Lindner O, Lamp B, Holzinger J, Kammeier A, et al. Myocardial oxygen consumption and perfusion before and after cardiac resynchronization therapy: Experimental observations and clinical implications. Eur Hear Journal, Suppl. 2004;6.

97. Koepfli P, Wyss CA, Gaemperli O, Siegrist PT, Klainguti M, Schepis T, et al. Left bundle branch block causes relative but not absolute septal underperfusion during exercise. Eur Heart J [Internet]. 2009;30:2993–9. Available from: http://www.ncbi.nlm.nih.gov/pubmed/19734552

98. Stankovic I, Aarones M, Smith H-J, Vörös G, Kongsgaard E, Neskovic AN, et al. Dynamic relationship of left-ventricular dyssynchrony and contractile reserve in patients undergoing cardiac resynchronization therapy. Eur Heart J [Internet]. 2014;35:48–55. Available from: http://www.ncbi.nlm.nih.gov/pubmed/23918757

99. Bellina CR, Parodi O, Camici P, Salvadori PA, Taddei L, Fusani L, et al. Simultaneous in vitro and in vivo validation of nitrogen-13-ammonia for the assessment of regional myocardial blood flow. J Nucl Med [Internet]. 1990;31:1335–43. Available from: http://www.ncbi.nlm.nih.gov/pubmed/2384801

100. Knaapen P, van Campen L (C.)M. C, de Cock CC, Götte MJW, Visser CA, Lammertsma AA, et al. Effects of Cardiac Resynchronization Therapy on Myocardial Perfusion Reserve. Circulation [Internet]. 2004 [cited 2018 Oct 25];110:646–51. Available from: https://www.ahajournals.org/doi/10.1161/01.CIR.0000138108.68719.C1

101. Zanco P, Desideri A, Mobilia G, Cargnel S, Milan E, Celegon L, et al. Effects of left bundle branch block on myocardial FDG PET in patients without significant coronary artery stenoses. J Nucl Med [Internet]. 2000;41:973–7. Available from: http://www.ncbi.nlm.nih.gov/pubmed/10855620

102. Shah A, Schelbert HR, Schwaiger M, Henze E, Hansen H, Selin C, et al. Measurement of regional myocardial blood flow with N-13 ammonia and positron-emission tomography in intact dogs. J Am Coll Cardiol [Internet]. 1985;5:92–100. Available from: http://www.ncbi.nlm.nih.gov/pubmed/3871096

103. Choi Y, Huang SC, Hawkins RA, Kim JY, Kim BT, Hoh CK, et al. Quantification of myocardial blood flow using 13N-ammonia and PET: comparison of tracer models. J Nucl Med [Internet]. 1999;40:1045–55. Available from: http://www.ncbi.nlm.nih.gov/pubmed/10452323

104. Ypenburg C, Westenberg JJ, Bleeker GB, de Veire N Van, Marsan NA, Henneman MM, et al. Noninvasive Imaging in Cardiac Resynchronization Therapy-Part 1: Selection of Patients. Pace-Pacing Clin Electrophysiol. 2008;31:1475–99.

105. Cvijic M, Duchenne J, Unlü S, Michalski B, Aarones M, Winter S, et al. Timing of myocardial shortening determines left ventricular regional myocardial work and regional remodelling in hearts with conduction delays. Eur Heart J Cardiovasc Imaging. 2018;19:941–9.

106. Russell K, Eriksen M, Aaberge L, Wilhelmsen N, Skulstad H, Remme EW, et al. A novel clinical method for quantification of regional left ventricular pressure-strain loop area: a non-invasive index of myocardial work. Eur Heart J [Internet]. Oxford University Press; 2012 [cited 2019 Feb 12];33:724–33. Available from: http://www.ncbi.nlm.nih.gov/pubmed/22315346

107. Vardas PE, Auricchio A, Blanc J-J, Daubert J-C, Drexler H, Ector H, et al. Guidelines for cardiac pacing and cardiac resynchronization therapy. The Task Force for Cardiac Pacing and Cardiac Resynchronization Therapy of the European Society of Cardiology. Developed in collaboration with the European Heart Rhythm Association. Europace [Internet]. 2007;9:959–98. Available from:

http://www.ncbi.nlm.nih.gov/pubmed/17726043
108. Castro P, Winter JL, Verdejo H, Orellana P, Quintana JC, Greig D, et al. Relationship between mechanical and metabolic dyssynchrony with left bundle branch block: evaluation by 18-fluorodeoxyglucose positron emission tomography in patients with non-ischemic heart failure. J Heart Lung Transplant [Internet]. 2012;31:1096–101. Available from: http://www.ncbi.nlm.nih.gov/pubmed/22975099
109. Mukherjee A, Patel CD, Naik N, Sharma G, Roy A. Quantitative assessment of cardiac mechanical dyssynchrony and prediction of response to cardiac resynchronization therapy in patients with nonischaemic dilated cardiomyopathy using gated myocardial perfusion SPECT. Nucl Med Commun [Internet]. 2015;36:494–501. Available from: http://www.ncbi.nlm.nih.gov/pubmed/25695610
110. Beela AS, Ünlü S, Duchenne J, Ciarka A, Daraban AM, Kotrc M, et al. Assessment of mechanical dyssynchrony can improve the prognostic value of guideline-based patient selection for cardiac resynchronization therapy. Eur Hear J - Cardiovasc Imaging [Internet]. 2018;1–9. Available from: https://academic.oup.com/ehjcimaging/advance-article/doi/10.1093/ehjci/jey029/4903003
111. Konstam MA, Kramer DG, Patel AR, Maron MS, Udelson JE. Left ventricular remodeling in heart failure: current concepts in clinical significance and assessment. JACC Cardiovasc Imaging [Internet]. 2011;4:98–108. Available from: http://www.ncbi.nlm.nih.gov/pubmed/21232712
112. Degtiarova G, Claus P, Duchenne J, Schramm G, Nuyts J, Verberne HJ, et al. Impact of left bundle branch block on myocardial perfusion and metabolism: A positron emission tomography study. J Nucl Cardiol [Internet]. 2019; Available from: http://www.ncbi.nlm.nih.gov/pubmed/31578659
113. Degtiarova G, Claus P, Duchenne J, Cvijic M, Schramm G, Nuyts J, et al. Low septal to lateral wall 18F-FDG ratio is highly associated with mechanical dyssynchrony in non-ischemic CRT candidates. EJNMMI Res [Internet]. 2019;9:105. Available from: http://www.ncbi.nlm.nih.gov/pubmed/31820130
114. Ypenburg C, Schalij MJ, Bleeker GB, Steendijk P, Boersma E, Dibbets-Schneider P, et al. Impact of viability and scar tissue on response to cardiac resynchronization therapy in ischaemic heart failure patients. Eur Heart J [Internet]. 2007;28:33–41. Available from: http://www.ncbi.nlm.nih.gov/pubmed/17121757
115. Heiberg E, Sjögren J, Ugander M, Carlsson M, Engblom H, Arheden H. Design and validation of Segment - freely available software for cardiovascular image analysis. BMC Med Imaging [Internet]. 2010;10:1. Available from: https://bmcmedimaging.biomedcentral.com/articles/10.1186/1471-2342-10-1
116. Duckett SG, Ginks M, Shetty A, Kirubakaran S, Bostock J, Kapetanakis S, et al. Adverse response to cardiac resynchronisation therapy in patients with septal scar on cardiac MRI preventing a septal right ventricular lead position. J Interv Card Electrophysiol [Internet]. 2012;33:151–60. Available from: http://www.ncbi.nlm.nih.gov/pubmed/22127378
117. Chalil S, Foley PWX, Muyhaldeen SA, Patel KCR, Yousef ZR, Smith REA, et al. Late gadolinium

enhancement-cardiovascular magnetic resonance as a predictor of response to cardiac resynchronization therapy in patients with ischaemic cardiomyopathy. Europace [Internet]. 2007;9:1031–7. Available from: http://www.ncbi.nlm.nih.gov/pubmed/17933857

118. Stankovic I, Belmans A, Prinz C, Ciarka A, Maria Daraban A, Kotrc M, et al. The association of volumetric response and long-term survival after cardiac resynchronization therapy. Eur Hear J - Cardiovasc Imaging [Internet]. 2017; Available from: https://academic.oup.com/ehjcimaging/article-lookup/doi/10.1093/ehjci/jex188

119. Murray CJ, Lopez AD. Alternative projections of mortality and disability by cause 1990-2020: Global Burden of Disease Study. Lancet. 1997;349(9064):1498–504.

120. Mozaffarian D, Benjamin EJ, Go AS, Arnett DK, Blaha MJ, Cushman M, et al. Heart disease and stroke statistics-2015 update : A report from the American Heart Association. Circulation. 2015;131:290–322.

121. Klocke F, Baird M, Lorell B, Bateman T, Messer J, Berman D, et al. ACC/AHA/ASNC guidelines for the clinical use of cardiac radionuclide imaging–executive summary: a report of the American College of Cardiology/American Heart Association Task Force on Practice Guidelines (ACC/AHA/ASNC Committee to Revise the 1995 Guidelin. J Am Coll Cardiol. 2003;42:1318–33.

122. Zheng Y, Ji S, Tomaselli E, Ernest C, Freiji T. Effect of co-ligands on chemical and biological properties of (99m)Tc(III) complexes [(99m)Tc(L)(CDO)(CDOH)2BMe] (L=Cl, F, SCN and N3; CDOH2=cyclohexanedione dioxime). Nucl Med Biol. 2014;41:813–24.

123. Narra RK, Nunn AD, Kuczynski BL, Feld T, Wedeking P, Eckelman WC. A neutral technetium-99m complex for myocardial imaging. J Nucl Med. 1989;3011:1830–7.

124. Li Q, Solot G, Frank TL, Wagner HN, Becker LC. Tomographic myocardial perfusion imaging with technetium-99m-Teboroxime at rest and after dipyridamole. J Nucl Med. 1991;32:1968–77.

125. Johnson LL, Seldin DW. Clinical experience with technetium-99m Teboroxime, a neutral, lipophilic myocardial perfusion imaging agent. Am J Cardiol. 1990;66:63–7.

126. Seldin DW, Johnson LL, Blood DK, Muschel MJ, Smith KF, Wall RM, et al. Myocardial perfusion imaging with technetium-99m SQ30217: comparison with thallium-201 and coronary anatomy. J Nucl Med. 1991;32:1968–76.

127. Abraham SA, Mirecki FN, Levine D, Nunn AD, Strauss HW. Myocardial technetium-99m-Teboroxime activity in acute coronary artery occlusion and reperfusion: relation to myocardial blood flow and viability. J Nucl Med. 1995;36:1062–9.

128. Sherif HM, Nekolla SG, Saraste A, Reder S, Yu M, Robinson S, Schwaiger M. Simplified Quantification of Myocardial Flow Reserve with flurpiridaz F 18 : Validation with Microspheres in a Pig Model. J Nucl Med. 2011;52:617–24.

129. Rimoldi O, Schäfers KP, Boellaard R, Turkheimer F, Stegger L, Law MP, Lammerstma AA CP. Quantification of subendocardial and subepicardial blood flow using 15O-labeled water and PET:experimental validation. J Nucl Med. 2006;47(1):163–72.

130. Christian TF, Frankish ML, Sisemoore JH, Christian MR, Gentchos G, Bell SP J-HM. Myocardial perfusion imaging with first-pass computed tomographic imaging: Measurement of coronary flow reserve in an animal model of regional hyperemia. J Nucl Cardiol. 2010;17 (4):625–30.
131. Mahnken AH, Klotz E, Pietsch H, Schmidt B, Allmendinger T, Haberland U et al. Quantitative whole heart stress perfusion CT imaging as noninvasive assessment of hemodynamics in coronary artery stenosis: preliminary animal experience. Invest Radiol. 2010;45:298–305.
132. . Lautamaki R, George RT, Kitagawa K et al. Rubidium-82 PET-CT for quantitative assessment of myocardial blood flow: validation in a canine model of coronary artery stenosis. Eur J Nucl Med Mol Imaging. 2009;36:576–86.
133. Maublant JC, Moins N, Gachon P, Renoux M, Zhang Z, Veyre A. Uptake of technetium-99m-Teboroxime in cultured myocardial cells: comparison with thallium-201 and technetium-99m-sestamibi. J Nucl Med [Internet]. 1993;34:255–9. Available from: http://www.ncbi.nlm.nih.gov/pubmed/8429344
134. Zanco P, Chierichetti F, Fini A, Cargnel S, Ferlin G. Myocardial perfusion, glucose utilization and oxidative metabolism in a patient with left bundle branch block, prior myocardial infarction and diabetes. J Nucl Med [Internet]. 1998;39:261–3. Available from: http://www.ncbi.nlm.nih.gov/pubmed/9476932

CURRICULUM VITAE

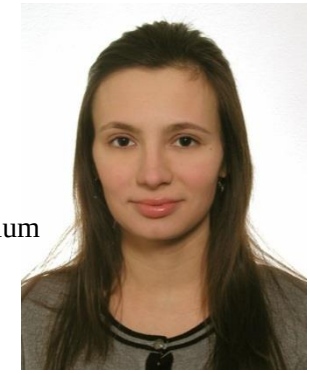

PERSONAL INFROMATION

Name:	**GANNA DEGTIAROVA**
Date and place of birth:	20 June 1989 | Donetsk, Ukraine
Address:	Vaartstraat 35, 3000 Leuven Belgium
E-mail:	ganna.degtiarova@kuleuven.be
Mobile:	+32485878584

CURRENT POSITION

2017 - present	Dept. of Imaging & Pathology, Nuclear Medicine & Molecular Imaging Unit, And Department of Cardiovascular Sciences University of Leuven, Leuven, Belgium	Doctoral research fellow

EDUCATION

Date	University	City	Type of education
2014-2015	M.Gorkiy Donetsk National Medical University; Dept. of Internal medicine & Cardiology, V.K.Gusak Institute of Emergency and Reconstructive Surgery	Donetsk, Ukraine	Residency in Internal Medicine. Diploma: Specialist in Internal medicine
2012-2014	M.Gorkiy Donetsk National Medical University; Dept. of Internal medicine & Cardiology, V.K.Gusak Institute of Emergency and Reconstructive Surgery	Donetsk, Ukraine	Residency in General Medicine. Diploma: Specialist in General medicine
2006-2012	M.Gorkiy Donetsk National Medical University	Donetsk, Ukraine	Medical education. Graduated with great distinction

CERTIFIED TRAINING & EDUCATION COURSES

Date	Type of course	University
June 2019	ESMIT Level 3 Cardio Course "Quantification of myocardial perfusion"	Caen University Hospital, Caen, France
February 2018	Basic Kinetic Modeling in PET and MR imaging	University of Copenhagen, Copenhagen, Denmark
September 2016	Course in Echocardiography	KULeuven, Leuven, Belgium
April 2016	Educational Salzburg Medical Seminars	Salzburg Duke University, Salzburg, Austria
January 2016	Course in radiation protection	KULeuven, Leuven, Belgium
January 2016	Course on Laboratory animal Science (FELASA B level European certification)	KULeuven, Leuven, Belgium
May-June 2014	Educational medical course "Vital Signs: Understanding What the Body Is Telling Us"	University of Pennsylvania, Philadelphia, USA (distant learning)

GRANTS & AWARDS

Date	Grant
August 2019	Travel grant from YouReCa (Young Research Career)
May 2019	Travel grant from European Society of Cardiology
February 2018	Travel grant from Leuven Academic Foundation

April 2016	Travel grant from Amerikanischen Österreichischen Stiftung
April 2016	Award for the best clinical case presentation, Salzburg Medical Seminars, Salzburg, Austria

SCIENTIFIC FELLOWSHIPS:

Date	Fellowship	Place
Sept 2019 – Oct 2019	Short research stay abroad Supervisor: R.Büchel/O.Gheysens Key words: CRT, mechanical dyssynchrony, phase analysis, SPECT, PET	Department of Nuclear Medicine, University hospital of Zurich, Zurich, Switzerland
Sept 2015 – Dec 2016	Pre-doctoral research fellowship Supervisor: O.Gheysens/P.Claus Key words: SPECT, absolute myocardial perfusion, ^{99m}Tc-Teboroxime	Dept. of Imaging & Pathology, Nuclear Medicine & Molecular Imaging Unit, University of Leuven, Leuven, Belgium
Sept 2014 – Sept 2015	Research fellowship Supervisor: N.Vatutin/L.Natrus Key words: Arterial hypertension, hyperaldosteronism, aldosterone antagonists	Dept. of Internal medicine & Cardiology, V.K.Gusak Institute of Emergency and Reconstructive Surgery, Donetsk, Ukraine

PERSONAL SKILLS AND COMPETENCES

Mother tongues:	Ukrainian, Russian
Other languages:	English – C1, Dutch – B2, German – B2, French –A2
Computer skills:	**Microsoft Office:** Word, Excel, PowerPoint **Statistical software:** R statistics, STATISTICA, IBM SPSS **Programming:** Matlab (basic knowledge)

LIST OF PUBLICATIONS

Publications in peer-reviewed scientific journals

1. Degtiarova G, Claus P, Duchenne J, Bogaert J, Nuyts J, Larsen CK, Aalen J, Fjeld JG, Stokke C, Hopp E, Smiseth OA, Voigt J-U, Gheysens O. Left ventricular regional glucose metabolism in combination with septal scar extent identifies CRT responders. [Under review at the journal]
2. Degtiarova G, Claus P, Duchenne J, Schramm G, Nuyts J, Bogaert J, Voros G, Willems R, Verberne HJ, Voigt J-U, Gheysens O. Can nuclear imaging accurately detect scar in ischemic CRT candidates? [Under review at the journal]
3. Degtiarova G, Claus P, Duchenne J, Cvijic N, Schramm G, Nuyts J, Voigt J-U, Gheysens O. Low Septal to Lateral Wall 18 F-FDG Ratio Is Highly Associated With Mechanical Dyssynchrony in Non-Ischemic CRT Candidates, EJNMMI Res 2019; 9 (1), 105. DOI: 10.1186/s13550-019-0575-9
4. Degtiarova G, Claus P, Duchenne J, Schramm G, Nuyts J, Verberne HJ, Voigt J-U, Gheysens O. Impact of left bundle branch block on myocardial perfusion and metabolism: a positron emission tomography study. JNC 2019. Ahead of print.
5. Degtiarova G, Gheysens O, Van Cleemput J, Wuyts W, Bogaert J Natural evolution of cardiac sarcoidosis in an asymptomatic patient: a case report. Eur Heart J – Case Reports, 2019; 3(3). DOI: 10.1093/ehjcr/ytz099
6. Larsen CK, Aalen J, Stokke C, Fjeld JG, Kongsgaard E, Duchenne J, Degtiarova G, Gheysens O, Voigt J-U, Smiseth OA, Hopp E. Regional Myocardial Work by Cardiac Magnetic Resonance and Non-Invasive Left Ventricular Pressure: A Feasibility Study in Left Bundle Branch Block. Eur Heart J Cardiovasc Imaging 2020; 21 (2), 143-153
7. Duchenne J, Turco A, Bézy S, Ünlü S, Pagourelias ED, Beela AS, Degtiarova G, Vunckx K, Nuyts J, Coudyzer W, Claus P, Rega F, Gheysens O, Voigt JU. Papillary muscles contribute significantly more to left ventricular work in dilated hearts. Eur Heart J Cardiovasc Imaging. 20(1), 84-91, 2019
8. Duchenne J, Turco A, Ünlü S, Pagourelias ED, Vunckx K, Degtiarova G, Bézy S, Cvijic M, Nuyts J, Claus P, Rega F, Gheysens O, Voigt JU Left Ventricular Remodelling Results in Homogenization of Myocardial Work Distribution. Circ Arrhythm Electrophysiol. 2019;12(5), e007224. DOI: 10.1161/CIRCEP.118.007224

9. Pedrosa J, Duchenne J, Queirós S, Degtiarova G, Gheysens O, Claus P, Voigt JU, D'hooge J. Non-invasive myocardial performance mapping using 3D echocardiographic stress-strain loops. Phys Med Biol. 2019; 64 (11), 115026. DOI: 10.1088/1361-6560/ab21f8

Scientific presentations as first author

1. Oral presentation. Myocardial Function Imaging meeting 2020. Leuven, Belgium.
   Prediction of CRT response. Is there any place for nuclear imaging?
   Degtiarova G, Claus P, Duchenne J, Bogaert J, Nuyts J, Larsen CK, Aalen J, Fjeld JG, Stokke C, Hopp E, Smiseth OA, Voigt J-U, Gheysens O.
2. Oral presentation. EANM 2019. Barcelona, Spain.
   Low septal to lateral wall ^{18}F-FDG ratio is highly associated with mechanical dyssynchrony in non-ischemic CRT candidates.
   Degtiarova G, Claus P, Duchenne J, Cvijic M, Schramm G, Nuyts J, Voigt JU, Gheysens O.
3. Poster presentation. ICNC 2019. Lisbon, Portugal.
   Absolute vs semiquantitative ^{13}N-NH_3 myocardial perfusion and ^{18}F-FDG metabolism in non-ischemic patients with LBBB selected for cardiac resynchronization therapy.
   Degtiarova G, Claus P, Duchenne J, Voigt JU, Verberne HJ, Schramm G, Nuyts J, Gheysens O.
4. Oral presentation ICNC 2019. Lisbon, Portugal.
   Natural evolution of cardiac sarcoidosis in an asymptomatic patient: a case report.
   Degtiarova G, Gheysens O, Van Cleemput J, Wuyts W, Bogaert J.
5. Oral presentation EANM 2018. Dusseldorf, Germany.
   Impact of left bundle branch block on myocardial perfusion and metabolism in patients with non-ischemic dilated cardiomyopathy prior to cardiac resynchronization therapy.
   Degtiarova G, Claus P, Duchenne J, Schramm G, Nuyts J, Verberne HJ, Voigt JU, Gheysens O
6. Poster presentation EANM 2018. Dusseldorf, Germany.
   Absolute myocardial perfusion and flow reserve with ^{99m}Tc-Teboroxime dynamic SPECT in a porcine model.
   Degtiarova G, Claus P, Verberne HJ, M.Wu, Vanbilloen B, Bormans G, Gheysens O

ACKNOWLEDGEMENT, PERSONAL CONTRIBUTION AND CONFLICT OF INTEREST

Scientific acknowledgements

This PhD project was funded by:

- KU Leuven research grant [OT/12/084].
- Travel grants provided by:
  - ✓ The Young Researchers' Careers Organization (YouReCa)
  - ✓ The European Society of Cardiology (ESC)
  - ✓ The Leuven Academic Foundation (ASL)

Personal contribution

I hereby assert that the my personal contributions to this thesis included but were not limited to:

- Execution of clinical trials.
- Collecting and analyzing clinical data.
- Development and management of clinical databases.
- Conducting large animal experiments in the cardiac catheterization laboratory and nuclear department.
- Collecting and analyzing experimental data.
- Writing the chapters included in this manuscript.

Conflict of interest

I hereby assert that none of the authors of the manuscript have any conflicts of interest relevant to the work reported in this thesis.

PERSONAL ACKNOWLEDGEMENTS

This journey started in November 2015, when I stepped out of the plane in Brussels, being welcomed by surprisingly sunny Belgium. Several months of terrible homesickness, culture and weather adjustment turned into one of the most fascinating experiences of my life, leaving memories that I will always keep very close to my heart. This trip would not have been so memorable and successful without the people, who were guiding and accompanying me during all this period. In this chapter of my thesis I would like to take an opportunity to thank all of them.

My first words of gratitude go to my promoters Prof. Olivier Gheysens and Prof. Piet Claus. Thank you for choosing me among the whole list of candidates, for giving an opportunity to embark on this challenging and rewarding journey, to work in your team and to perform research in such a nice place and atmosphere. Thank you for putting your trust in everything I was doing and for your support all through the ups and downs. I was lucky to have you by my side and I am thankful for the time that we succeeded and struggled together.

I would like to extend my deep and sincere gratitude to my co-promoters Prof. Jens-Uwe Voigt and Prof. Johan Nuyts. Even though you officially co-supervised only part of my PhD program, I cannot thank you enough for your help, support and contribution throughout all these years! Thank you for your commitment and time to read my manuscripts and for the valuable and constructive feedback that always only improved my work and results. Johan, I have never met so kind, helpful and big-hearted person, whose door is always open for any questions and requests. Professor Voigt, your guidance, fruitful ideas, immense support and the most amazing barbeque parties I have ever attended, will be impossible to forget. I will also miss our heart-to-heart talks, both in English and in German.

I would like to express my gratitude to the members of the jury for the willingness to evaluate my PhD work and for the interest and time taken to help me to improve my PhD thesis. Professor S.Janssens, Professor J.Bogaert, Professor E.Donal and Professor A.Saraste, it is an honor for me that four of you are the part of the examining committee. I would like to acknowledge Prof. Werner Budts for chairing the defence.

Furthermore, I would love to express my deep appreciation to the staff members of the nuclear department for the opportunity to be a part of your team, for your help and support during the scans, educational journal clubs, wonderful parties, dinners and all the memorable events. Thank you Prof K.Van Laere, Karolien, Chris, Christophe, Sander, Michel, Wis, Kristof, Christelle and all the technologists, including Kwinten, Guido, Jef. A special word to Peter Vermaelen, Francine Reniers and Jens Wouters for logistical help and all the administrations over the years. You were always very helpful, I deeply appreciate it.

A special gratitude goes to my colleagues from Medical Imaging Research Center (MIRC). Probably never in my life will I have another chance to work in such a multicultural environment and among so wonderful colleagues, some of whom have already become friends. In particular, I would like to thank my nuclear group, including Jenny, Laura, Martijn, Eline, Aline, Donatienne, Melissa, Anna-Maria, Heleen, Ludovic, Sezgin and Patrick. Thank you for your help, for lunch time chats and for the wonderful time that we spent together during the conferences. Thanks to Nathalie for being an amazing neighbor and for understanding me sometimes without the words. Thanks to Georg, for constructive comments and lessons on physics. Special thanks to June. I was lucky to start my PhD with you as a colleague and to finish it with you as a friend. Words are powerless to express my gratitude for your support, trust, pep talks, innumerable chats and so many dear to my heart memorable moments together.

A warm thanks to the colleagues from the cardio group for the great time at and outside work: Ahmed, Boudewijn, Serkan, Alexis, Razvan, Geo, Maria, Anni. Separate thanks to Marta for the clinical and scientific advices and fruitful discussions; to Stephanie for the wonderful sense of humor and for the ability to spread any news within the seconds ☺. An important word of appreciation goes to Jurgen, my valuable and endless source of knowledge. Thank you immensely for your help, support, professional and personal discussions, for sharing the scientific interests and research projects. Thank you also for being a great friend and motivator, and for dealing with my straightforwardness. A special word goes to Monica and Aniela. Monica, I have sincerely admired your positive attitude, kindness, big smile and how you pronounce "Braaavo". Thank you for my hard drive full of pictures, which will remind me about my PhD adventure for the rest of my life. Thank you, Aniela, for our late evenings and weekends at work, you made them special and cozy, for our chats, for our breakfasts and for your friendship, despite the distance. Girls, thanks for amazing time together, I will cherish these sweet memories for a long time.

I give deep thanks to the group of Jan D'hooge. We were connected neither by work, nor by the similar scientific interest. We didn't have any common projects and never discussed the research ideas. But we were all foreigners and probably that banded us together very tight. Thank you all for solidarity, for the interest to each-other culture, for weekends and holidays that we spent together. Nuno, Pedro, Joao, Alessandro thanks for forgiving my special pronunciation of your names, for unforgettable nights-out, picnics and table games. Bidisha, Alejandra, Adriyana for our long chats, weekend trips and skype conversations. I appreciate so much that despite the distance, we still keep in touch regularly. Thank you, girls, for all your efforts of trying to get me accustomed to high-quality food and I am so sorry that you failed ☺. Alejandra, you cultivated my love to sport and you were one of the best gym and lunch partners ever. Special thanks goes to Nataliya. Your contribution to my comfortable Belgian life has been enormous. Your support and advices were priceless. I am thankful and grateful to have you as a friend. I extend my gratitude to Jan D`hooge for the ability to select amazing colleagues, most of whom have become my friends.

Another thanks goes to other researches whom I met and with whom I shared the memorable moments over time: Charlotte, Hanan, Mahvish, Natasa, I would like to thank you for all those evenings that we spent together making sushi and pizza; Ruben, for the chats, lunches and walks home. I adore listening all your stories with your perfect English accent. Thank you for being always kind and helpful. Marta, Mathias, Mahdi, Vangjush, Sophi, Kobe, Olivia, Tim, Wentao, Nadia, Brecht, Paulo, Katya, Kate, Sjoerd, Helena, Marcus, Ahmed, Joke, Gwen, Janne thank you all for very warm and friendly relationships that we established and for the wonderful atmosphere that you created.

A special word goes to the colleagues that helped me in the animal lab: Bert, Ming, Patricia, Roxana, David, Matthew, Sebastian, Peter. Without you my experimental work wouldn't have been so successful. During all these years of research I couldn't develop any love for the animal experiments, but all of you made the long days in the Cath lab brighter! Thanks for this!

During my PhD I had a unique opportunity to learn cardiac CMR and for this amazing and valuable experience I would like to thank Professor Jan Bogaert. I deeply admire you as a radiologist, as a scientist and as a person. I have never met anyone who is so dedicated to work, who loves so much his profession and contaminates with this love everyone around. You inspire and you motivate. Thank you for letting me to be a part of your team. I owe you a lot for all the

knowledge and experience I gained! I would also like to thank my colleagues without whom my CMR experience would not have been so amazing: Sara, Pierpaolo, Emanuel, Veronica, Rafaella, Tom, Lui and all the CMR technologists. Special thanks to Tom for the infinite patience during CMR physics lessons and to Professor Dymarkowski, for the generosity with which you shared all your knowledge and for your great sense of humor. Jan, Tom and Professor Dymarkowski, I feel extremely privileged to have worked with you and to have learned from you!

In September 2019 I had a chance to carry-out a short term research in the Nuclear Medicine Department of Zurich University Hospital. I would like to thank the amazing team that hosted me and made my stay in Switzerland fruitful and memorable, especially senior staff members: Ronny, Tobias, Aju and residents: Hannes, Adam, Aleksandra.

I would not be able to cope with the homesickness so easily if it wasn't for my Russian-speaking friends, whom I met in Belgium. Enormous thanks for our day and night chats, parties, trips, crazy shopping, a lot of Prosecco and Aperol, for all the laughs, support and magnificent moments that gave me a feeling of home, while being so far away. I will remember all our adventures and every time recollect them with a big smile. Alena, Kristina, Anna, Valeriya these words of thanks go to you! I'm grateful for the chance to meet you and to enjoy your company during all these years. You contribute a lot in making my PhD trip very memorable.

Separate thanks to my Ukrainian friends. Now I know for sure that the distance is not an obstacle for the friendship. I appreciate so much our regular phone calls, chats and trips. Thank you for your continuous support and for offering a help hand each time it was needed.

I would like to thank the KULeuven, UZ Leuven, Leuven Academic Foundation, Young Research`s Career Foundation (YouReCa) and European Society of Cardiology for their support of this PhD project, for the travel grants and the opportunity to perform fellowship in Zurich University Hospital.

Last but not least I would like to thank my family and my husband in my mother tongue.
Моей семье. Не верится, что у меня в руках одно из самых больших достижений в жизни. Этого бы не случилось без вашей неустанной помощи и поддержки. Спасибо вам за то, что прошли со мной этот путь рука об руку, за то, что верили в меня, гордились и были рядом в минуты сомнений. Я благодарна за вашу любовь и за душевную теплоту, которую я чувствую даже через тысячу километров! Благодарна за усердие и трудолюбие, которые вы воспитывали во мне на протяжении всей жизни. Без всего этого, мне было бы не справиться.
Моему мужу. Все мои взлеты и падения, победы и поражения, слёзы и радость, абсолютно всё ты делил со мной поровну. Я и мечтать не могла о лучшем партнёре. Спасибо, что гордишься мной, мотивируешь и делаешь мою жизнь удивительной! Спасибо, за искреннюю веру в мой успех, даже когда провал очевиден и за то, что несмотря на трудности, ни разу не позволил опустить руки. Я уверена, что никогда не была бы там, где сейчас, без твоего надёжного плеча. Спасибо тебе за это!

Эту книгу я посвящаю памяти своего дедушки Валентина - профессора, доктора технических наук, лауреата Государственной премии Советского Союза. Уверенна, что сегодня он был бы бесконечно горд.